AD A129564

(12)

Research and Development Technical Report

DELET-TR-81-0420-2

Studies Leading to the Development of High-Rate Lithium-Sulfuryl Chloride Battery Technology

John C. Hall, Mark Koch and Faruq Marikar
Gould Research Center, Materials Laboratory
40 Gould Center
Rolling Meadows, IL 60008

December 1982

Final Report for the Period 1 September 1981 to 31 August 1982

APPROVED FOR PUBLIC RELEASE: DISTRIBUTION UNLIMITED

Prepared for:
ELECTRONICS TECHNOLOGY AND DEVICES LABORATORY

ERADCOM

US ARMY ELECTRONICS RESEARCH AND DEVELOPMENT COMMAND
FORT MONMOUTH, NEW JERSEY 07703

NOTICES

Disclaimers

The findings in this report are not to be construed as an official Department of the Army position, unless so designated by other authorized documents.

The citation of trade names and names of manufacturers in this report is not to be construed as official Government indorsement or approval of commercial products or services referenced herein.

Disposition

Destroy this report when it is no longer needed. Do not return it to the originator.

UNCLASSIFIED

SECURITY CLASSIFICATION OF THIS PAGE (When Data Entered)

REPORT DOCUMENTATION PAGE

READ INSTRUCTIONS BEFORE COMPLETING FORM

1. REPORT NUMBER: DELET-TR-81-0420-2	2. GOVT ACCESSION NO.
3. RECIPIENT'S CATALOG NUMBER	
4. TITLE (and Subtitle): Studies Leading to the Development of High-Rate Lithium-Sulfuryl Chloride Battery Technology	5. TYPE OF REPORT & PERIOD COVERED: 9/1/81 to 8/31/82
	6. PERFORMING ORG. REPORT NUMBER: 827-055
7. AUTHOR(s): John C. Hall, Mark Koch, and Faruq Marikar	8. CONTRACT OR GRANT NUMBER(s): DAAK20-81-C-0420
9. PERFORMING ORGANIZATION NAME AND ADDRESS: Gould Research Center, Materials Laboratory, 40 Gould Center, Rolling Meadows, IL 60008	10. PROGRAM ELEMENT, PROJECT, TASK AREA & WORK UNIT NUMBERS: IL162705AH94-11-021
11. CONTROLLING OFFICE NAME AND ADDRESS: U.S. Army Elect Tech & Dvcs Laboratory, Attn: DELET-PR, Fort Monmouth, NJ 07703	12. REPORT DATE: December 1982
	13. NUMBER OF PAGES: 154
14. MONITORING AGENCY NAME & ADDRESS (if different from Controlling Office)	15. SECURITY CLASS. (of this report): UNCLASSIFIED
	15a. DECLASSIFICATION/DOWNGRADING SCHEDULE

16. DISTRIBUTION STATEMENT (of this Report)

17. DISTRIBUTION STATEMENT (of the abstract entered in Block 20, if different from Report)

Approved for public release; distribution unlimited

18. SUPPLEMENTARY NOTES

19. KEY WORDS (Continue on reverse side if necessary and identify by block number)

Sulfuryl chloride, lithium, primary cells, lithium batteries, high energy batteries.

20. ABSTRACT (Continue on reverse side if necessary and identify by block number)

DD FORM 1 JAN 73 1473 EDITION OF 1 NOV 65 IS OBSOLETE

UNCLASSIFIED

SECURITY CLASSIFICATION OF THIS PAGE (When Data Entered)

The overall aim of the program was to examine the viability of an active electrolyte, lithium-sulfuryl chloride battery system. The specific objectives were

- Quantify the stability of lithium in sulfuryl chloride solution.
- Explore means to stabilize lithium in sulfuryl chloride.
- Establish the limits of performance of carbon/TEFLON® cathodes.

During the course of the contract we carried out the following activities:

- Optimization of the cell design with respect to leakage and lithium stability.
- Studied the stability of the lithium anode with respect to electrolyte composition and stabilizing coating by calorimetry and complex plane impedance.
- Determined the performance of both electrodes as a function of electrode and electrolyte composition, current density and temperature.
- Measured both the density and conductivity of sulfuryl chloride electrolyte.
- Carried out limited mechanistic studies of cathode discharge and cell safety.

We have found that

- The fundamental long term corrosion rate of lithium sulfuryl chloride electrolyte is less than 1 mil per year (mpy) at room temperature.
- The corrosion rate of lithium in an operating cell is considerably increased due to impurities in the cell hardware. We have been successful in reducing this corrosion rate to 5 mpy with the chlorine additive and cyanoacrylate coating, which are also effective in minimizing voltage delay.
- Lithium sulfuryl chloride cells are capable of delivering close to 110% of capacity at current densities of up to 100mA/cm^2. Neither reduces cell performance by a statistically significant amount.

Based on this work lithium-sulfuryl chloride appears to be a viable system for Army applications. Demonstration of viability requires the solution to materials compatability issues which are as much economic as technical. To meet Army safety requirements it is recommended that a follow-on effort also address safety questions.

Contents

List of Tables

List of Figures

List of Figures (continued)

List of Figures (continued)

List of Figures (continued)

List of Figures (continued)

List of Figure (continued)

List of Figures (continued)

I. INTRODUCTION

Batteries built with an inorganic catholyte (e.g., thionyl chloride and sulfuryl chloride) are of interest for military applications on the basis of their high demonstrated energy density and high discharge rate capability when compared with organic electrolyte lithium cells. By far the greatest attention has been given to the lithium-thionyl chloride ($Li/SOCl_2$) system; cells and batteries have been demonstrated with energy densities in excess of 600Wh/kg (1). Less attention has been given to the development of lithium-sulfuryl chloride batteries possibly because of a somewhat lower theoretical energy density (1700 and 1500 Wh/kg for $Li/SOCl_2$ and Li/SO_2Cl_2 respectively).

Despite the impressive levels of performance demonstrated with $Li/SOCl_2$, wide spread deployment has not yet occurred principally due to unresolved safety issues. One of the probable causes for explosion of $Li/SOCl_2$ cells during overheating either as a result of short circuiting or an external heat source is the reaction between lithium and sulfur (2), which is formed by cell discharge according to the discharge reaction (3)

$$4Li + 2SOCl_2 = 4LiCl + SO_2 + S \qquad [1]$$

In this regard Li/SO_2Cl_2 may be a fundamentally safer system as no sulfur is formed in the discharge reaction (4)

$$2Li + SO_2Cl_2 = 2LiCl + SO_2 \qquad [2]$$

---

1. D.I. Chua, J.O. Crabb and S.L. Despande, "Proceedings of the 28th Power Sources Symposium," Atlantic City, N.J. 28 247 (1978).

2. A.N. Dey, "Proceedings of the 26th Power Sources Symposium," Atlantic City, N.J. 27 42 (1976).

3. W.K. Behl, "Proceedings of the 28th Power Sources Symposium," Atlantic City, N.J. 28 30 (1978).

4. W.K. Behl, J. Electrochem. Soc., 127 1444 (1980).

Development of potentially safer Li/SO_2Cl_2 cells for military applications will require the demonstration of cells with long shelf lives and performance which at least approach that of $Li/SOCl_2$. The former requirement is principally a function of controlling the rate of lithium corrosion; the latter requirement entails optimization of the anode with respect to voltage delay and the cathode with respect to voltage and capacity in the range of 1 to 20 mA/cm^2 at temperatures down to -40°C. Both were examined in the present study.

The full scope of this study was as follows:

- Investigation of anode passivation and the properties of the passive film with respect to materials selection, electrolyte composition and means of stabilizing the anode.

- Fundamental studies of the operation of the bromine additive and safety related reaction during discharge and cell reversal.

- Characterization of anode performance after storage (i.e., voltage delay) with respect to electrolyte composition and anode design.

- Statistical characterization of cathode performance as a function of current density and temperature. These studies have been carried out with respect to both cathode and electrolyte composition.

- Measurements of physicochemical properties of sulfuryl chloride electrolytes.

The results of these studies are presented sequentially below, followed by a section containing conclusions drawn and recommendations for future work.

II. MECHANISTIC STUDIES OF ANODE OPERATION

The objectives of these studies were to characterize the processes which determine the life and performance of the lithium anode in active electrolyte lithium-sulfuryl chloride cells. The two anode processes of greatest concern with regard to the viability of Li/SO_2Cl_2 cells for Army applications are

- Anode corrosion in sulfuryl chloride. Active electrolyte Li/SO_2Cl_2 cells are only viable if an adherent, non-porous insulating film of LiCl forms over the anode surface.

- Voltage delay after storage. Voltage delay results if the protective film becomes overly thick, resulting in a large increase in internal cell resistance which, in turn, depresses the initial cell voltage on discharge.

The above two effects are somewhat related. If a thin adherent film rapidly forms both corrosion and film build-up will be minimized. In this section studies of the passivating film as a function of design, time and applied current are described.

II.1 Experimental Approach

The two methods we have applied to the study of anode processes are complex plane impedance and microcalorimetry. The former method has the potential for nondestructively supplying microscopic information on the nature of the anode protective film. The latter method yields data on the rate of film forming reactions.

Complex Plane Impedance Technique: The impedance of the electrochemical cell at any given frequency f is measured using a low amplitude ac signal (ca 5 mV peak to peak) applied to the cell at rest or

under polarization. For a parallell coupled resistance and capacitance (the most frequently encountered equivalent circuit in the studies described here), the impedance Ze can be represented as a function of the resistance R, the capacitance C and the angular frequency $\omega(=2\pi f)$ by either of the following equations.

$$Ze = \frac{R}{1+j\omega CR} = \frac{R}{1+(\omega CR)^2}(1-j\omega CR) \qquad [3]$$

$$Ze = \frac{R}{[1+(\omega CR)^2]^{\frac{1}{2}}} \text{ arc } [\tan^{-1}(-\omega CR)]$$

The locus of impedance for this simple electrical network is a semicircle as shown in Figure 1. The addition of a resistance in series with the circuit shown will cause the semicircular plot to shift to the right on the x-axis. It is customary in presenting electrochemical results to employ the first quadrant by simply inverting the y axis.

A typical complex plane impedance spectrum of a Li/SO_2Cl_2 cell four hours after filling with electrolyte is shown in Figure 2. The frequency range available for impedance measurement was 25 kHz to 0.05 Hz. The intersection of the high frequency end of the semicircle with the x-axis gives a measure of the sum of the terminal and electrolyte resistances (R_{el}). The center of the first semicircle lies below the X-axis. The resistance of the circuit element is 28Ω and the capacitance calculated from the frequency at the maximum of the semicircle is 1.14 μF. This capacitance value is over an order of magnitude smaller than the 10 to 40 $\mu F/cm^2$ expected of solid/electrolyte solution interfaces. Based on the changes in the electrical characteristics on storage and polarization of the cell (described below) the reactance obtained can be attributed to the presence of a dielectric film on the lithium anode. The presence of a film of LiCl on lithium in $SOCl_2$-based electrolytes is well known. A similar film exists on lithium in SO_2Cl_2-electrolytes.

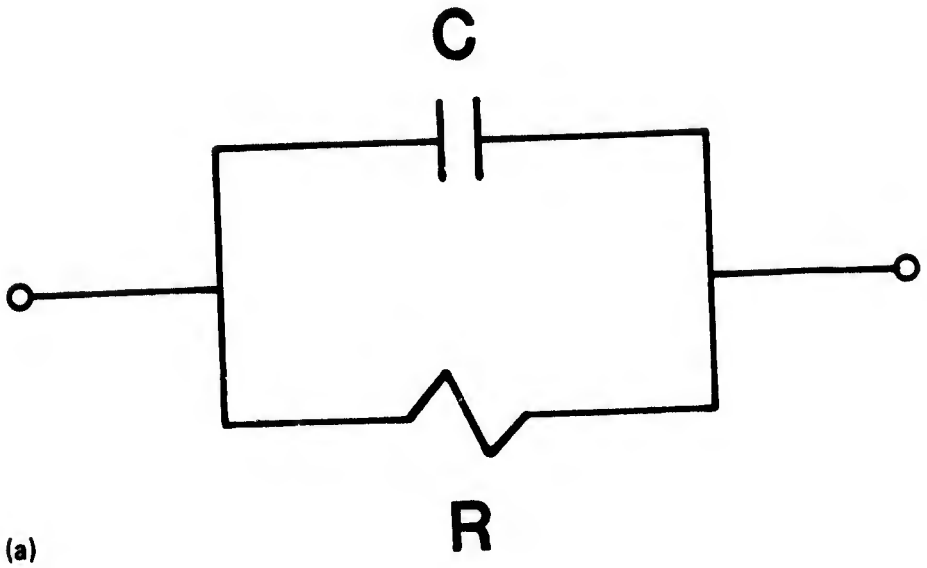

(a)

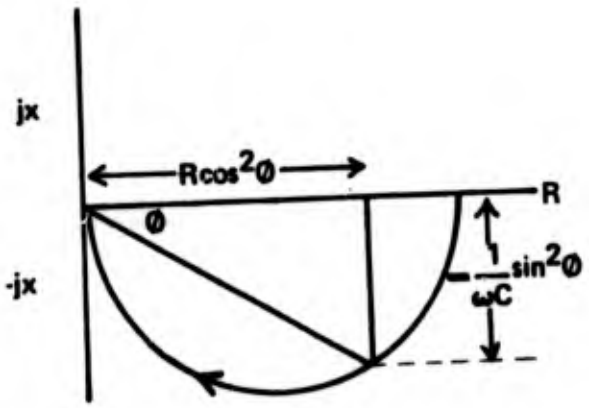

(b)

(1576)

Figure 1 a) Resistance – Capacitance Network and b) Locus of Impedance Plot

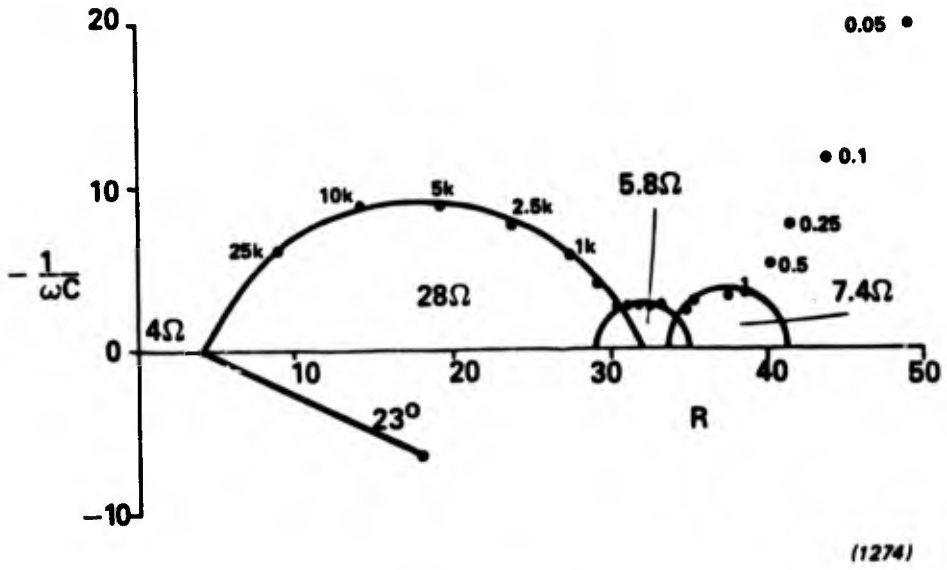

Figure 2 Complex plane impedance spectrum of a Li/SO_2Cl_2 cell 4 hours after fill

The thickness of the film d can be calculated from the capacitance C using the equation

$$C = \frac{\varepsilon A}{3.6 \times 10^{12} \pi d}$$

where A is the geometric area and ε the dielectric constant of LiCl is 11.05. The film thickness, four hours after cell filling is 283Å.

The semicircles observed at lower frequencies arise from resistance-capacitance couples associated with charge transfer impedances and inter-particle contact impedances in the cell. When the semicircle at the high frequency end grows in size, the low frequency side degrades in resolution and the frequency range available is no longer sufficient to delineate fully the spectrum. This effect is already evident in Figure 3 which is a spectrum obtained two hours after the one in Figure 2.

Battery Microcalorimetry: Battery microcalorimeters such as the Tronac 351R used in this work are capable of measuring heat fluxes of less then 1 μω. For the most probable corrosion/film formation reaction in Li/SO_2Cl_2 cells of the size built for this study

$$2Li + SO_2Cl_2 = SO_2 + 2LiCl \qquad \Delta H^\circ_{298} = 744 kJ/mole \qquad [2]$$

the sensitivity of the Tronac 351R allows reaction [2] to be measured at a rate correspondong to 0.05 mils per year (mpy) of lithium surface.

Although microcalorimetry is a very sensitive tool for determining reaction rates it is not discriminatory. That is, the output data is a heat flux and if more than one source of heat exists the total heat must be divided between the sources to estimate reliably reaction rates. For example, Hall,

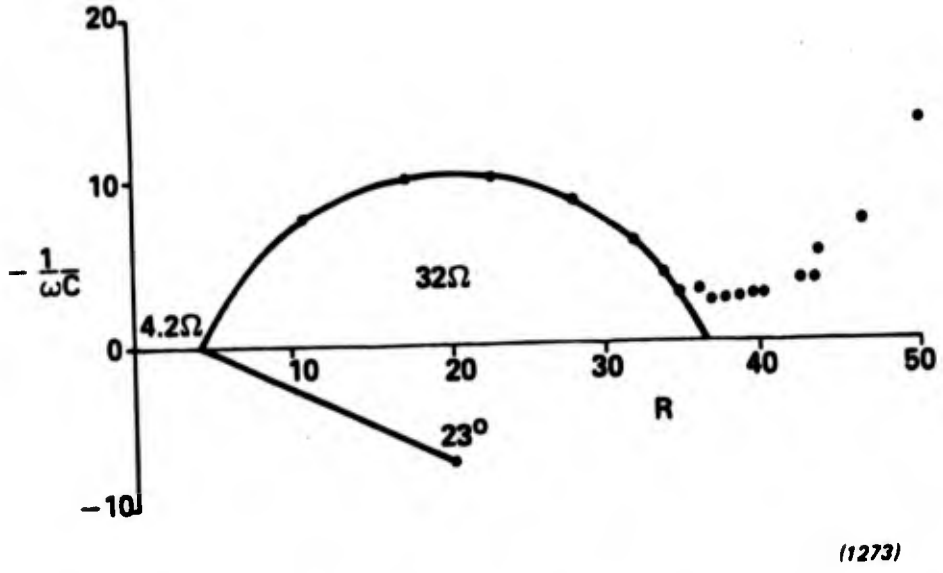

Figure 3 Complex Plane Impedance Spectrum of a Li/SO_2Cl_2 cell 6 hours after fill

et.al. (5) were able to partition the heat generated by zinc-air cell self discharge between direct oxidation and corrosion by measuring the heat flux in the presence and absence of oxygen. For sealed Li/SO_2Cl_2 cells extraneous sources of heat may arise from corrosion of cell components. In this work we have largely ignored these sources of heat and assigned the total heat flux to reaction [4]. Our estimated corrosion values thus represent a worst case situation.

In future work, if partitioning of the heat is desired, differential calorimetry between filled cells with and without lithium is recommended.

II.2. Materials Selection and Cell Design

The chief result of all of the early calorimetric work was a cell design of sufficient life and stability to allow parametric performance characterization. A schematic of the initial cell design is given in Figure 4. In this design a 304 SS case is employed with one electrode grounded to the case. Electrical connection to the second electrode is made with a glass-to-metal feedthrough whose insulated terminal also serves as a fill tube. The feedthrough is bonded to the case with soft tin or tin-lead solder.

Corrosion data for two such cells using a 1.5 M $LiAlCl_4/SO_2Cl_2$ electrolyte and a negative grounded design are given in Figure 5. Corrosion is high when the electrolyte is prepared from reagent grade sulfuryl chloride. When the reagent is distilled, refluxed over lithium and distilled again and then used, the corrosion rate diminishes considerably. The highest corrosion rate measured here is an order of magnitude lower than the rate estimated from the initial gassing rate found by Gilman and Wade (6). In

---

5. J.C. Hall, H.F. Gibbard and M.J. Montgomery, Fall Meeting of the Electrochemical Society, Extended Abstract No. 104, Los Angeles, California, October 14-19, 1979.
6. S. Gilman and W. Wade, J. Electrochem. Soc., 127, 1427 (1980).

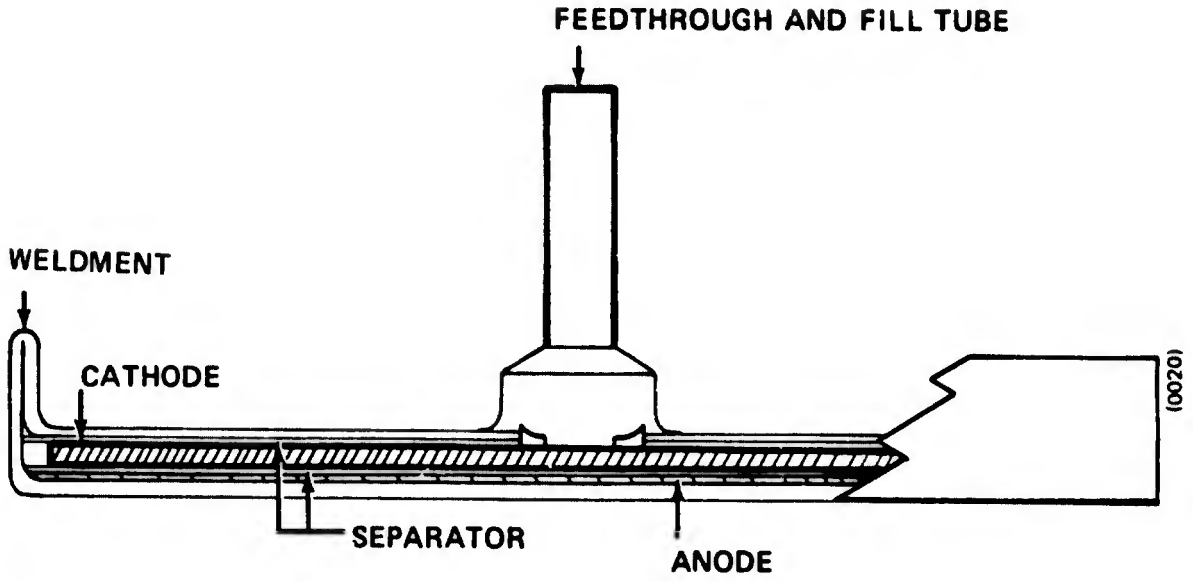

Figure 4 Schematic Cross Section of 25mm and 50mm Diameter Cells

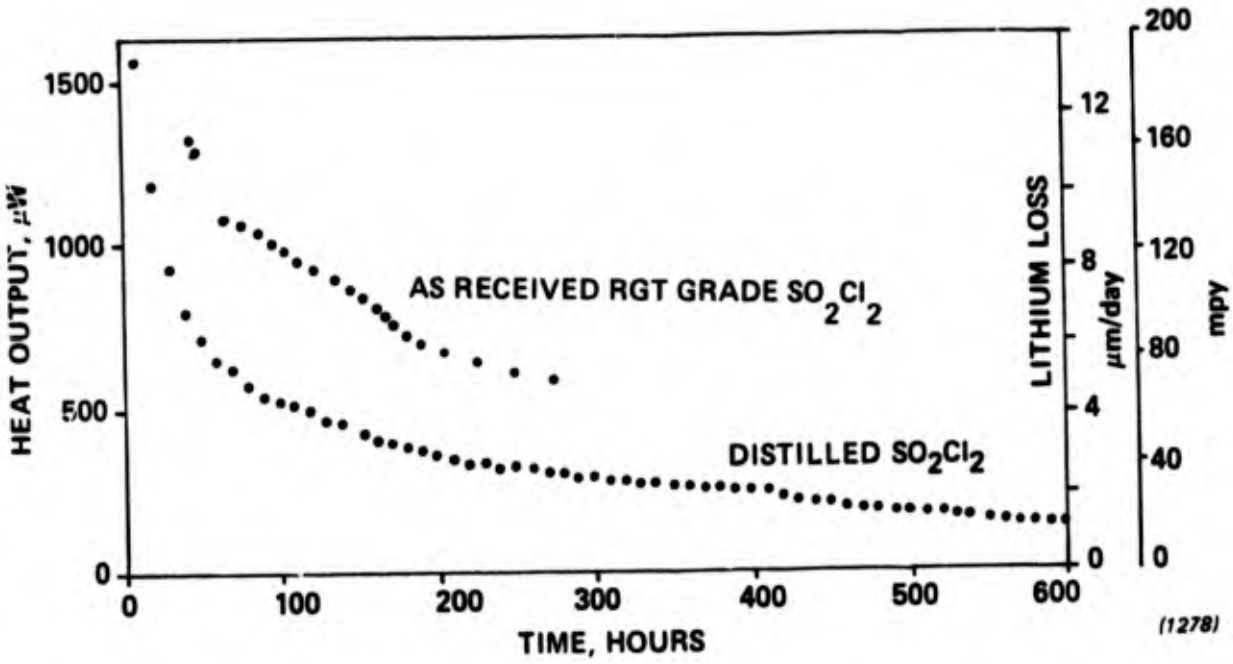

Figure 5 Heat Evolution from Li/SO_2Cl_2 cells

translating the heat outputs to corrosion rates it was assumed that only one face of the lithium foil pressed into the metal case is available for corrosion. If both the faces i.e., 2x3.3 cm^2 are indeed available for corrosion the effective corrosion rate would be half that shown in Figure 5.

The corrosion rate of lithium in the cell containing purified SO_2Cl_2 is about 125 mils per year, one day after cell filling. It decreases to 40 mpy after 10 days and 20 mpy after 23 days. The corrosion rate continues to decrease on further storage, but, after 600 hours of storage it is still greater than 10 mpy, which is clearly unacceptable for Army applications.

One possible cause for this high rate of corrosion is that stainless steel is corroded in sulfuryl chloride, and the heavy metal corrosion products may plate on the anode surface and create a local cell. In addition it was unclear what the optimum electrode grounding choice is with respect to cell shelf life. Finally the studies to this point were not carried out with performance additives which may impact lithium stability in an unforeseen way.

The design of the next series of cells tested are summarized in Table 1. In cells 2 and 3, where the negative electrode floats with respect to the case, the electrodes were made by pressing 2 0.01 inch lithium foils to both faces of a 0.002" Ni foil. In the case of cell 1 the negative electrode was fabricated by pressure bonding a 0.01 inch lithium foil to the nickel can.

Calorimetic heat generation, corrosion and film resistance data for the three cells are summarized in Table 2. Although none of the cells demonstrated an acceptable rate of corrosion it does appear that floating the negative electrode with respect to the case (cells 2 and 3) leads to a lower corrosion rate than negative grounding. For cell 3 the rate of corrosion is exponentially decreasing with time as shown in Figure 6.

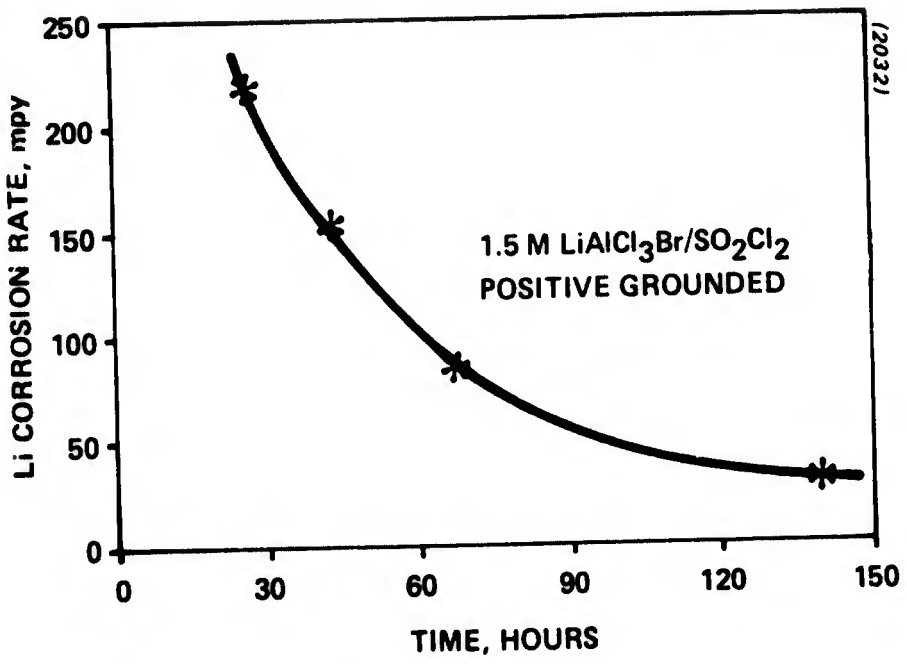

Figure 6 Lithium Corrosion Data in Sulfuryl Chloride

Table 1

Design Characteristics of 1-inch Diameter Cells
for Anode Stability Testing

- 200 Ni case
- Glass to metal feedthrough
- $LiAlCl_4/SO_2Cl_2$ electrolyte
- Bromine Additive
- 90% Shawinigan Black, 10% PTFE cathode
- 0.005 inch glass mat separator

Cell No.	Anode Area (cm^2)	Grounding
1	1.27	Negative
2	2.50	Floating
3	2.50	Positive

Table 2

Calorimetric and AC Impedance Data for Li/SO_2Cl_2 Cells

Time	Cell #1 Negative Grounded			Cell #2 Both Electrodes Floating			Cell #3 Positive Grounded		
	Heat Generation ($\mu W/cm^2$)	Corrosion Rate (mpy)	Film Resistance (Ω)	Heat Generation ($\mu W/cm^2$)	Corrosion Rate (mpy)	Film Resistance (Ω)	Heat Generation ($\mu W/cm^2$)	Corrosion Rate (mpy)	Film Resistance (Ω)
25	1470	562	22	1134	453	41	554	218	57
45	1050	420	38	785	314	89	381	153	80
70	790	316	-	-	-	-	209	83	-
140	162	56	-	-	-	-	78	31	-

All the cells summarized in Table 2 developed leaks at the tin solder joint between the feedthrough eyelet and the case. The leakage precluded longer term testing and may have led to an increase in the apparent corrosion rate as a result of

- Corrosion heat due to electrolyte attack on the solder and case material. To assess this an empty cell case was filled with electrolyte and its heat generation measured. 24 hours after construction the empty cell case was generating 241 μW of heat. Thus as much as 40% of the heat ascribed to anode corrosion could arise from a secondary corrosion process.

- If soluble heavy metal products arise from secondary corrosion processes they would be expected to plate out on the anode and increase anode corrosion through the formation of a local cell.

Based on these results it was not clear whether lithium is inherently unstable in sulfuryl chloride or the measured corrosion rates are representative of materials selection problems. To this end we have carried out a series of ampule experiments where the heat generation from lithium foils in contact with electrolyte inside sealed glass ampules was measured.

The first questions addressed by the ampule experiments were the inherent stability of lithium in $LiAlCl_4/SO_2Cl_2$ electrolytes and the possible local cell effect. Figure 7 shows the heat evolution due to exposure of 3.3 cm^2 area lithium foil. The heat output is high during the first day of exposure but it diminishes thereafter and amounts to only about 6 mpy corrosion rate after the second day. Corrosion is only about 2 mpy after ten days, and the decrease continues on further storage. Thus it does not appear that lithium is inherently unstable in a $LiAlCl_4/SO_2Cl_2$ solution.

Figure 8 shows the effect on corrosion rate of contacting the lithium foil with a piece of nickel foil of equal geometric area. In the absence of

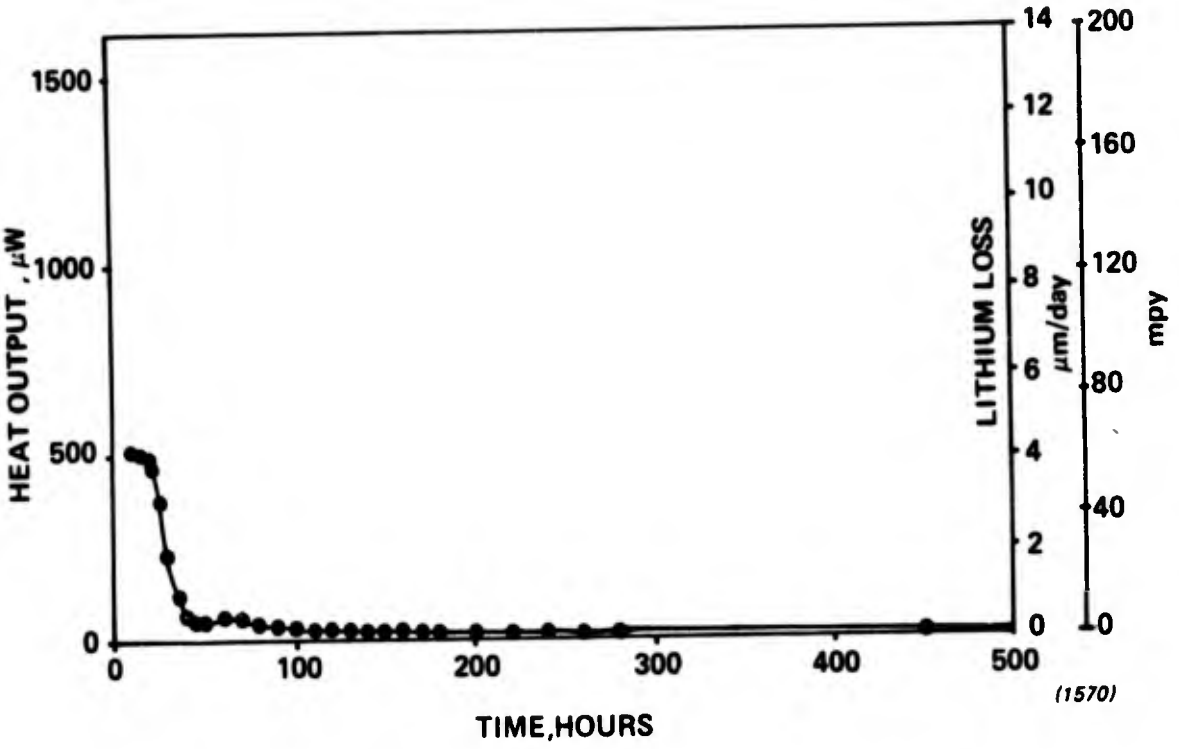

Figure 7 Corrosion Rate of Lithium Foil in SO_2Cl_2 – $LiAlCl_4$ Solution

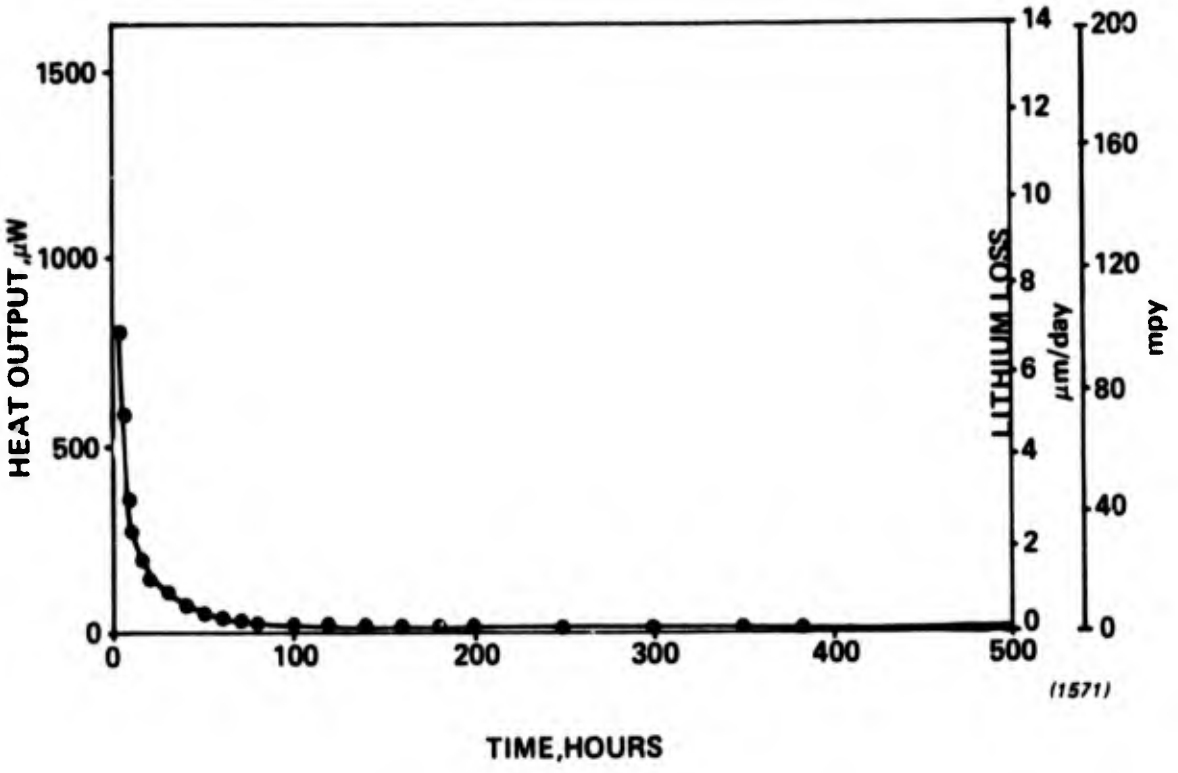

Figure 8 Corrosion Rate of Lithium Foil in SO_2Cl_2 – $LiAlCl_4$ Solution in contact with Nickel foil of equal area

nickel both the reduction of SO_2Cl_2 and the oxidation of Li to Li^+ have to occur on the lithium surface. Nickel provides a convenient substrate for the reduction reaction. Probably because of this the film formed on lithium could be more compact and the corrosion reaction moderates much more swiftly and smoothly. The corrosion rate is 16 mpy at the end of the first day and it drops to 2 mpy in eight days.

We have also evaluated the intrinsic rate of lithium corrosion in the bromine-containing electrolyte used in the second series of cell tests. This electrolyte was formed by mixing 1.0 mole of $LiAlCl_4$ and 0.5 moles of $LiAlCl_3Br$ per liter of sulfuryl chloride. The bromide containing solute is oxidized by SO_2Cl_2 according to the reaction

$$2LiAlCl_3Br + SO_2Cl_2 = SO_2 + LiAlCl_4 + Br_2 \qquad [4]$$

Based on spectroscopic studies reaction [4] proceeds to at least 80%. Thus the actual electrolyte composition for this ampule test was 1.4M $LiAlCl_4$, 0.2M So_2, 0.2M Br_2, 0.1M $LiAlCl_3Br/SO_2Cl_2$.

Corrosion data for the ampule experiment using the above Br_2, SO_2 containing electrolyte are given in Figure 9. As can be seen in Figure 9 with the additive the corrosion rate of lithium falls to zero within 9 hours. This is remarkably better than the cell data and a much lower corrosion rate than we previously reported for lithium corrosion in sulfuryl chloride electrolyte without bromine.

The above results indicate a strong materials/purity effect on the shelf life of cells. The immediate challenge was to translate ampule results into real cells. The obvious weakness of the cell design was the solder joint between the feedthrough eyelet and the case. A new feedthrough has been designed (shown in Figure 10) which combines the cell lid with a glass to metal seal. This design eliminates the need for solder and only TIG welding is required to seal the cell.

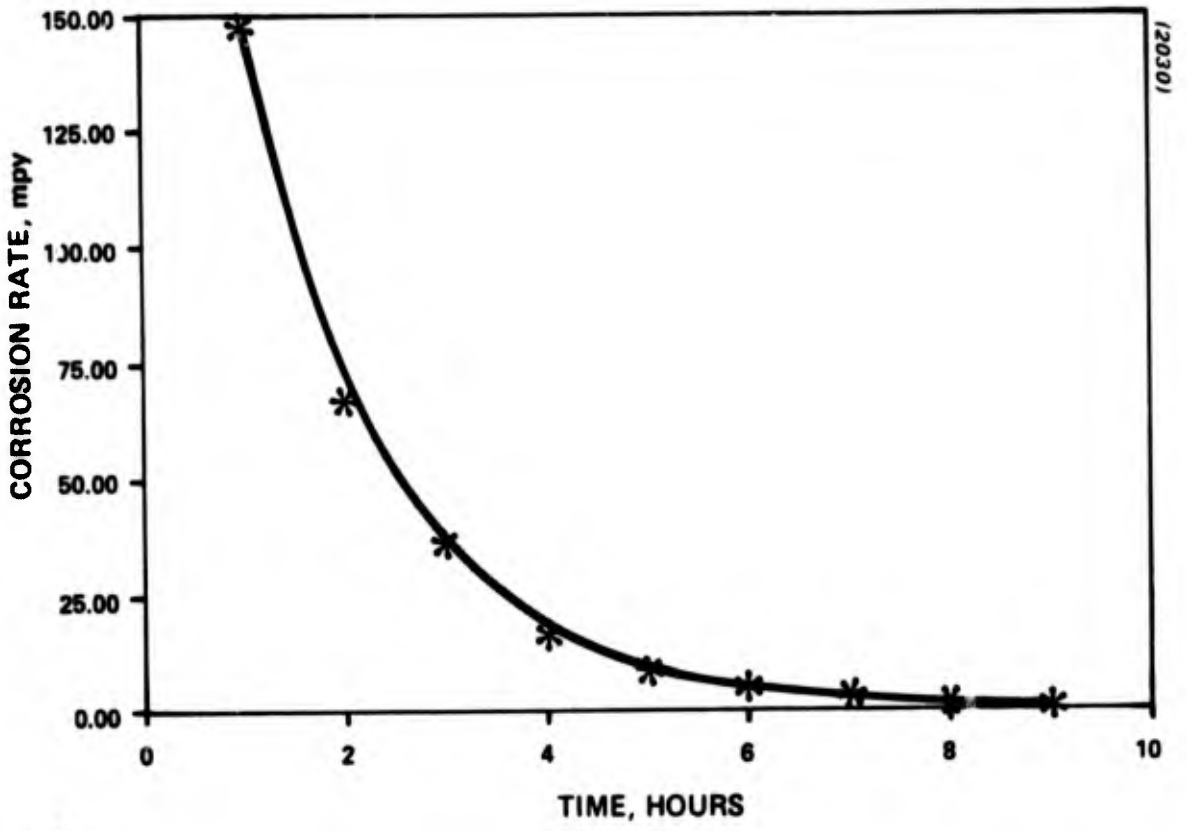

Figure 9 Lithium Corrosion Rate in a Glass Ampule at 25C. Ampule Contains 3.3cm_2 of Lithium in 1.0M $LiAlCl_4$, 0.5M $LiAlCl_3Br/SOCl_2$.

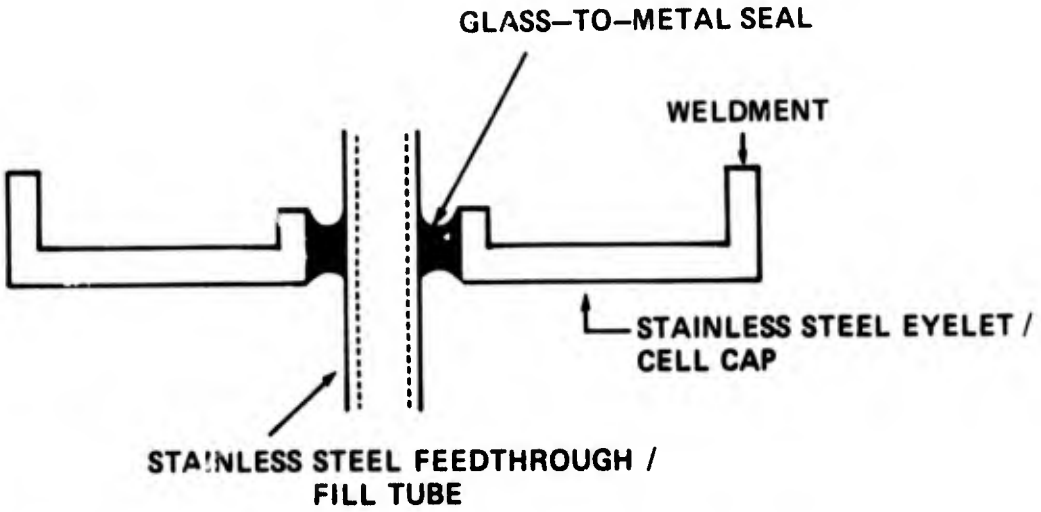

Figure 10 Design of Solderless Feedthrough/Fill Tube/Cell Cap

Unfortunately, use of the designs shown in Figure 10 also requires the use of stainless steel cell parts, since glass cannot be joined satisfactorily to more inert materials such as nickel. The baseline design described in detail in Section II.3 used the Figure 10 feedthrough and a 304 stainless steel positive grounded case.

We have evaluated the intrinsic lithium corrosion rate of this design with the glass ampule technique. Lithium and stainless steel $10cm^2$ foils were placed in a glass ampule but electrically isolated from each other with glass mat separator. The ampule was filled with 1.5 M $LiAlCl_4/SO_2Cl_2$ electrolyte. To eliminate extraneous effects due to stainless steel corrosion an ampule containing $10cm^2$ of stainless steel, glass mat separator and electrolyte was placed in the second compartment of the Tronac calorimeter. The experiment was thus differential in nature with sources of heat other than lithium corrosion substracted out.

Heat generation and corrosion data for the above experiment are given in Figure 11. Through 70 hours of testing the corrosion rate was found to be at least double that found in the previous ampule experiments (12mpy at t=60 as opposed to > 6mpy). This indicates a need for improved case materials to be developed as part of a follow-on effort.

II.3 Anode Stability on Storage

During the first two quarters of the contract work anode stability studies were carried out using cells with soldered feedthrough. Some of the results of this work and problems with the cell design were discussed in the previous section. A full description of the work is given in quarterly reports DELET-TR-81-0420-1 and DELET-TR-81-0420-2.

During the last two quarters all work was carried out with the solderless design. The cell design used in this work is summarized in Table 3. In general cells built with this design were leak-free and had relatively

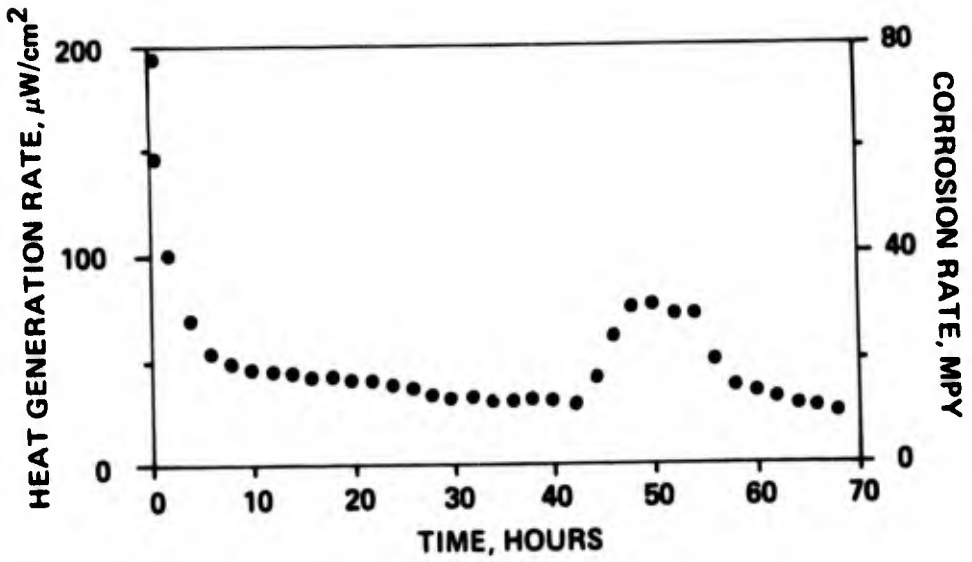

Figure 11 Corrosion Data for a $10cm^2$ Lithium Foil and a $10cm^2$ Stainless Steel Foil in a Sealed Glass Ampule Containing 1.5M $LiAlCl_4/SO_2Cl_2$ vs. a $10cm^2$ SS Foil in a Glass Ampule Containing 1.5M $LiAlCl_4/SO_2Cl_2$

Table 3

Design Characteristics for Second Generation Cells
Employed in Anode Stability Studies

- 304 stainless steel case with integral glass to metal seal
- Positive grounded
- 90% Shawinigan Black, 10% PTFE cathode, 0.02" thick, nickel Exmet supported
- 0.002" negative nickel sheet current collector
- 0.004" porous Teflon insulator between the anode and the case
- Cell TIG welded

stable voltages for at least two months. The actual life time of the cell is unknown or no unexpected failures have been observed.

The first problem addressed with the new design was the effect of electrolyte composition on anode stability and the nature of the passivating film. The three electrolytes used in this study were: 1.5M $LiAlCl_4/SO_2Cl_2$; 1.4M $LiAlCl_4$, 0.1M $LiAlCl_3Br$, 0.2M Br_2, 0.2M SO_2/SO_2Cl_2 and 1.5M $LiAlCl_3$, 0.2M Cl_2/SO_2Cl_2. The chlorine was added by bubbling gaseous chlorine through a presaturation and addition apparatus schematically shown in Figure 12. Thus the initial SO_2 concentration for this cell was probably lower than that normally present due to thermal decomposition due to removal by the gas stream.

In Figure 13 corrosion data from 0 to 700 hours after activation are given for the cell with the bromine electrolyte. The benefit of the solderless design is clearly evident if these data are compared with that in Table 2. The initial corrosion rate of the solderless design is only 25% of that found in cells built with solder.

Although we were successful in reducing the initial corrosion rate no improvement was seen in the long term corrosion rate as can be seen by comparing the data in Figure 13 with that in Figure 5. After 600 hours of testing the rate of corrosion in both cells is ~ 20 mpy.

This may indicate that cells which contain bromine are more sensitive to trace, corrosion-promoting impurities. This was confirmed by the tests of the $LiAlCl_4/SO_2Cl_2$ and $LiAlCl_4$, Cl_2/SO_2Cl_2 cells. Corrosion data for these cells through 700 and 500 hours of storage respectively are given in Figures 14 and 15. Both cells show a much more steeply declining corrosion rate than the cell built with the bromine additive. Although the cell containing chlorine initially has a slightly higher corrosion rate, after 500 hours of storage its corrosion rate has declined to 5 mpy or about half that of the cell without additives.

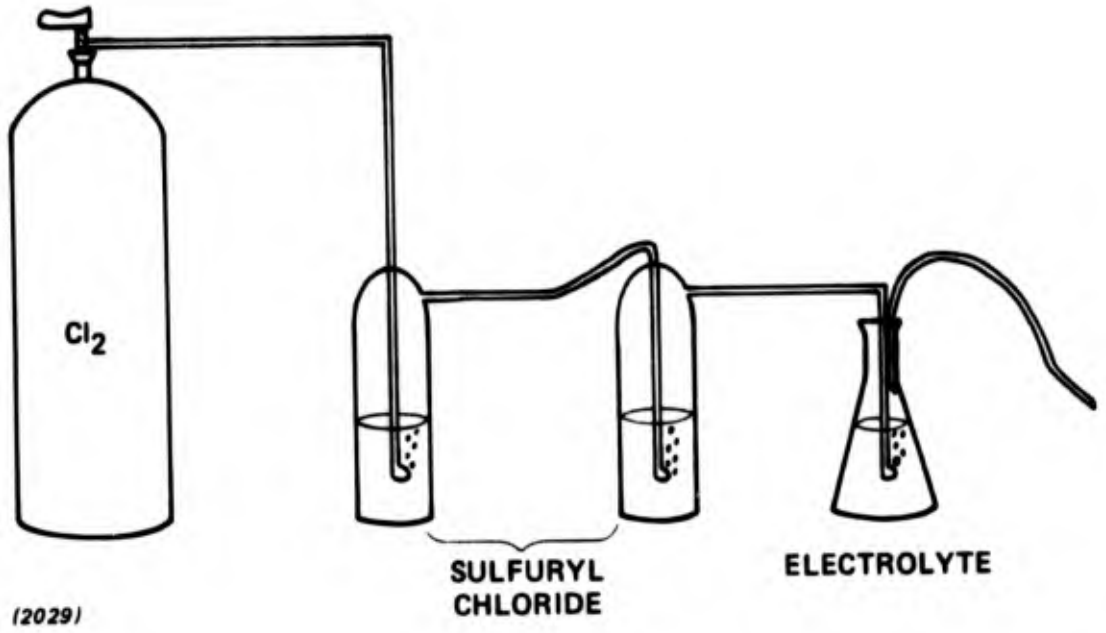

Figure 12 Cl_2 Gas Scrubbing Apparatus

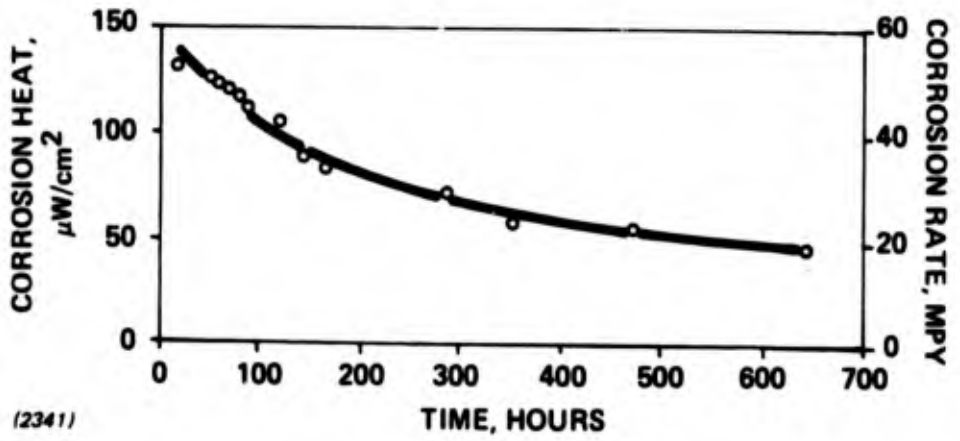

Figure 13 Long Term Corrosion Data for a Li/SO_2Cl_2 Cell with Added Br_2

- 1.25" Ø Cell, 1" Ø Electrode
- Positive Grounded SS Case
- 25°C

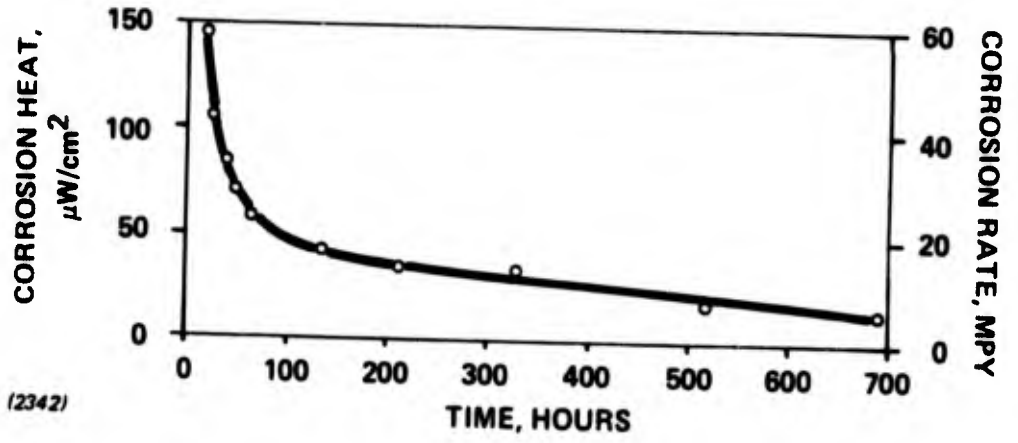

Figure 14 Long Term Corrosion Data for a Li/SO_2Cl_2 Cell without Additives

- 1.25" Ø Cell, 1" Ø Electrodes
- Positive Grounded SS Case
- 25°C

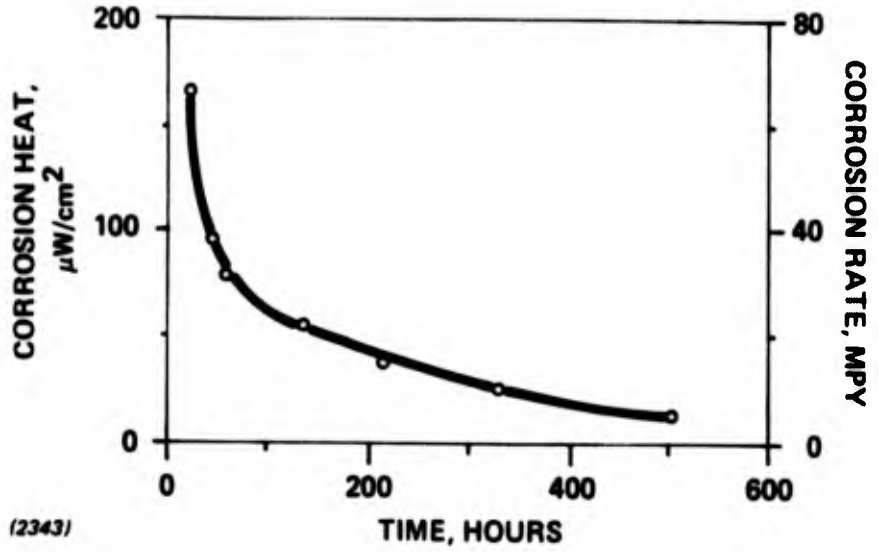

Figure 15 Long Term Corrosion Data for a Li/SO_2Cl_2 Cell with Added Chlorine

- 1.25" Ø, 1" Ø Electrodes
- Positive Grounded
- T = 25°C

Complex plane impedance spectra are given in Figures 16-19 for the cell with the bromine additive at 20, 68, 144 and 168 hours after activation. As summarized in Figure 20, film resistance increases with time, as does calculated film thickness.

Complex plane impedance data for the cell without additives are given in Figure 21-25 for periods of storage between 2 and 138 hours. A summary of the variation in film resistance and calculated thickness is given in Figure 26. Comparing the data in Figure 26 with those in Figure 20 the two striking differences are

- Film resistance is increasing at a much faster and apparently linear rate for the cell without additives.

- Film thickness is increasing at a much slower rate for the cell without additives.

The thickness results appear to mirror the greater rate of corrosion with the bromine additive which should result in an accumulation of corrosion (e.g., film) at the anode surface. The greater resistance and faster rate of film resistance increase in the absence of bromine probably indicates a purer (e.g., less doped) film. A more rapidly increasing film resistance should lead to a lower corrosion rate as

- It probably indicates a more adherent, denser film which will physically protect the lithium anode.

- It may lead to a lower corrosion rate if the electronic resistances also increases as in the absence of a local cell film growth and corrosion require electronic conductor through the film.

In Figures 27-30 complex plane impedance spectra are given for the cell with added gaseous chlorine. The variations in film resistance and thickness

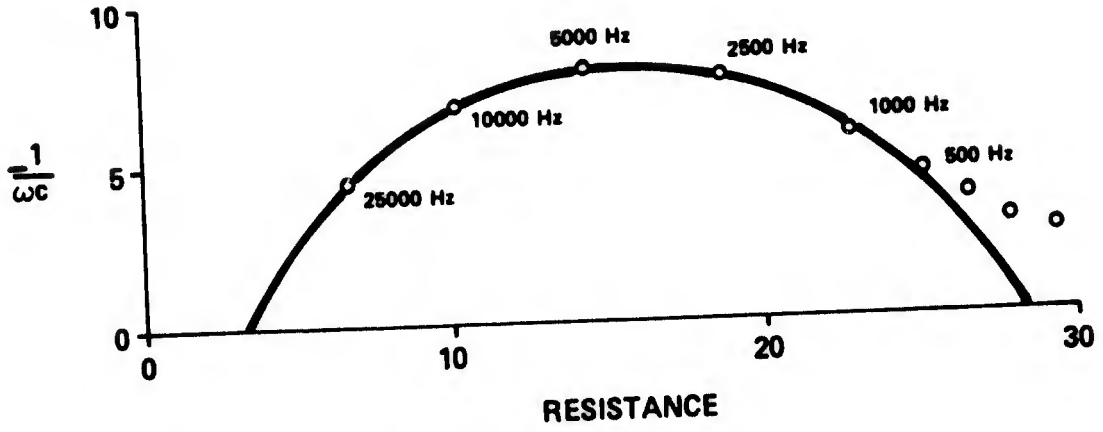

Figure 16 Complex Plane Impedence Spectra of $Li/SO_2Cl_2+Br_2$

20 hours after activation

R_{film} = 25 ohms (13×10^7 ohm–cm)
C_{film} = 5.1 μ F
Thickness = 19.1 Å

(2065)

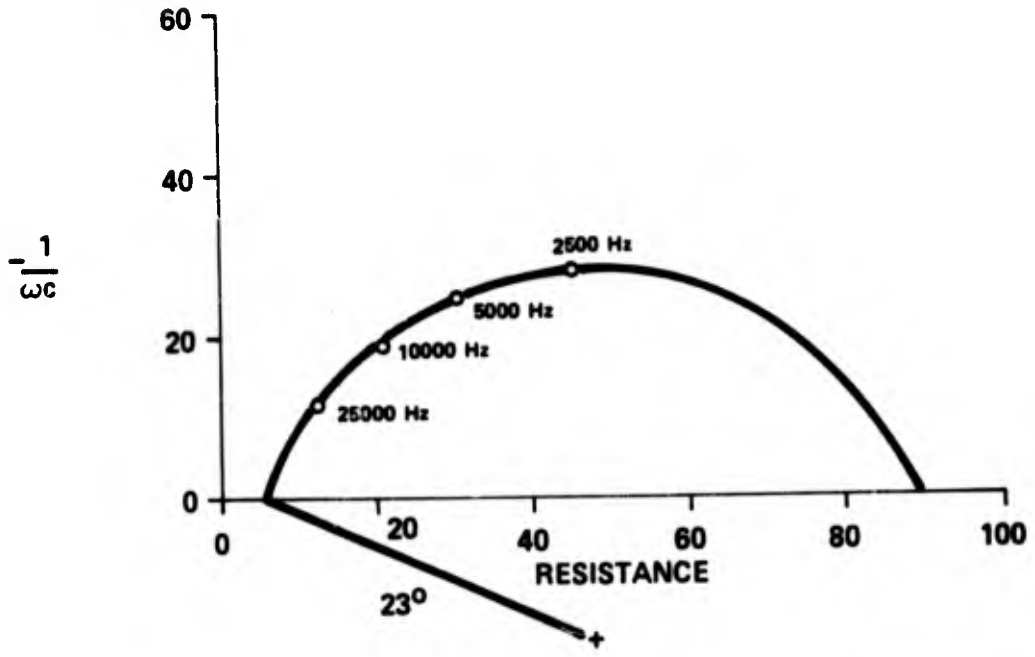

Figure 17 Complex Plane Impedence Spectrum of $Li/SO_2Cl_2+Br_2$
68 hrs. after fill
R_{film} = 86 ohms (25 x 10^8 ohm-cm)
C_{film} = 2.83 μ F
Thickness = 345 Å

(2069)

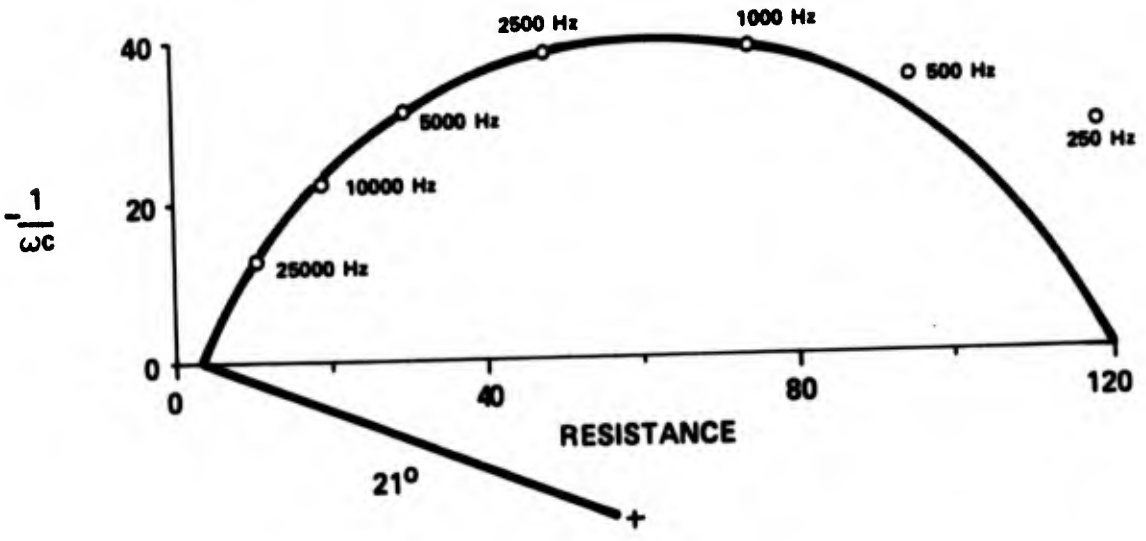

Figure 18 Complex Plane Impedence Spectrum of $Li/SO_2Cl_2+Br_2$

144 hrs. after fill
R_{film} = 117 ohms (28×10^7 ohm–cm)
C_{film} = 2.3 μ f
Thickness = 420Å

(2068)

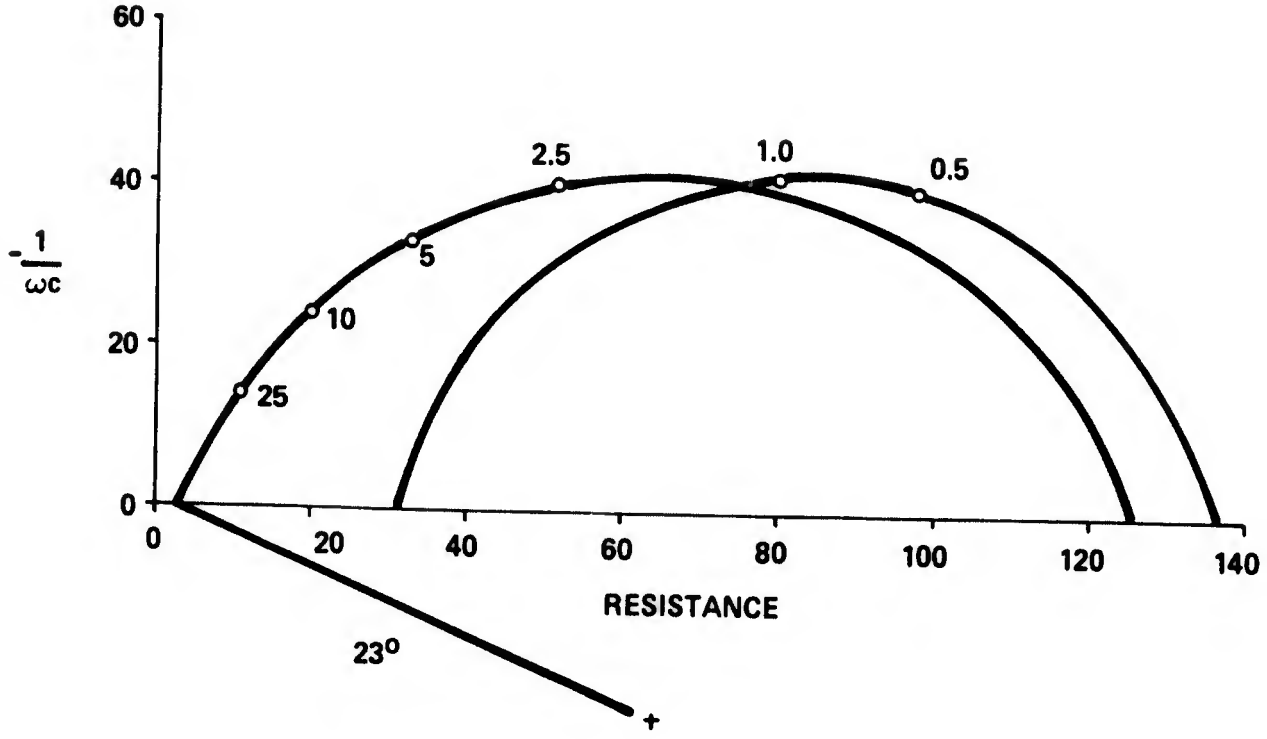

Figure 19 Complex Plane Impedence Spectrum of $Li/SO_2Cl_2+Br_2$ 163 hrs. after fill
R_{film} = 123 Ω (24x10^7 Ω–cm)
C_{film} = 2.0 μ F
Thickness = 510 Ω

(2067)

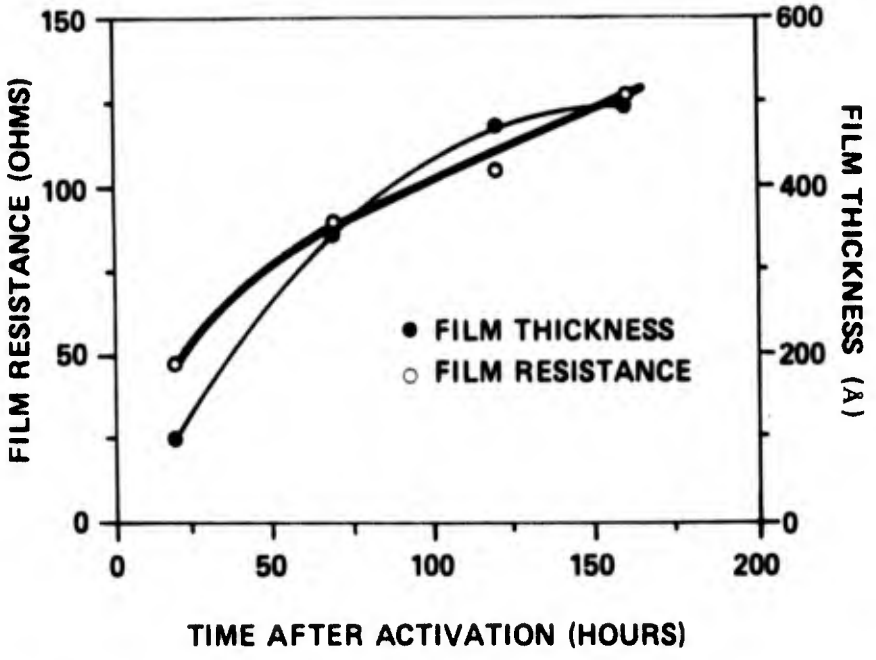

Figure 20 Change in Film Resistance and Thickness During Storage of Li/SO_2Cl_2+Br_2

(2058)

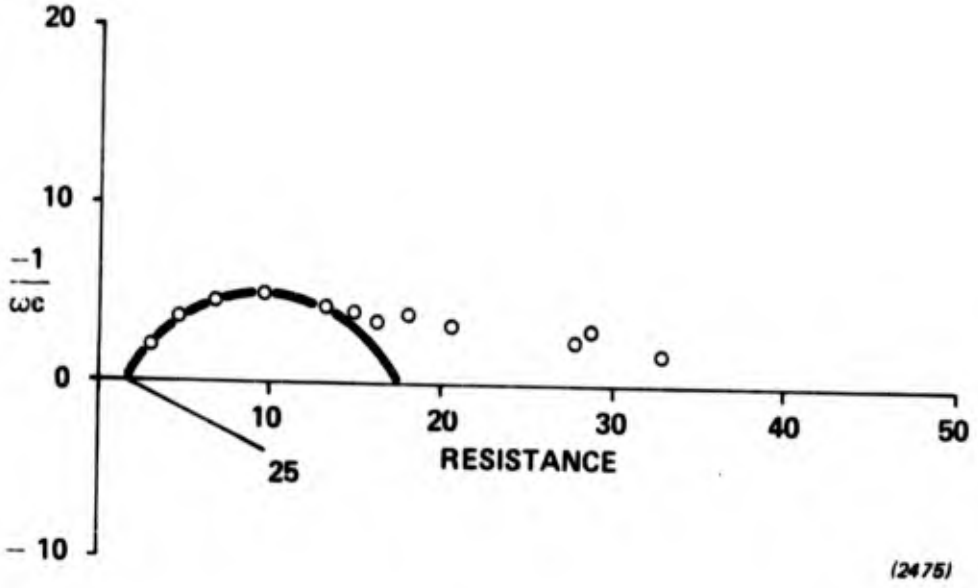

Figure 21 Complex Plane Impedance Spectrum of a Lithium—Sulfuryl Chloride Cell Built without Additives 2hr after Fill

R_{film} = 16 ohms

C_{film} = 12.0 μ F

Thickness = 85 Å

Film Specific Resistance in Ohm-cm = 19E + 007

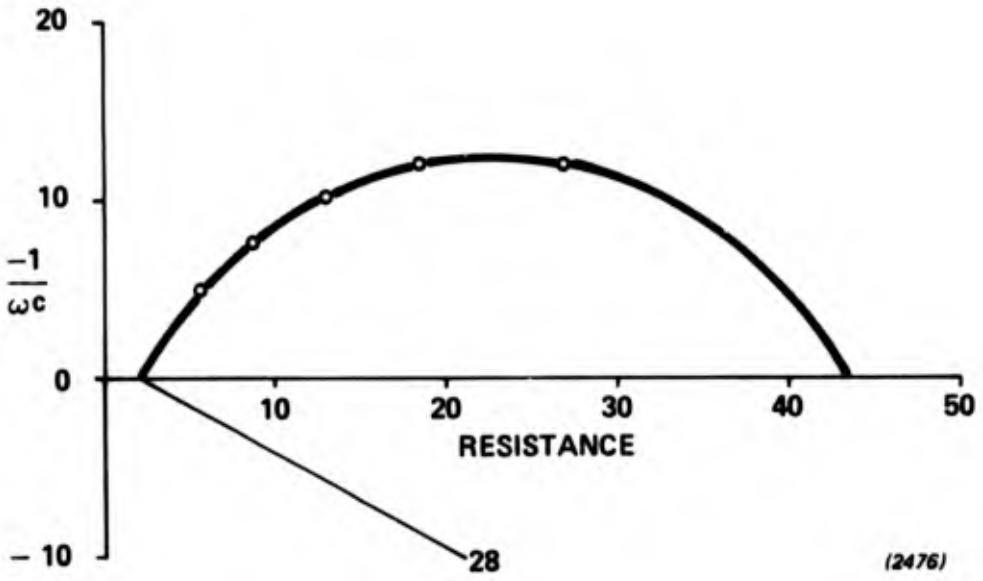

Figure 22 Complex Impedance Spectrum of a Lithium–Sulfuryl Chloride Cell Built without Additives 19hr after Fill

R_{film} = 41 ohms

C_{film} = 7.4 μ F

Thickness = 137 Å

Film Specific Resistance in Ohm-cm = 30E + 007

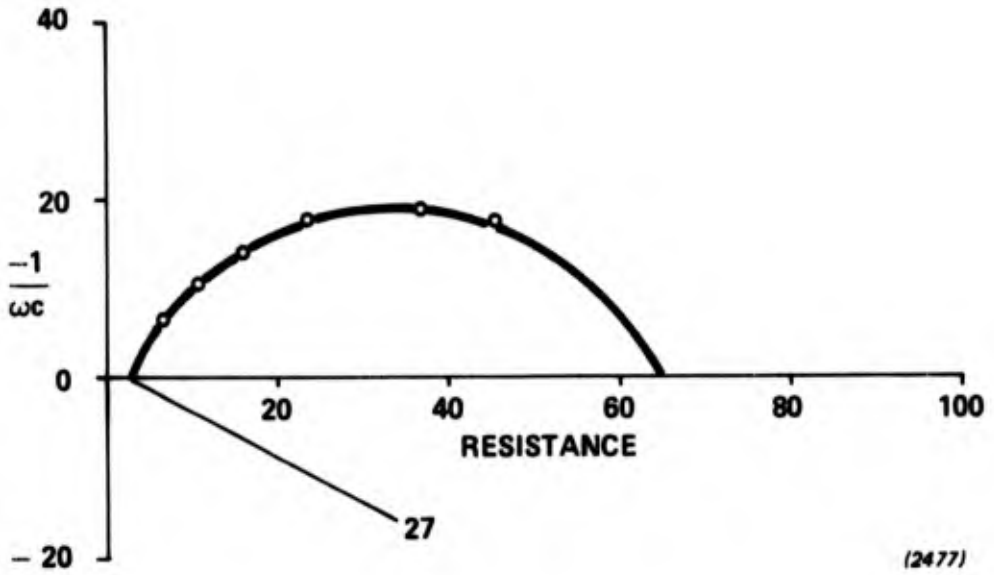

Figure 23 Complex Plane Impedance Spectrum of a Lithium–Sulfuryl Chloride Cell Built without Additives 44hr after Fill

R_{film} = 62 ohms

C_{film} = 6.1 μ F

Thickness = 167 Å

Film Specific Resistance in Ohm-cm = 37E + 007

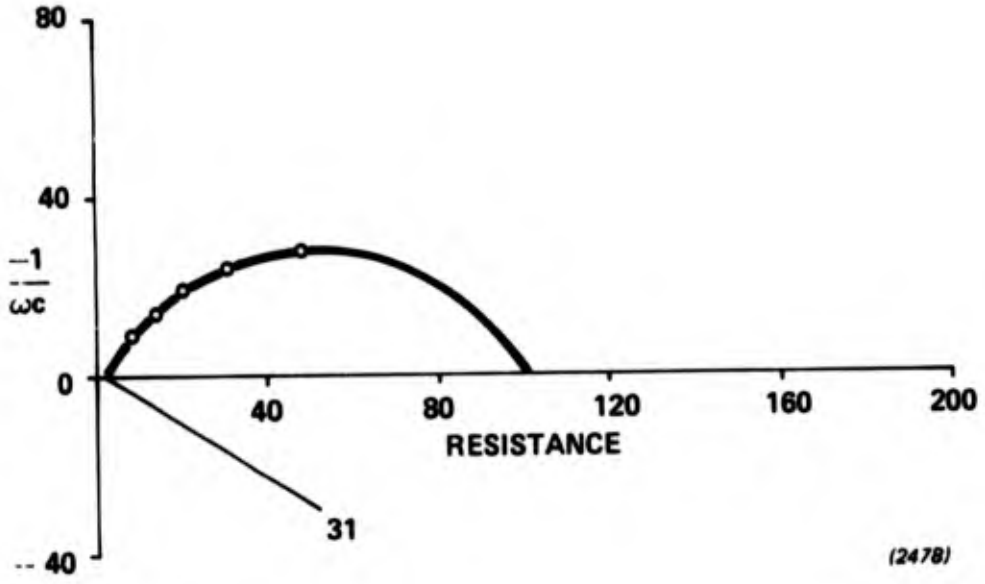

Figure 24 Complex Plane Impedance Spectrum of a Lithium–Sulfuryl Chloride Cell Built without Additives 69hr after Fill

R_{film} = 99 ohms

C_{film} = 4.8 μ F

Thickness = 214 Å

Film Specific Resistance in Ohm-cm = 46E + 007

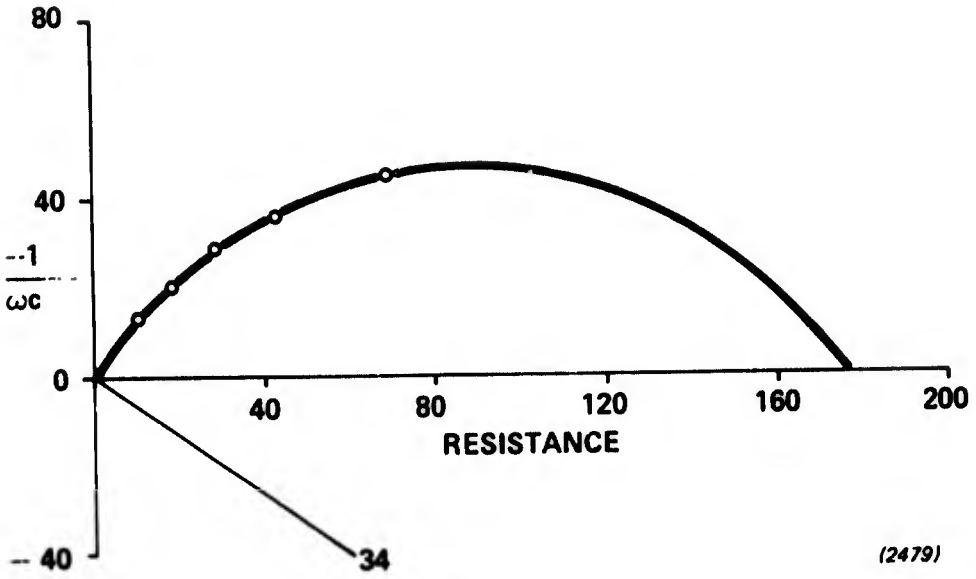

Figure 25 Complex Plane Impedance Spectrum of a Lithium-Sulfuryl Chloride Cell Built without Additives 138hr after Fill

R_{film} = 178 ohms

C_{film} = 3.4 μ F

Thickness = 299 Å

Film Specific Resistance in Ohm-cm = 59E + 007

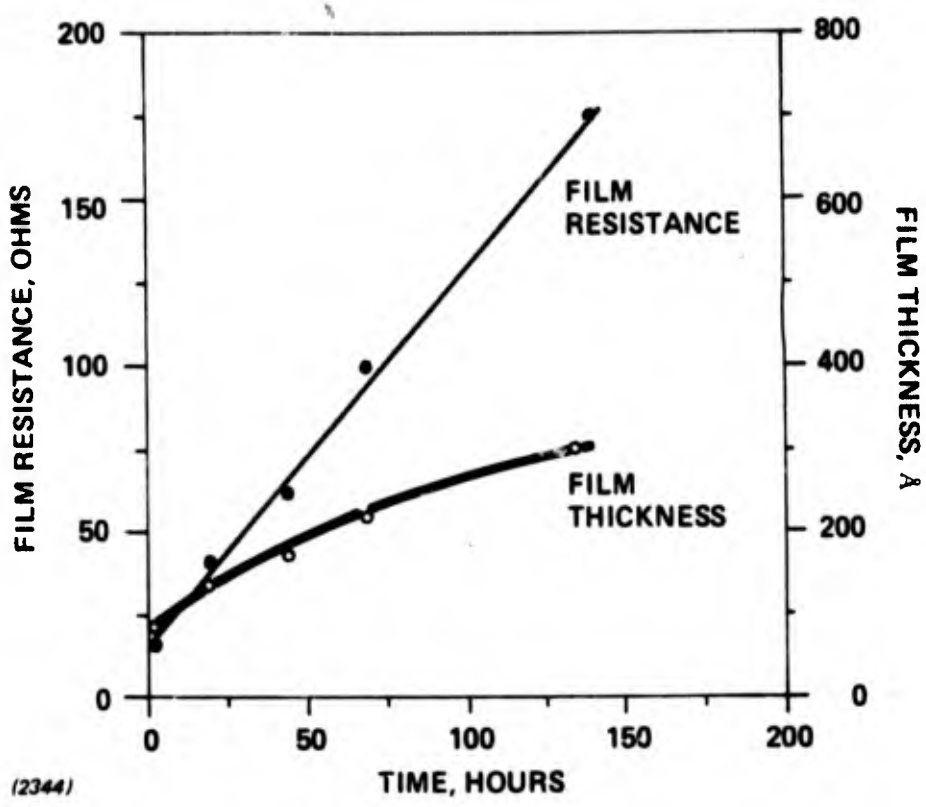

Figure 26 Changes in Anode Film Resistance and Thickness with Storage Time for a Li/SO_2Cl_2 Cell without Additives

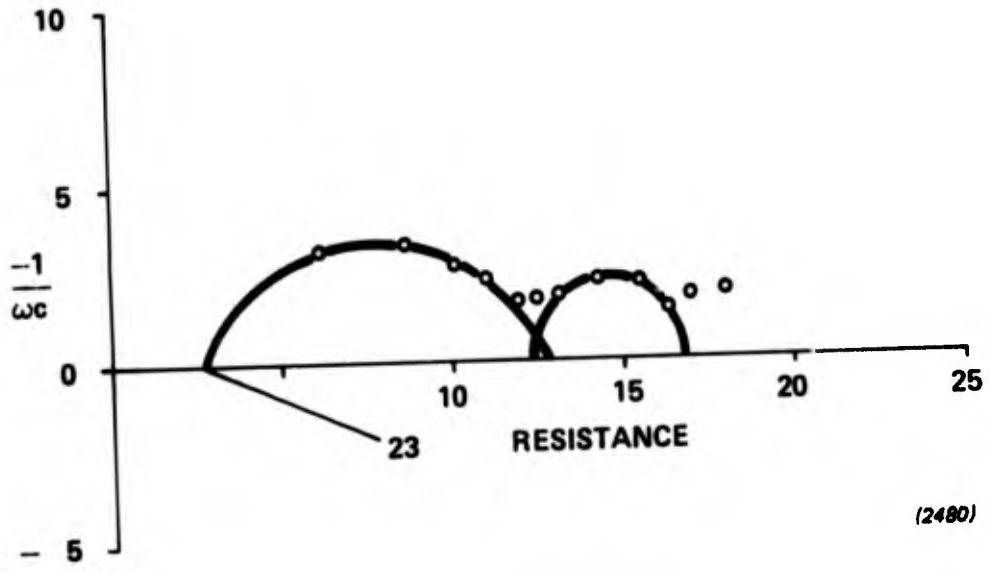

Figure 27 Complex Plane Impedance Spectrum of a Lithium–Sulfuryl Chloride Cell with Added Gaseous Chlorine 2 hr after Fill

R_{film} = 10 ohms

C_{film} = 3.0 μ F

Thickness = 334 Å

Film Specific Resistance in Ohm-cm = 30E + 006

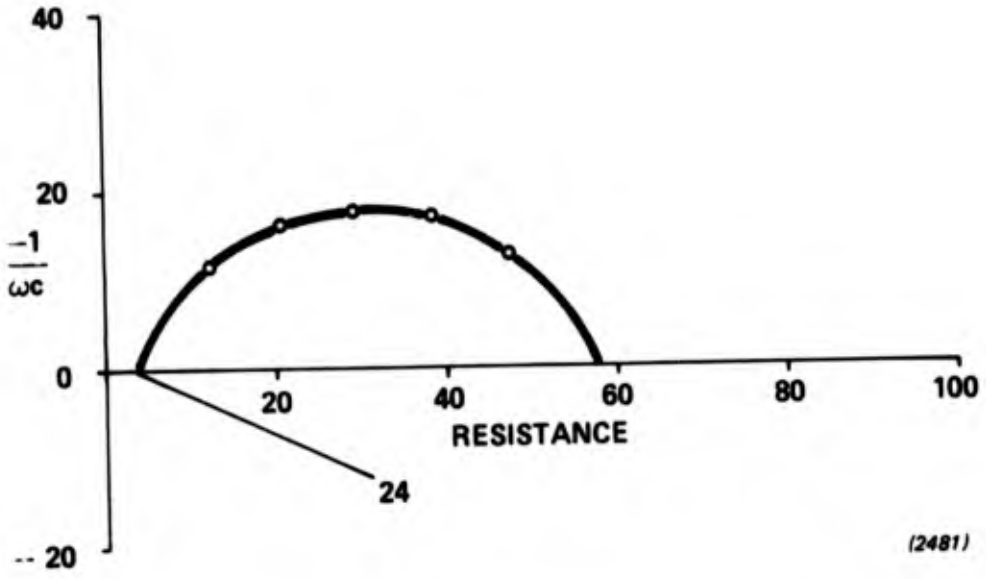

Figure 28 Complex Plane Impedance Spectrum of a Lithium--Sulfuryl Chloride Cell with Added Gaseous Chlorine 19hr after Fill

R_{film} = 55 ohms

C_{film} = 1.9 μ F

Thickness = 522 Å

Film Specific Resistance in Ohm-cm = 10E + 007

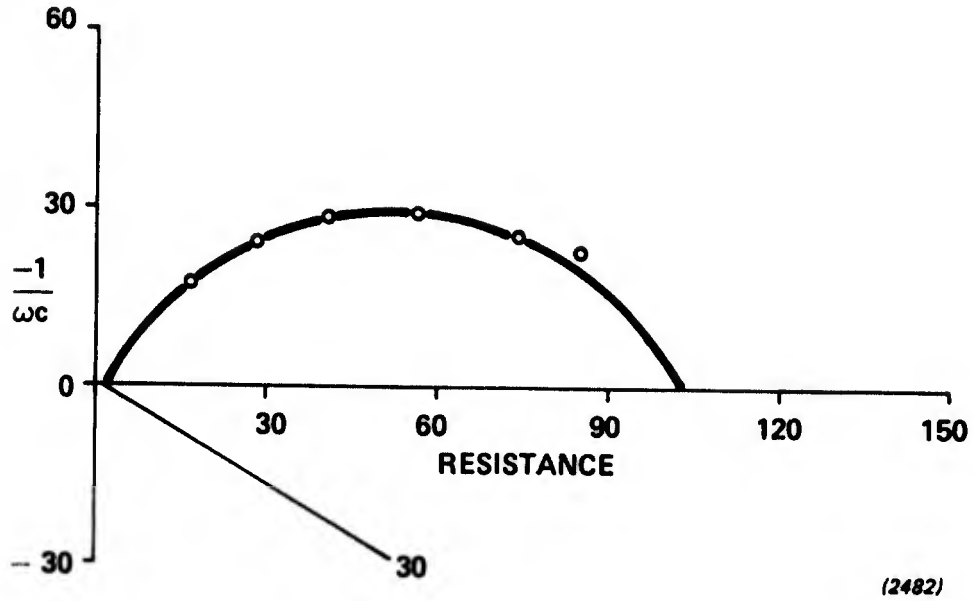

Figure 29 Complex Plane Impedance Spectrum of a Lithium-Sulfuryl Chloride Cell with Added Gaseous Chlorine 44hr after Fill

R_{film} = 102 ohms

C_{film} = 1.7 μ F

Thickness = 604 Å

Film Specific Resistance in Ohm-cm = 17E + 007

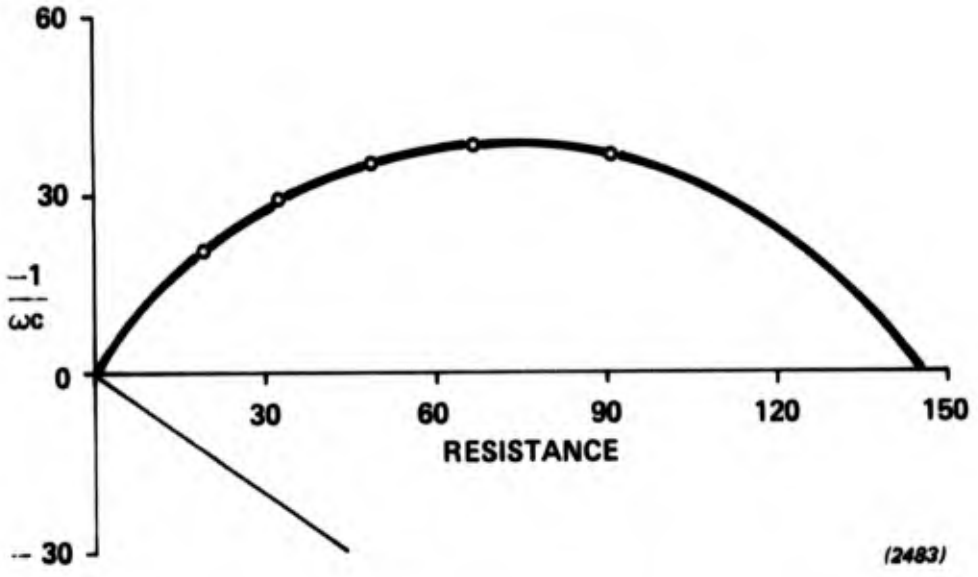

Figure 30 Complex Plane Impedance Spectrum of a Lithium–Sulfuryl Chloride Cell with Added Gaseous Chlorine 69hf after Fill

R_{film} = 146 ohms

C_{film} = 1.9 μ F

Thickness = 530 Å

Film Specific Resistance in Ohm-cm = 27E + 007

with time summarized in Figure 31. As was the case in the cell without additives an apparent linear increase in film resistance is evident. In fact the rate in increase is even more rapid with added chlorine which is possibly reflected in the lower long term corrosion rate.

The thickness of the film in the presence of added chlorine starts out a very high value (~ 340°A). This probably reflects the higher molecular chlorine activity which will result in film formation by the reaction

$$2Li + Cl_2 = 2LiCl \qquad [5]$$

rather than the reaction

$$2Li + SO_2Cl_2 = 2LiCl_2 + SO_2 \qquad [2]$$

One might expect that reaction [5] would occur more rapidly than reaction [2]. In addition as volatile products are not formed in reaction [5] a more adherent film may be formed by this reaction which would be reflected in greater thickness values.

The apparent decrease in film thickness shown in Figure 31 may be an anomally. However, it might also indicate a sloughing off of an outer film layer.

After this initial set of experiments and prior to further parametric tests experiments were carried out to

- Reexamine the design parameters summarized in Table 3 with respect to anode stability.

- Investigate semiempirical approaches to stabilization of the lithium anode.

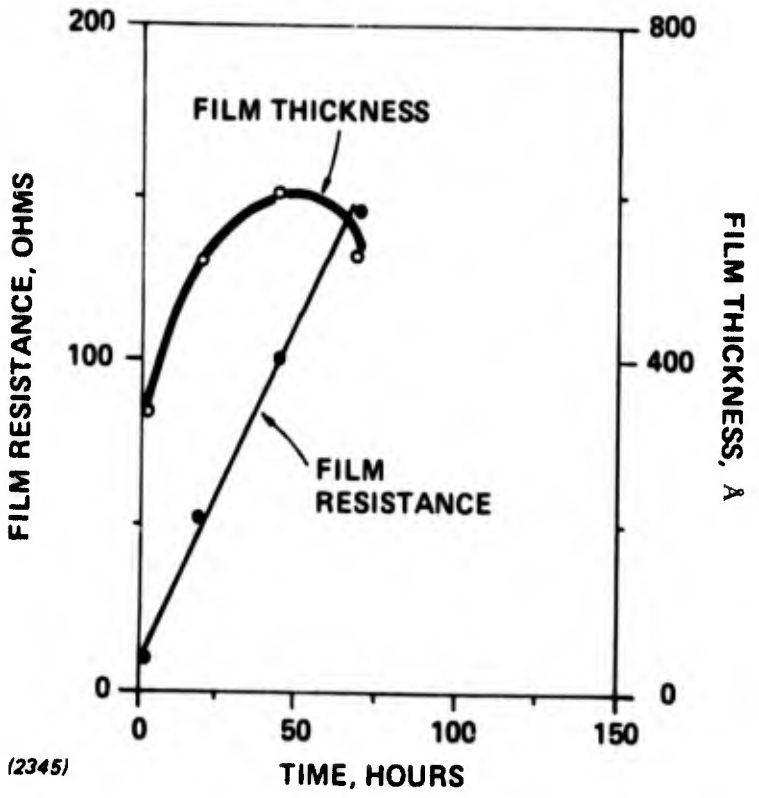

Figure 31 Variation in Film Resistance and Thickness for a Li/SO_2Cl_2 Cell with Added Gaseous Chlorine

Two elements of the Table 3 design are suspect with respect to anode stability. The selection of positive grounding was based on results obtained with an unstable solder connection between the feedthrough and cell case. The use of a porous PTFE insulator between the double faced anode and cell case may not be optimum as lithium and fluorocarbons react.

The choice of grounding was reexamined calorimetrically in a cell of the new design. Heat generation rate data through 250 hours of testing are given in Figure 32. The corrosion rate through 100 hours of testing is at least double that of a positive grounded cell without additives. The longer term data, however, suggest that a negative grounded cell built with stable materials will have a corrosion rate equivalent to a positive grounded cell.

The result in Figure 32 suggests that the stainless steel case is acting as a surface for the reduction of sulfuryl chloride. This is still a source of parasitic capacity loss, however, if prepassivation of the case is feasible, reduction of sulfuryl chloride on the case wall may be minimized. In any event it appears that only the initial corrosion rate is accelerated.

In Figure 33 long term corrosion data are given for a positive grounded Li/SO_2Cl_2 cell where the PTFE insulator is replaced with a glass mat insulator. Comparing the date in Figure 33 with that in Figure 14 for a cell of identical chemistry but built with the PTFE insulator it is seen that the elimination of the fluorocarbon-lithium contact reduces the apparent corrosion rate. The improvement seems to diminish as the cells age, but heat generation is still lower after 500 hours of storage for the cell built with the glass mat insulator.

The two semiempirical approaches explored for stabilizing the lithium anode in sulfuryl chloride cells are

- Coating the anode with methylcyanoacrylate. Such coatings are reported to reduce voltage delay in $Li/SOCl_2$ cells. Although their mechanism of

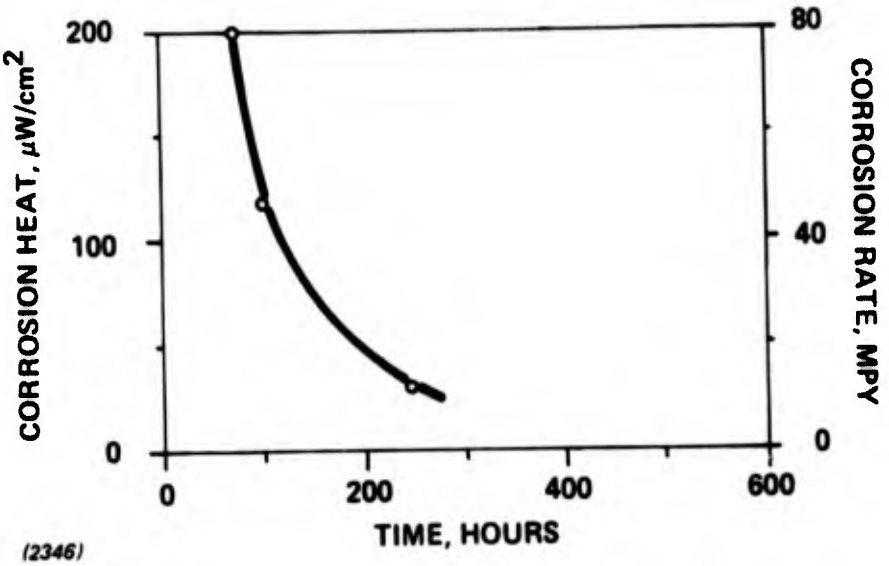

Figure 32 Long Term Corrosion Data for a Li/SO_2Cl_2 Cell without Additives

- 1.25" Ø Cell, 1" Ø Electrodes
- Negative Grounded SS Case
- 25°C

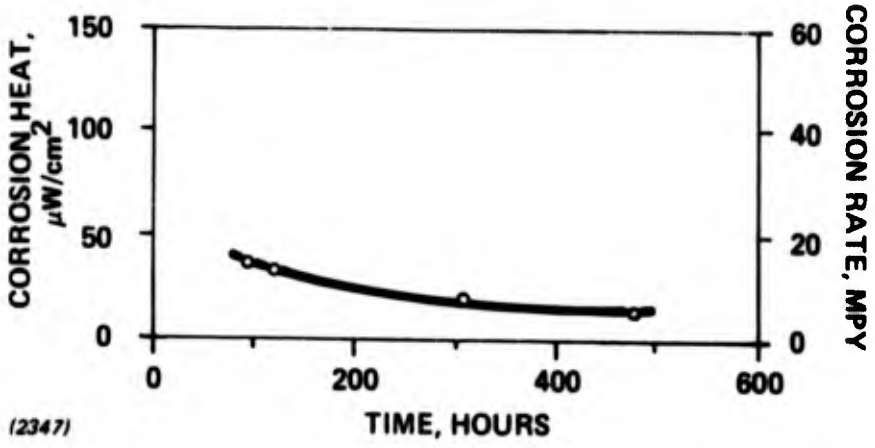

Figure 33 Long Term Corrosion Data for a Li/SO_2Cl_2 Cell without the PTFE Insulator

operation is unclear the possibility exists that they will enhance anode stability in Li/SO_2Cl_2 cells.

- Soaking the lithium anode for approximately 48 hours in a solution of 1.5M $LiAlCl_4/SOCl_2$. The rationale for this procedure is that the LiCl film formed in thionyl chloride may be more protective than that formed in sulfuryl chloride.

The methylcyanoacrylate coating was applied by repetitive dipping of the anode into a solution of methlcyanoacrylate in ethyl acetate. Heat generation rate data for a cell built with the coated anode is given in Figure 34. If we attribute the heat solely to lithium corrosion it appears that the coating sharply reduces the initial corrosion rate but does not effect the long term corrosion rate (see Figure 14).

In fact at least initially much of the measured heat must be due to the reaction of sulfuryl chloride with the coating. The mechanisms by which the coating operates in thionyl chloride is not fully understood. It is reported, however, that the coating is consumed by results in a more protective LiCl coating (7). We cannot separate the methylcyanoacrylate-sulfuryl chloride reaction from the corrosion heat. After 400 hr. the measured heat is equivalent to that found in a cell without methylcyanoacrylate (see Figure 14). If some of this heat is still due to the methylcyanoacrylate chemical reaction the rate of corrosion may be lower.

Complex plane impedance spectra for the cell built with the methylcyanoacrylate coating are given in Figures 35-40. Initially a spectrum could not be resolved. This presumably is due to the methylcyanoacrylate coating blocking the anode surface. After 90 hours of storage spectra became

7. N.A. Fleisher, "30th Power Sources Symposium," Atlantic City, N.J. (to be published).

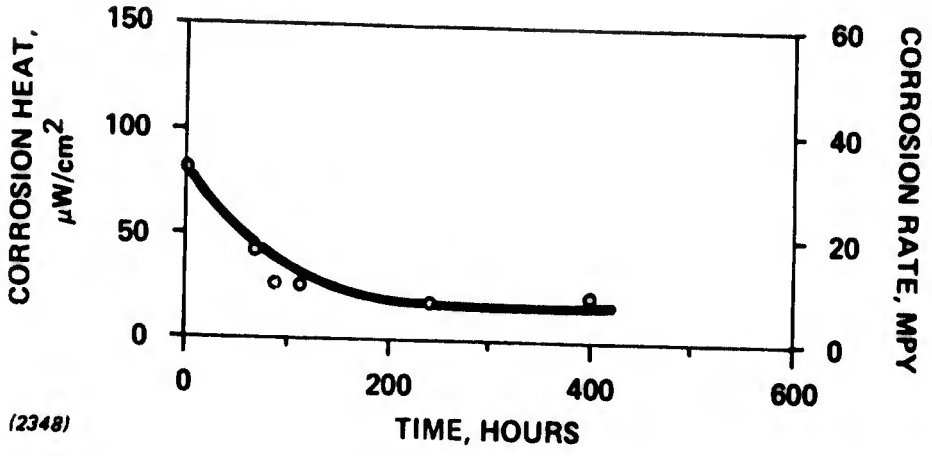

Figure 34 Long Term Corrosion Data for a Li/SO_2Cl_2 Cell with a Methylcyanoacrylate Coating on the Lithium Anode

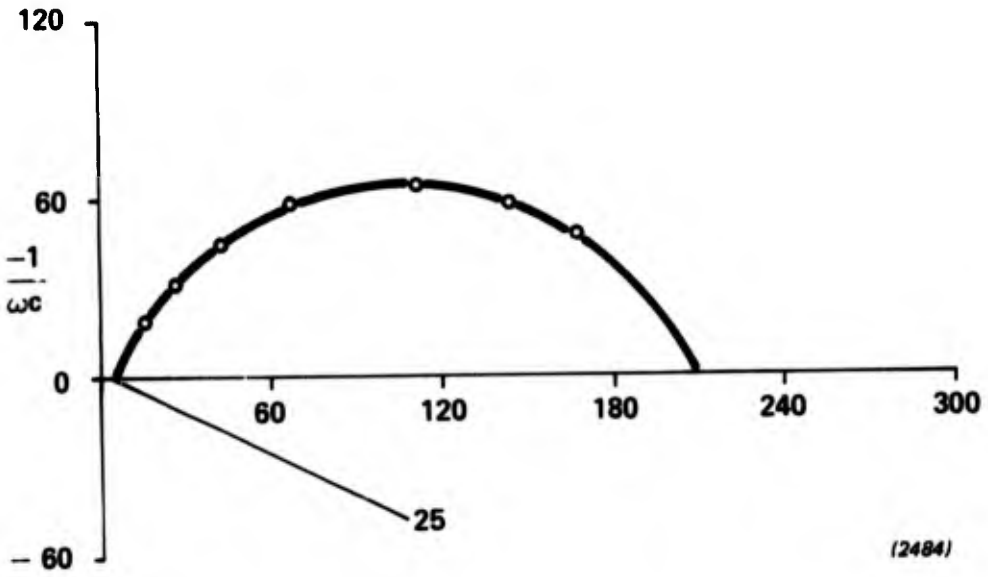

Figure 35 Complex Plane Impedance Spectrum of a Lithium--Sulfuryl Chloride Cell Built with a Methylcyanoacrylate Anode Coating 90hr after Fill

R_{film} = 204 ohms

C_{film} = 2.1 μ F

Thickness = 477 Å

Film Specific Resistance in Ohm-cm = 43E + 007

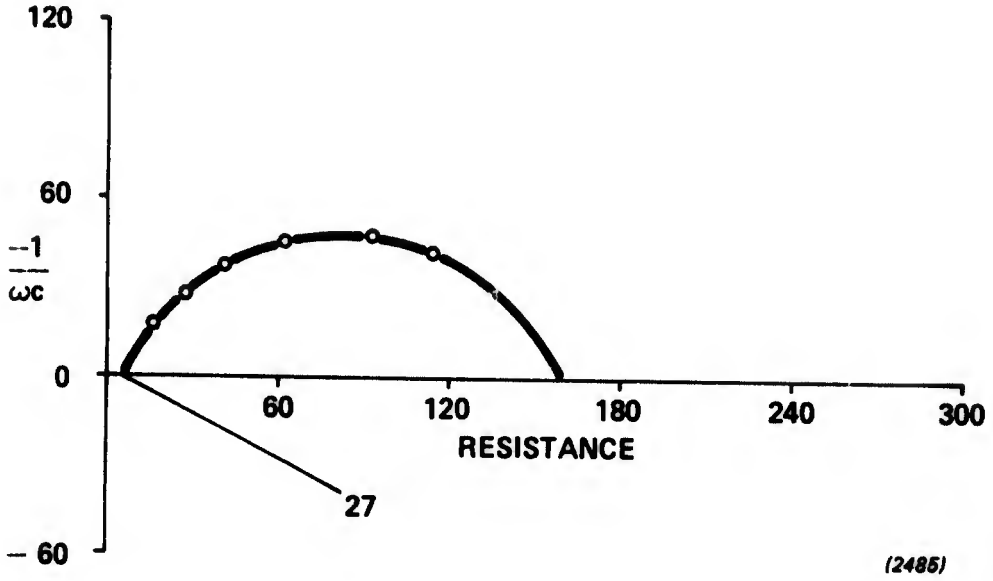

Figure 36 Complex Plane Impedance Spectrum of a Lithium–Sulfuryl Chloride Cell Built with a Methylcyanoacrylate Anode Coating 115hr after Fill

R_{film} = 155 ohms

C_{film} = 2.2 μ F

Thickness = 458 Å

Film Specific Resistance in Ohm-cm = 34E + 007

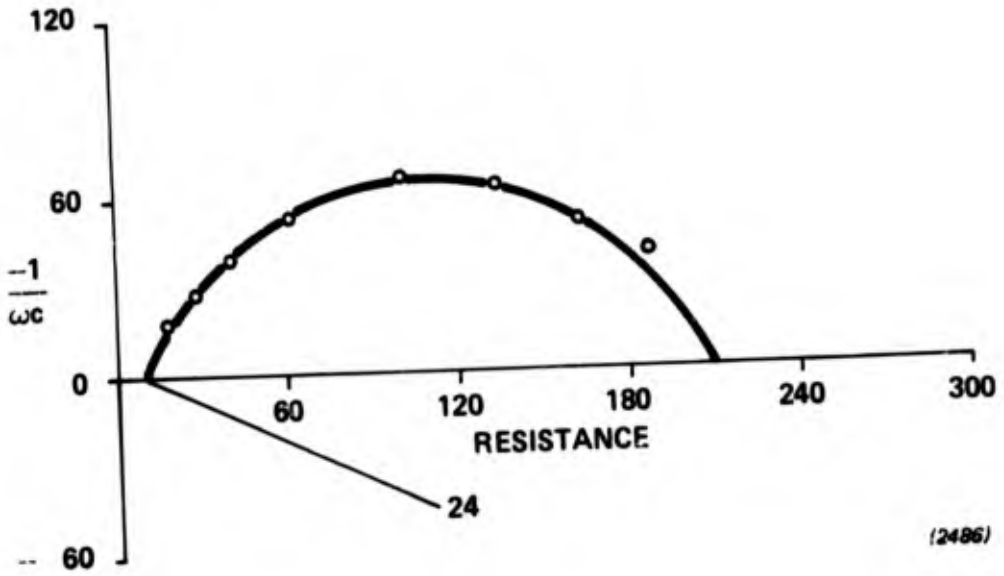

Figure 37 Complex Plane Impedance Spectrum of a Lithium–Sulfuryl Chloride Cell Built with a Methylcyanoacrylate Anode Coating 173hr after Fill

R_{film} = 200 ohms

C_{film} = 2.8 μ F

Thickness = 358 Å

Film Specific Resistance in Ohm-cm = 56E + 007

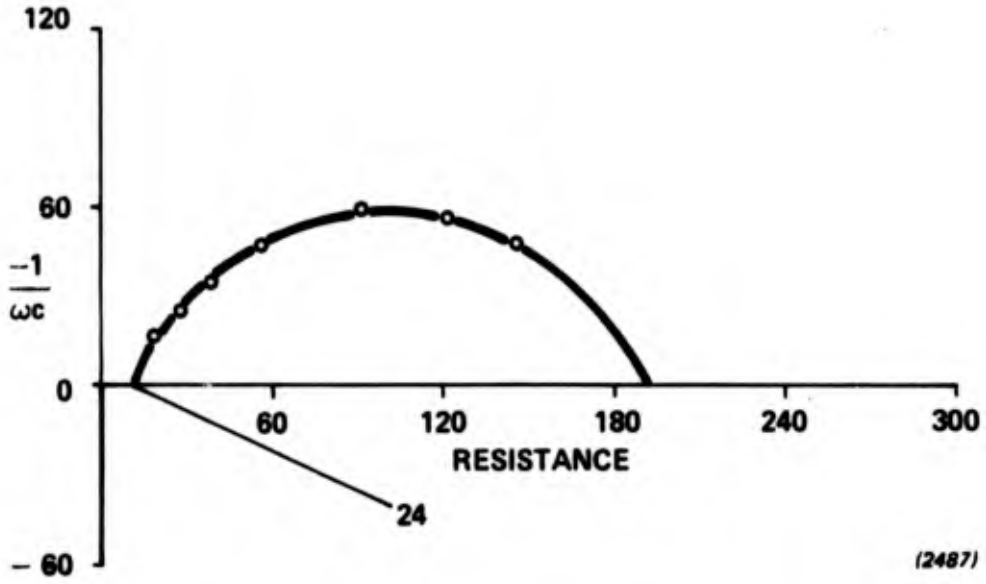

Figure 38 Complex Plane Impedance Spectrum of a Lithium–Sulfuryl Chloride Cell Built with a Methylcyanoacrylate Anode Coating 242hr after Fill

R_{film} = 181 ohms

C_{film} = 3.2 μ F

Thickness = 315 Å

Film Specific Resistance in Ohm-cm = 57E + 007

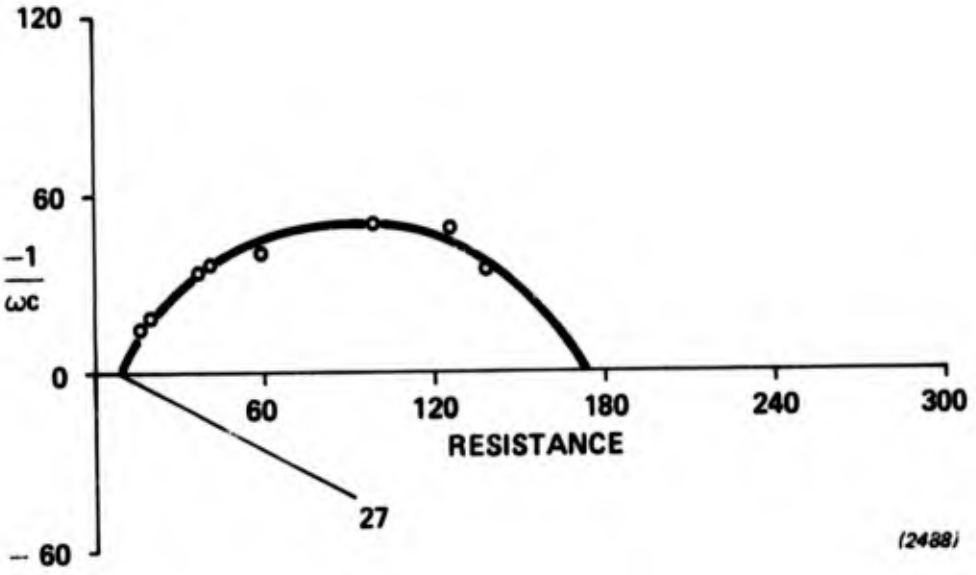

Figure 39 Complex Plane Impedance Spectrum of a Lithium–Sulfuryl Chloride Cell Built with a Methylcyanoacrylate Anode Coating 288hr after Fill

R_{film} = 165 ohms

C_{film} = 5.3 μ F

Thickness = 191 Å

Film Specific Resistance in Ohm-cm = 86E + 007

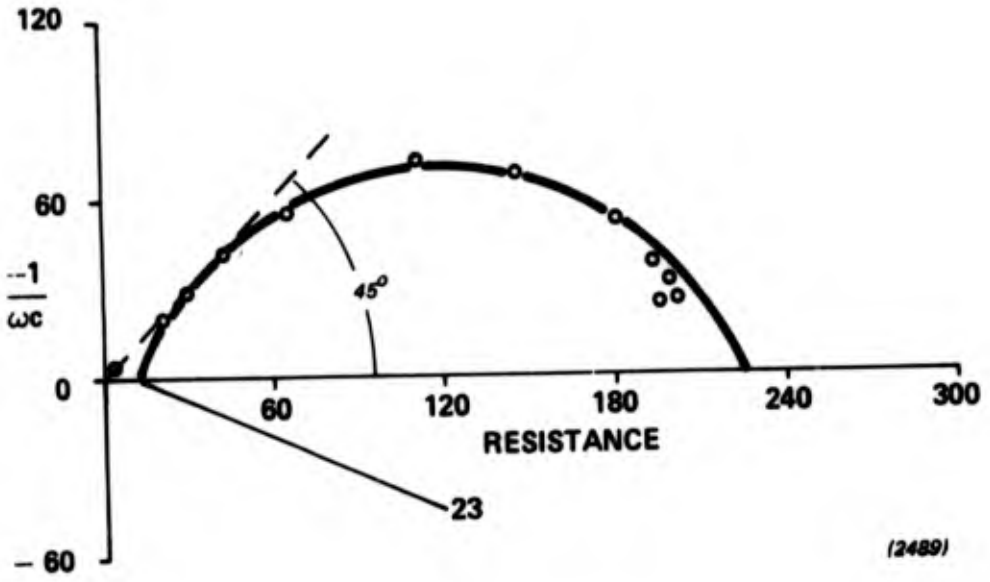

Figure 40 Complex Plane Impedance Spectrum of a Lithium--Sulfuryl Chloride Cell Built with Methylcyanoacrylate Anode Coating 462hr after Fill

R_{film} = 213 ohms

C_{film} = 5.1 μ F

Thickness = 201 Å

Film Specific Resistas ce in Ohm-cm = 11E + 008

resolveable presumably indicating at least partial consumption or modification of the methylcyanoacrylate coating.

Between 90 and 462 hours no consistant trend is seen in film resistance which remains ~ 200 ohms. Apparent film thickness actually appears to decrease with storage time as shown in Figure 41. Considering the probable complex nature of the film and the assumptions of the thickness calculation the trend in Figure 41 is viewed as purely qualitative. It is nonetheless noteworthy that film growth is a probable cause of voltage delay. A thinning of the film with storage time would be expected to lead to reduced voltage delay.

A final trend evident in the complex plane impedance spectra after about 200 hours of storage is the departure of the high frequency (i.e., low resistance) points from the semicircle. Normally these are the most precisely determined points. Their departure from the semicircle is then not an error but evidence for a new circuit element in the equivalent circuit. This is clearly evident in Figure 40 where after 462 hours of storage a line passing through the intersection of the axes at 45° can be drawn through the first four high frequency points (i.e., 25, 10, 5 and 2.5 kHz).

In ac measurements points forming a 45° line to the real axis are ascribed to a Warburg impedance which results from diffusion of a dilute reactant to an electrode surface (8). A high frequency Warburg impedance is predicted by the Nerst approximation where the thickness of the diffusion layer is finite.

The high frequency points in Figure 40 are in agreement with the Nerst approximation. As the only difference between this and previous cells is the methylcyanoacrylate coating it is a safe assumption that the diffusion layer

---

8. C. Gabrielli, "Identification of Electrochemical Processes by Frequency Response Analysis," Solartron Instruments Group.

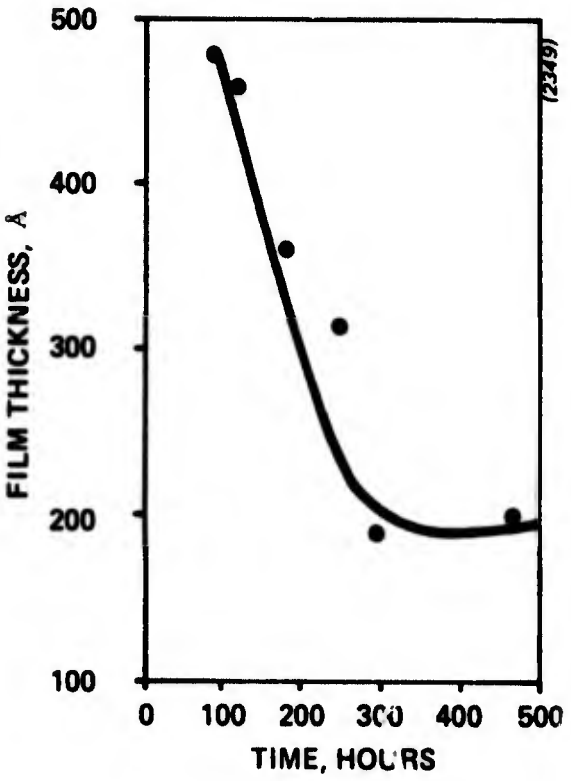

Figure 41 Change in Apparent Film Thickness with Storage Time for a Li/SO_2Cl_2 Cell Built with a Methylcyanoacrylate Anode Coating

is a result of the coating. The diffusion zone probably arises from the diffusion of lithium ions through a gradient of concentration between the anode surface and the bulk electrolyte.

Two months after the completion of the study all the cells used for studies of anode processes were tested for voltage delay. The tests were carried out by applying a constant $10mA/cm^2$ current. Only the cell built with the methylcyanoacrylate coating operated above zero volts; after a two minute startup transient of low voltage the cell discharged above 3V.

The question arises as to the possible errors which result from inclusion of high frequency Warburg points in calculating a semicircle for a pure RC network. In Figure 42 the spectrum at 462 hours has been recalculated without the first four points. The fit to semicircle is obviously better in Figure 42 as compared to Figure 40. However, the calculated data are not significantly different.

Heat generation rate data for a cell with a 1.5M $LiAlCl_4/SOCl_2$ anode pretreatment is given in Figure 43. The corrosion rate, while approximately 20% less than that of a cell without the pretreatment (see Figure 14), is still unacceptably high after 300 hours of testing.

We attribute the continued high corrosion rate after thionyl chloride pretreatment to indicate either incomplete passivation or that the thionyl chloride-formed passive film is unstable in sulfuryl chloride. That film modification continues after contacting the anode with sulfuryl chloride is demonstrated by the complex plane impedance spectra in Figures 44 and 45 taken 30 minutes and 4 hours after fill. These spectra clearly demonstrate continued film modification on contacting the anode with sulfuryl chloride. The mechanism of this modification appears to be fairly complex, since

- Unlike other tests no spectral resolution was possible after 20 hours of storage.

- The corrosion rate continues to be lower than that found in a cell without the pretreatment.

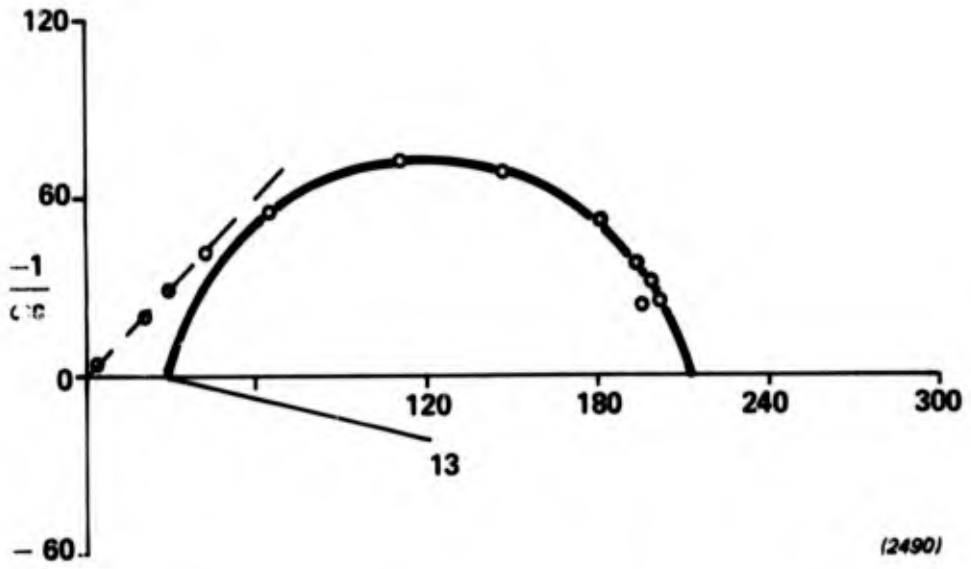

Figure 42 Complex Plane Impedance Spectrum of a Lithium–Sulfuryl Chloride Cell Built with a Methylcyanoacrylate Anode Coating 462hr after Fill with the High Frequency Data Points no included in the Semicircle Calculation

R_{film} = 183 ohms

C_{film} = 5.0 μ F

Thickness = 203 Å

Film Specific Resistance in Ohm-cm = 90E + 007

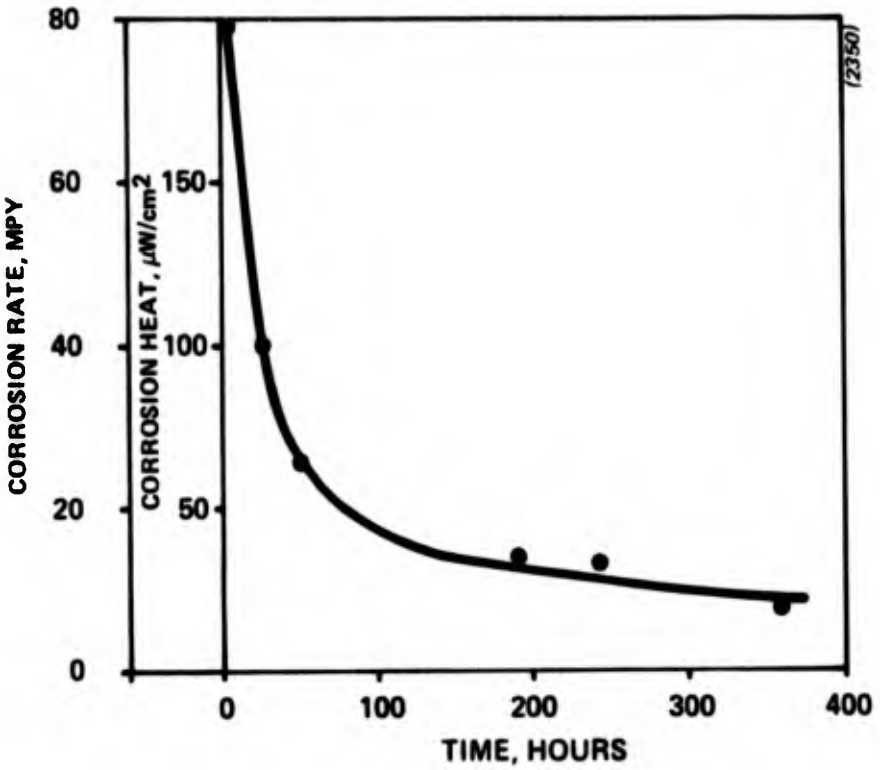

Figure 43 Long Term Corrosion Data for a Li/SO_2Cl_2 Cell with an Anode Pretreated in Thionyl Chloride

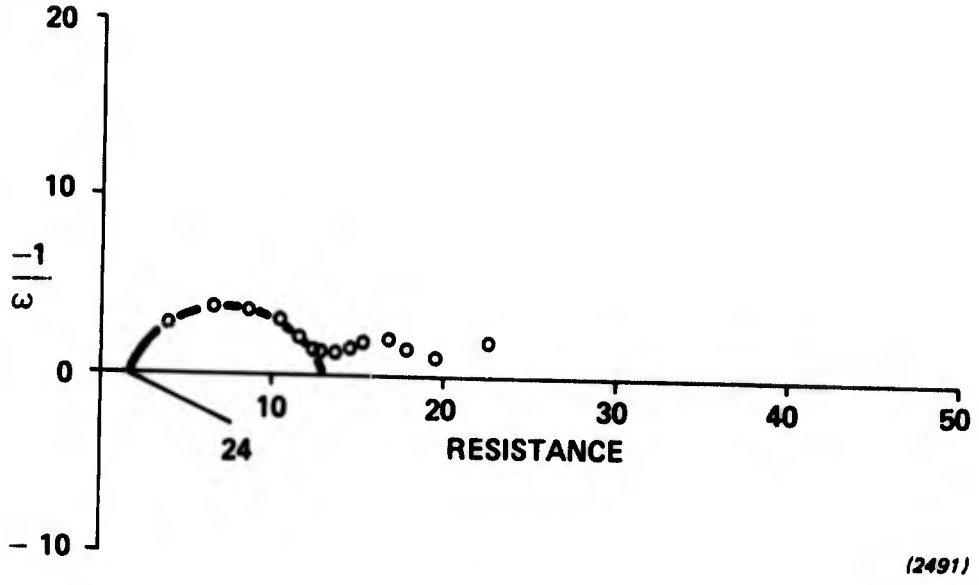

Figure 44 Complex Plane Impedance Spectrum of a Lithium–Sulfuryl Chloride Cell Built with a Thionyl Chloride Treated Anode 30min after Fill

R_{film} = 12 ohms

C_{film} = 5.1 μ F

Thickness = 198 Å

Film Specific Resistance in Ohm-cm = 59E + 006

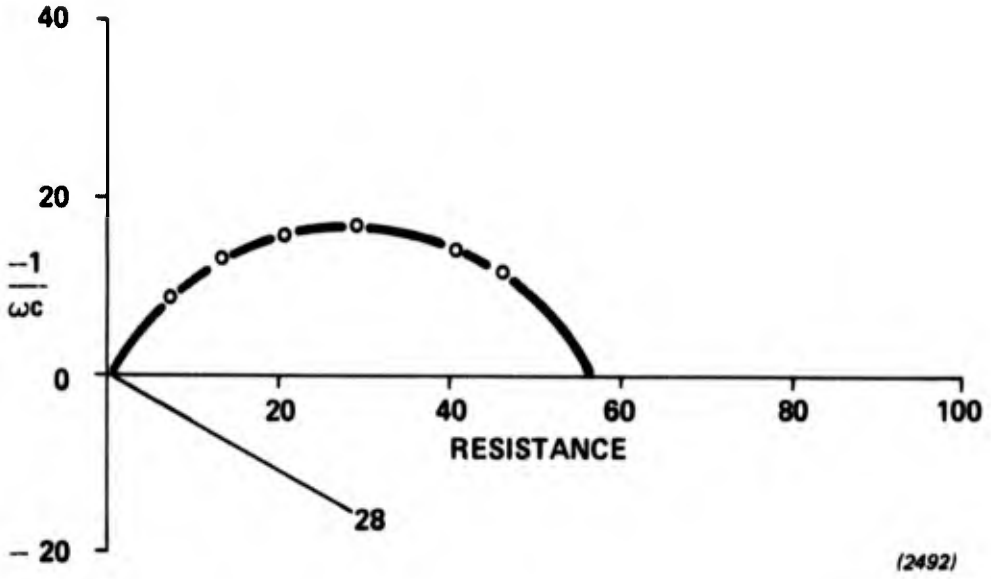

Figure 45 Complex Plane Impedance Spectrum of a Lithium–Sulfuryl Chloride Cell Built with a Thionyl Chloride Treated Anode 4hr after Fill

R_{film} = 56 ohms

C_{film} = 3.6 μ F

Thickness = 285 Å

Film Specific Resistance in Ohm-cm = 20E + 007

In the final phase of the studies of anode storability the effects of performance additives were examined with respect to the means by which they are introduced into the cell. The cell design for these tests was modified by replacing the PTFE insulator with glass mat to eliminate possible extraneous sources of heat. The three electrolyte compositions examined were

- 1.5M $LiAlCl_4$, 0.25M Br_2/SO_2Cl_2. In this test molecular liquid bromine was added to the electrolyte. This had the effect of eliminating SO_2 from the initial electrolyte composition which may in an unforeseen fashion effect anode stability.

- 1.5M $LiAlCl_4$, 0.3M Cl_2/SO_2Cl_2. For this electrolyte composition liquified chlorine was added to chilled 1.5M $LiAlCl_4/SO_2Cl_2$.

- 1.5M $LiAlCl_4$, 0.3M Cl_2, 0.25M Br_2/SO_2Cl_2. The objective of this test was to examine possible synergistic effects between the two additives with respect to anode stability.

Heat generation data for the 1.5M $LiAlCl_4$, 0.25M Br_2/SO_2Cl_2 cell are given in Figure 46. The complex-plane impedance spectra are shown in Figures 47-51. The corrosion rate through the first 200 hours of the test is approximately 30% lower than that observed when the bromine additive is formed in situ (see Figure 13). However, after 300 hours of storage no significant difference is evident between the two electrolytes. It appears that the in-cell rate of lithium corrosion in the bromine electrolyte is not greatly effected by the mode of electrolyte preparation.

Heat generation data for the chlorine-containing cell are presented in Figure 52. The steady corrosion rate, 5 mils per year, is well below the 30 mils per year rate for the bromine-containing cell.

Complex plane impedance spectra for the cell between 74 and 517 hours of storage are given in Figures 53-58. With the exception of the 517 hours spectrum film resistance is essentially constant at ~ 100 ohms. Apparent film thickness is effectively unvariant in all the spectra with a value on the

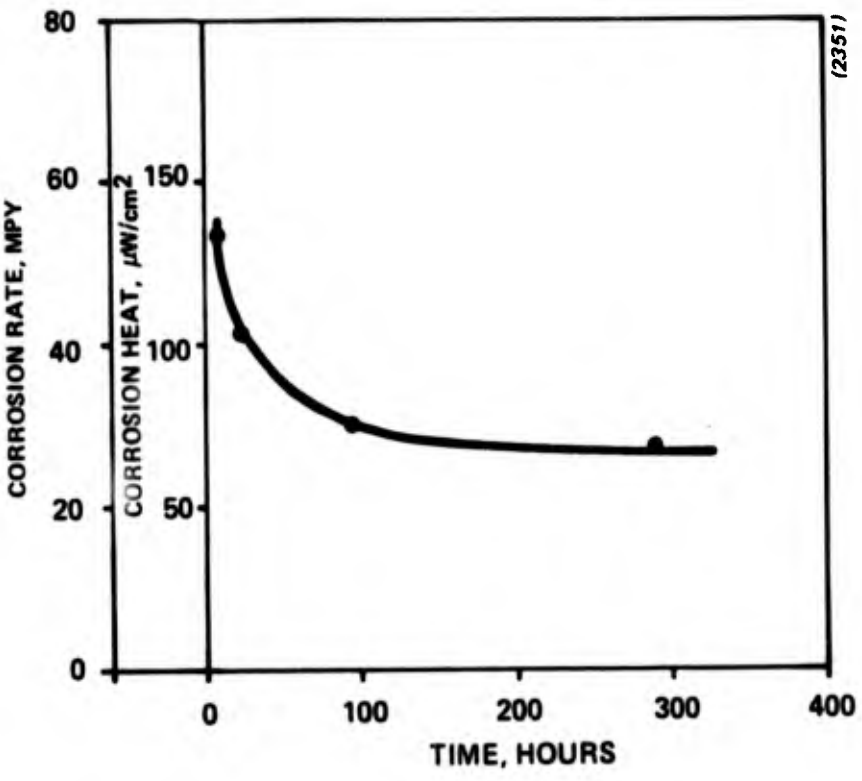

Figure 46 Long Term Corrosion Data for a Li/SO_2Cl_2 Cell with Added Liquid Bromine and No PTFE Insulator

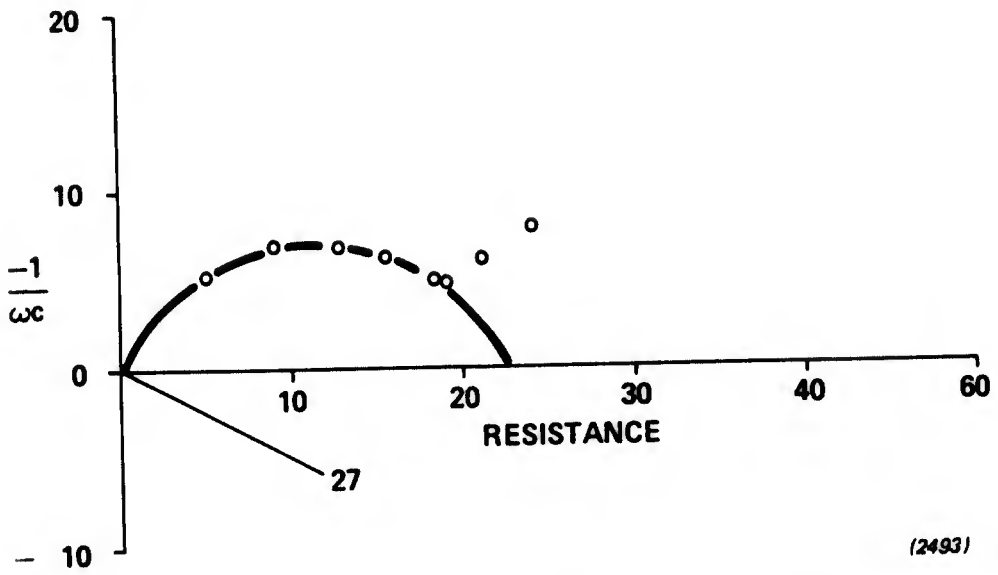

Figure 47 Complex Plane Impedance Spectrum of a Lithium–Sulfuryl Chloride Cell Built with Added Liquid Bromine 3hr after Fill

R_{film} = 23 ohms

C_{film} = 3.4 μF

Thickness = 303 Å

Film Specific Resistance in Ohm-cm = 75E + 006

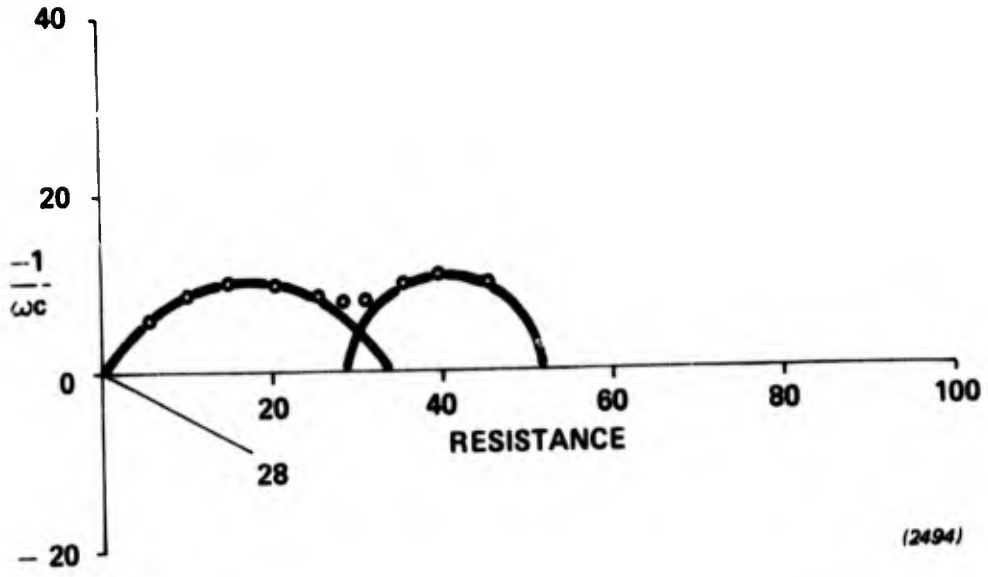

Figure 48 Complex Plane Impedance Spectrum of Lithium–Sulfuryl Chloride Cell BRL–1 Built with Added Liquid Bromine and No PTFE Insulator 27.5hr after Fill

R_{film} = 33 ohms

C_{film} = 4.0 μ F

Thickness = 253 Å

Film Specific Resistance in Ohm-cm = 13E + 007

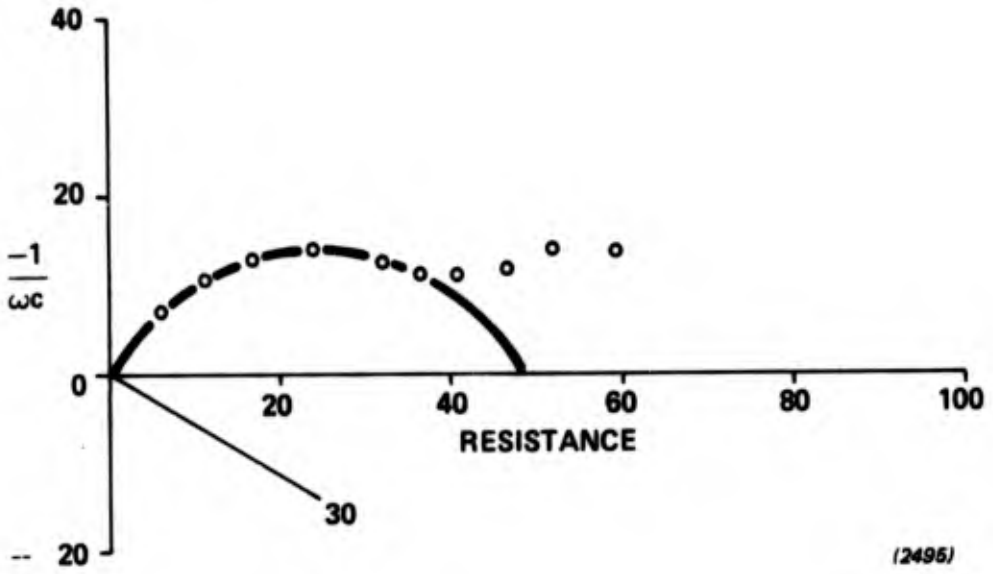

Figure 49 Complex Plane Impedance Spectrum of a Lithium--Sulfuryl Chloride Cell Built with Added Liquid Bromine 94hr after Fill

R_{film} = 48 ohms

C_{film} = 4.8 μ F

Thickness = 214 Å

Film Specific Resistance in Ohm-cm = 22E + 007

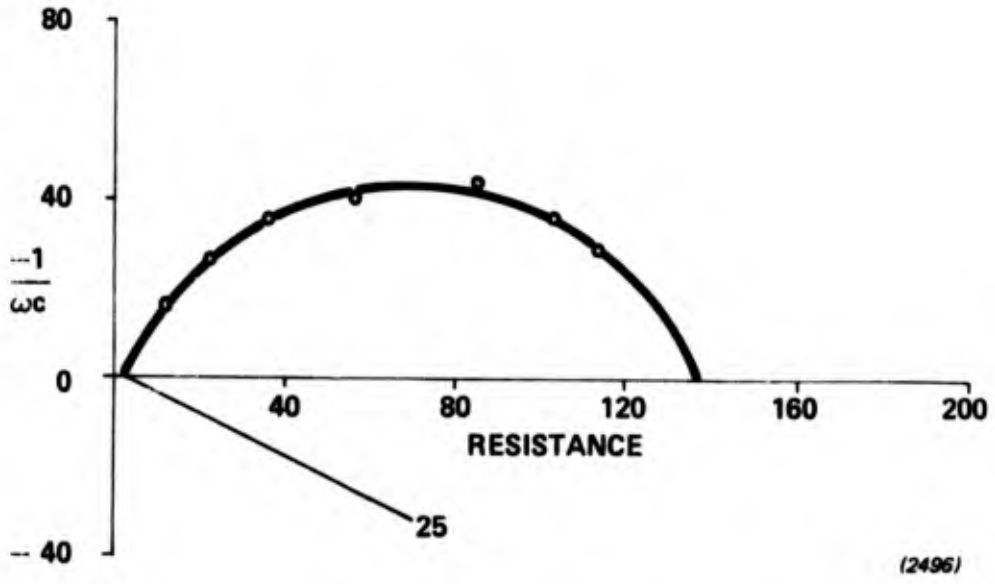

Figure 50 Complex Plane Impedance Spectrum of a Lithium–Sulfuryl Chloride Cell Built with Added Liquid Bromine 172hr after Fill

R_{film} = 135 ohms

C_{film} = 2.1 μ F

Thickness = 488 Å

Film Specific Resistance in Ohm-cm = 28E + 007

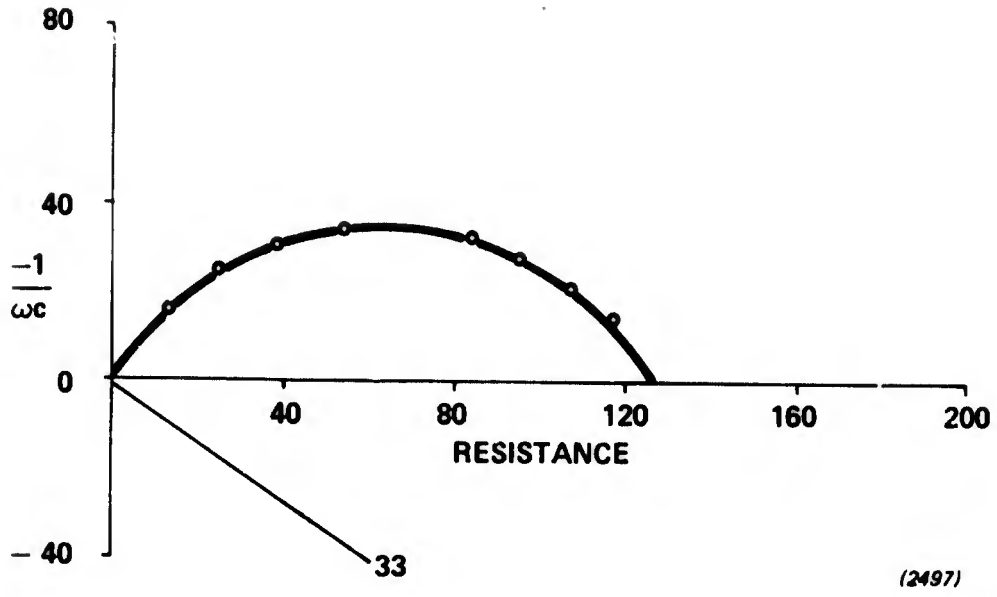

Figure 51 Complex Plane Impedance Spectrum of a Lithium--Sulfuryl Chloride Cell Built with Added Liquid Bromine 286hr after Fill

R_{film} = 128 ohms

C_{film} = 2.2 μ F

Thickness = 456 Å

Film Specific Resistance in Ohm-cm = 28E + 007

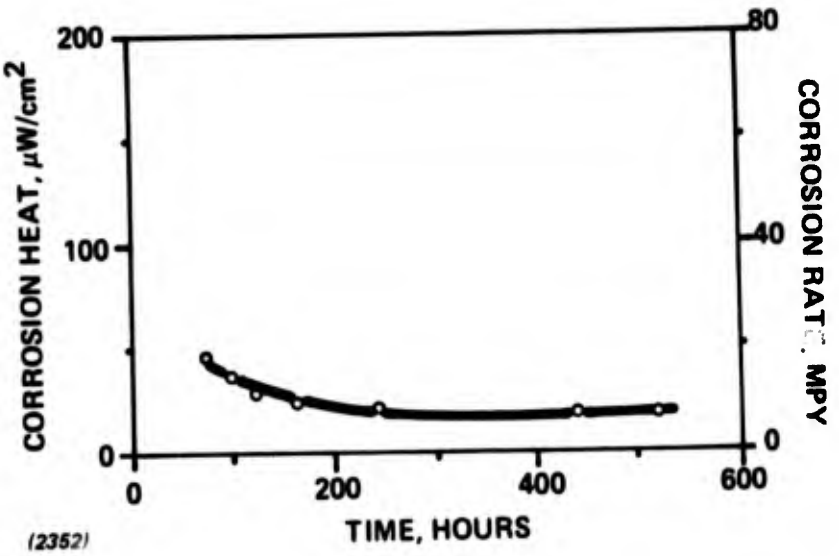

Figure 52 Long Term Corrosion Data for a Li/SO_2Cl_2 Cell with Added Liquid Chlorine

- 1.25" Ø, 1" Ø Electrode
- Positive Grounded
- T = 25°C

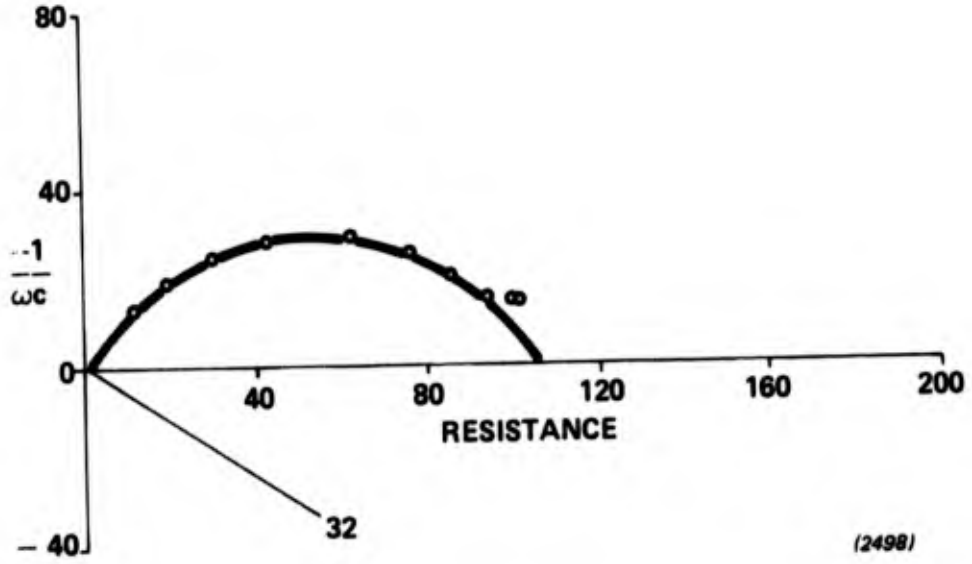

Figure 53 Complex Plane Impedance Spectrum of a Lithium--Sulfuryl Chloride Cell Built with Added Liquid Chlorine 74hr after Fill

R_{film} = 106 ohms
C_{film} = 3.3 μ F
Thickness = 306 Å
Film Specific Resistance in Ohm-cm = 34E + 007

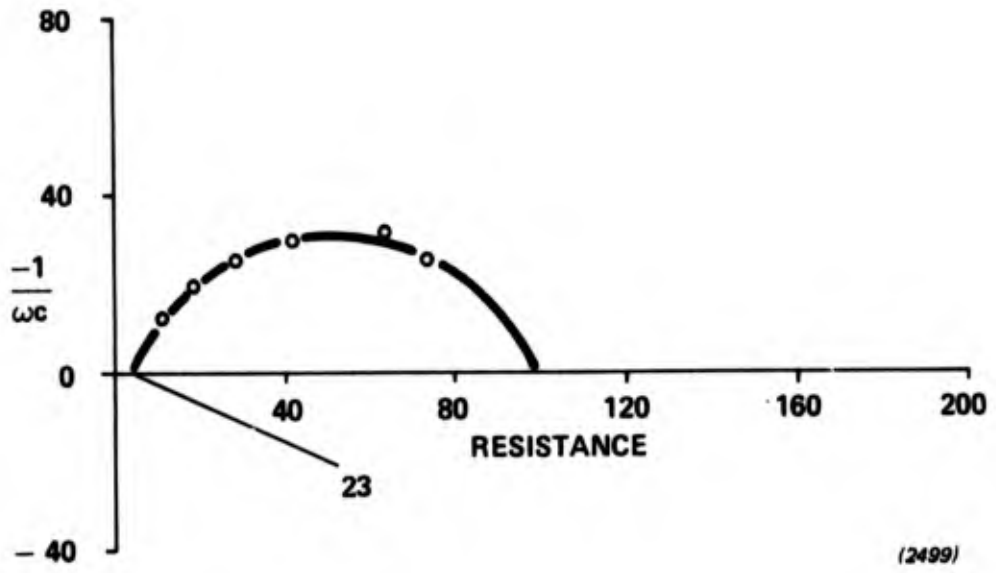

Figure 54 Complex Plane Impedance Spectrum of a Lithium–Sulfuryl Chloride Cell Built with Added Liquid Chlorine 94hr after Fill

R_{film} = 95 ohms

C_{film} = 2.8 μ F

Thickness = 362 Å

Film Specific Resistance in Ohm-cm = 26E + 007

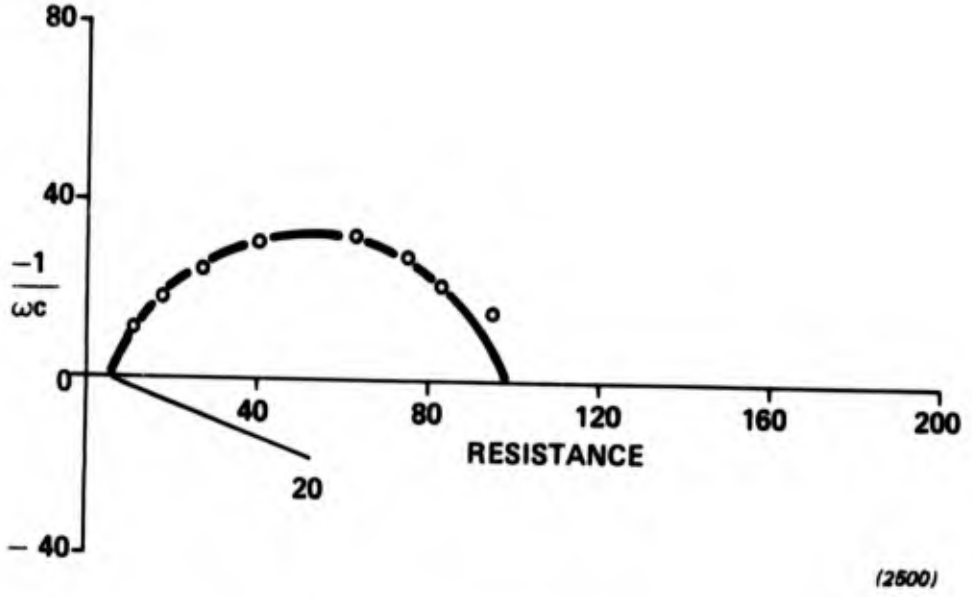

Figure 55 Complex Plane Impedance Spectrum of a Lithium–Sulfuryl Chloride Cell Built with Added Liquid Chlorine 120hr after Fill

R_{film} = 93 ohms

C_{film} = 2.9 μ F

Thickness = 353 Å

Film Specific Resistance in Ohm-cm = 26E + 007

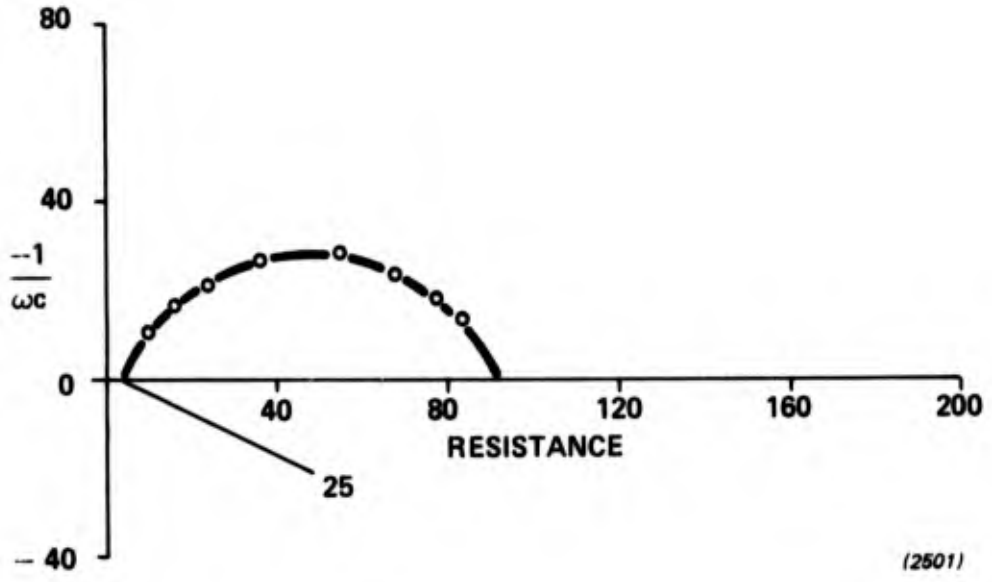

Figure 56 Complex Plane Impedance Spectrum of a Lithium--Sulfuryl Chloride Cell Built qith Added Liquid Chlorine 171hr after Fill

R_{film} = 88 ohms

C_{film} = 3.6 μ F

Thickness = 283 Å

Film Specific Resistance in Ohm-cm = 31E + 007

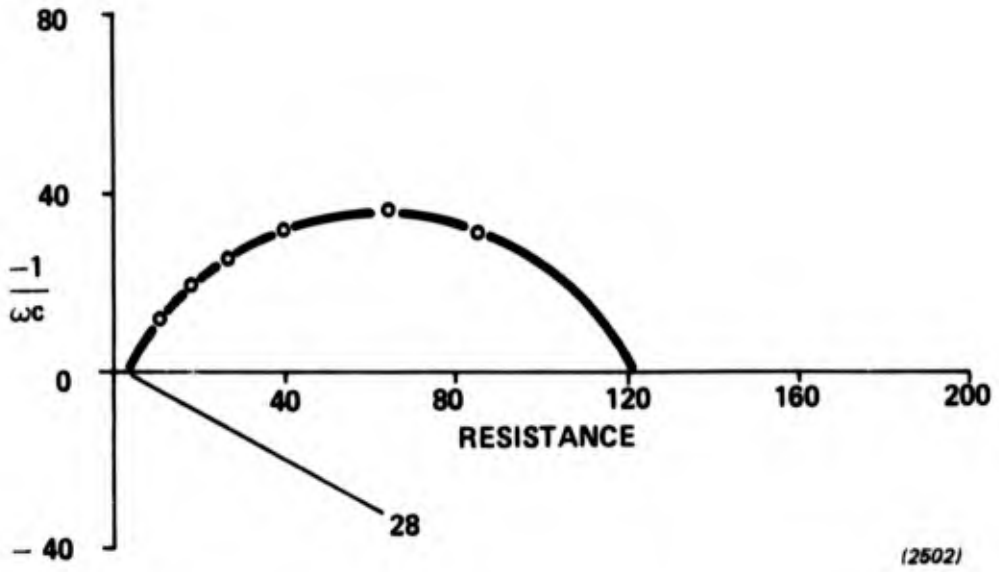

Figure 57 Complex Plane Impedance Spectrum of a Lithium–Sulfuryl Chloride Cell Built with Added Liquid Chlorine 246hr after Fill

R_{film} = 118 ohms

C_{film} = 4.0 μ F

Thickness = 257 Å

Film Specific Resistance in Ohm-cm = 46E + 007

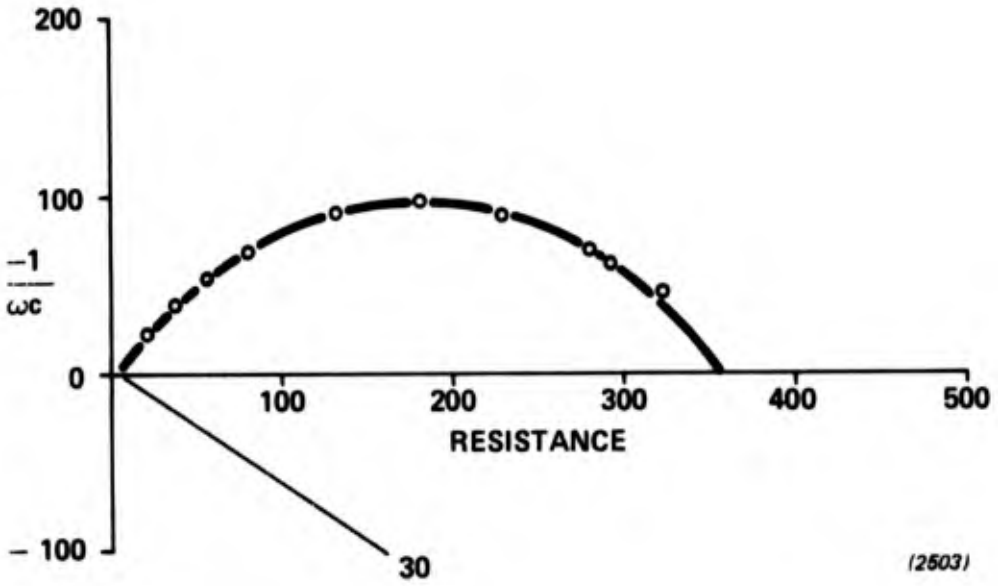

Figure 58 Complex Plane Impedance Spectrum of a Lithium–Sulfuryl Chloride Cell Built with Added Liquid Chlorine 517hr after Fill

R_{film} = 350 ohms

C_{film} = 3.4 μ F

Thickness = 300 Å

Film Specific Resistance in Ohm-cm = 12E + 008

order of 500Å. It should be noted that the fit of the points to a semicircle is good in all the spectra and in none is a high frequency Warburg impedance evident.

Heat generation rate data for the cell using a 1.5M $LiAlCl_4$, 0.3M Cl_2, 0.25M Br_2/SO_2Cl_2 electrolyte are given in Figure 59. The goal of this test was to increase anode stability in the presence of bromine by the addition of chlorine. Comparing the data in Figure 59 with that in Figure 46 it is evident that the long term corrosion rate with both additives is half that when only bromine is present. The corrosion rate is still higher than that observed with the pure chlorine additive, however (see Figures 15 and 52).

Complex plane impedance spectra for this cell are given in Figures 60-62. Variations in film resistance and thickness with storage time are summarized in Figure 63. Comparing the data in Figure 63 with that in Figure 20 for a cell with only the bromine additive, it is seen that film thickness is increasing at a much lower rate when chlorine is also present. In fact the film thickness is close to invariant as was found in the cell with added chlorine. The increase in film resistance is similar to that observed with added bromine. It appears that the two additives are both influencing anode stability in what is most likely a complex fashion.

II.4. Changes due to the Passage of Current

The presence of a resistive film on the lithium anode causes the cell voltage to be depressed upon initiation of cell discharge. The subsequent recovery of the voltage (characteristic of the phenomenon of "voltage delay") occurs due to the decrease in film resistance on polarization as is evident in Figure 64, for a cell employing a 1.5M $LiAlCl_4/SO_2Cl_2$ electrolyte. The film resistance of 85Ω on open circuit is progressively reduced to 58Ω, 39Ω and 31.5Ω on polarization by 0.1, 0.2 and 0.3V respectively. There is approximately 1.5Ω increase in electrolyte resistance due to the addition to the porous film caused by disruption of the compact film. The film builds up

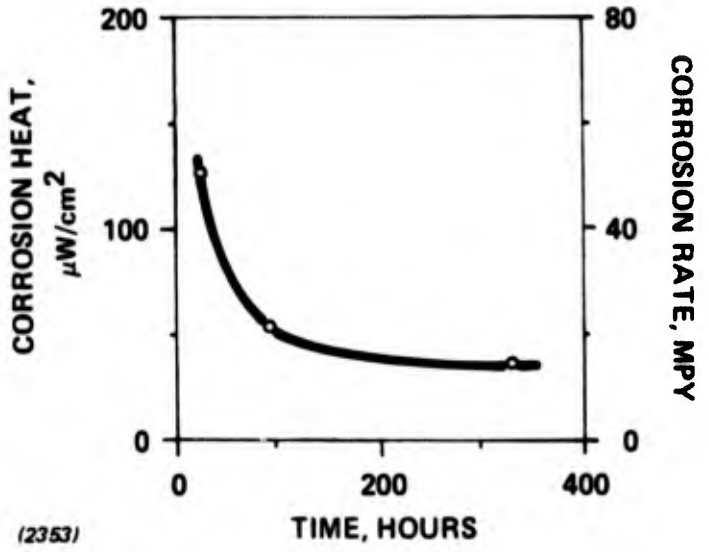

Figure 59 Long Term Corrosion Data for a Li/SO_2Cl_2 Cell Built with Added Liquid Chlorine and Bromine and No PTFE Insulator

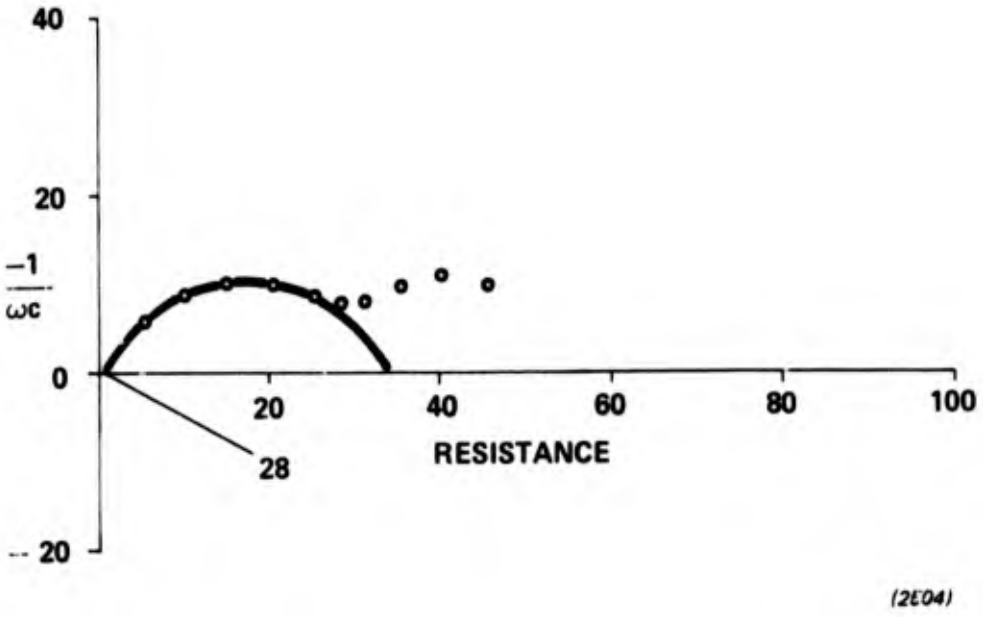

Figure 60 Complex Plane Impedance Spectrum of a Lithium–Sulfuryl Chloride Cell Built with Added Liquid Chlorine and Bromine 27hr after Fill

R_{film} = 33 ohms

C_{film} = 4.0 μ F

Thickness = 253 Å

Film Specific Resistance in Ohm-cm = 13E + 007

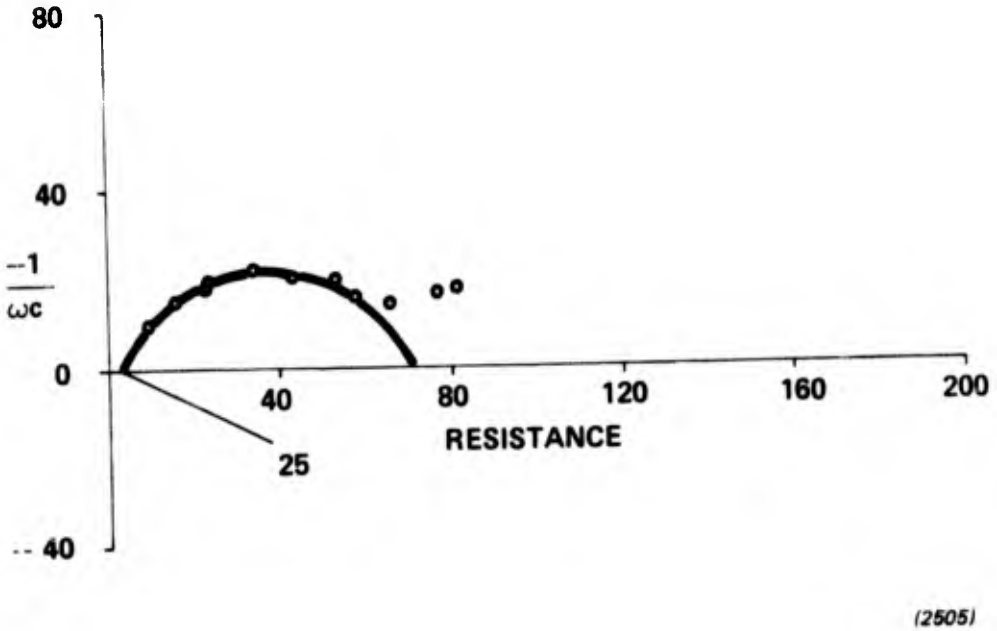

Figure 61 Complex Plane Impedance Spectrum of a Lithium--Sulfuryl Chloride Cell Built with Added Liquid Chlorine and Bromine 94hr after Fill

R_{film} = 69 ohms

C_{film} = 3.7 μ F

Thickness = 276 Å

Film Specific Resistance in Ohm-cm = 25E + 007

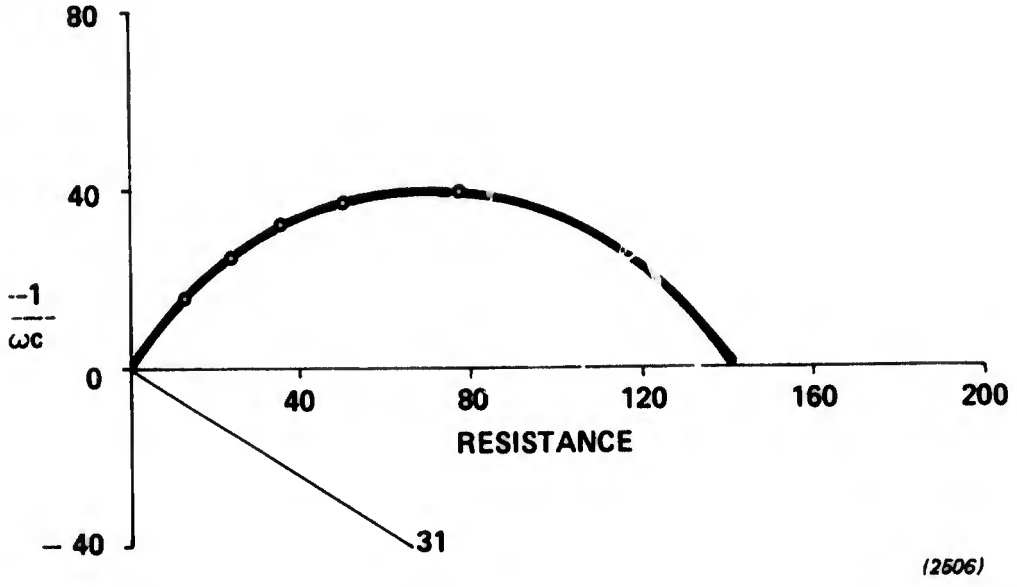

Figure 62 Complex Plane Impedance Spectrum of a Lithium–Sulfuryl Chloride Cell Built with Added Liquid Chlorine and Bromine 333hr after Fill

R_{film} = 141 ohms

C_{film} = 3.0 μ F

Thickness = 342 Å

Film Specific Resistance in Ohm-cm = 41E +007

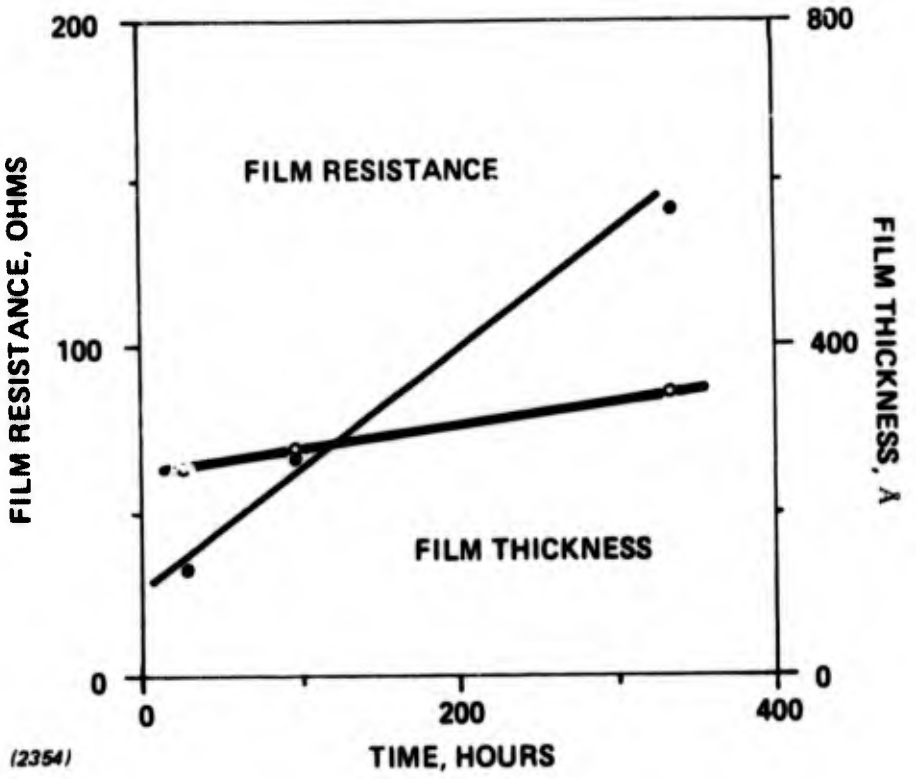

Figure 63 Variations in Film Resistance and Thickness with Time for a Li/SO_2Cl_2 Cell Employing a 1.5M $LiAlCl_4$, 0.3M Cl_2, 0.25M Br_2/SO_2Cl_2 Electrolyte

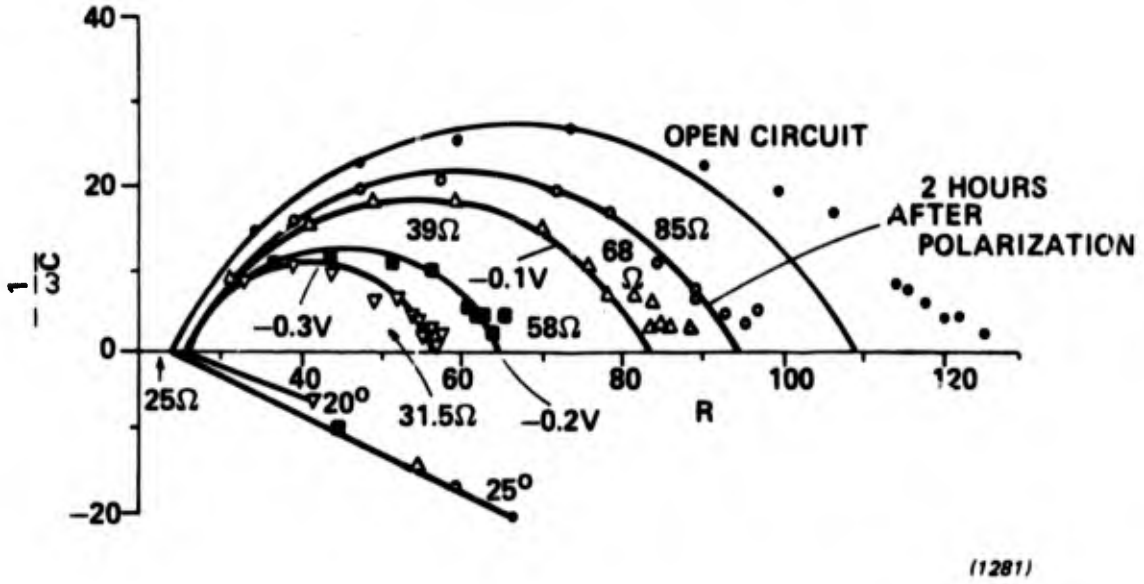

Figure 64 Complex Plane Impedance Spectrum of a Li/SO_2Cl_2 Cell on Polarization

in thickness quite rapidly on leaving the cell on open circuit after polarization.

The recovery of resistance due to film growth after polarization was followed by the complex plane impedance technique. Figure 65 shows the semicircles associated with the LiCl film on 300 mV polarization and 5, 15, 40, 120, 180, 300 and 1200 minutes following termination of polarization. The corresponding resistances are 12, 23, 38, 64, 105, 121, 128 and 182 ohms respectively. The film resistance continues to increase further; the spectrum in Figure 66 obtained 11 days after polarization shows a resistance of 348Ω, and Figure 67, a spectrum taken 6 weeks after polarization indicates a resistance of 920Ω. There is also a significant increase in electrolyte resistance on extended storage of the cell.

The capacitance, film thickness and film resistivity following polarization are listed in Table 4. A thickness vs. time plot during the initial period of recovery is shown in Figure 68. The film thickens rapidly until it approaches the thickness value prior to polarization. The rate of build-up then slackens abruptly, and some twenty hours after termination of polarization, the rate is virtually identical to that before polarization.

Effects of a similar nature are also observed with chlorine containing electrolyte and cells built with the methylcyanoacrylate anode coating. In Figures 69 and 70 complex plane impedance spectra for various degrees of polarization are given for these two cases. Both show a decrease in film resistance with increasing polarization. It is most likely that the decreasing film resistance corresponds to a disruption of the passivating LiCl layer. No evidence is seen in Figure 70 for a high Warburg impedance due to the methylcyanoacrylate coating and we can draw no conclusion as to the fate of this coating during and after polarization.

A disruption of the passivating film during has been previously shown by Gibbard (9) to lead to an increased rate of lithium corrosion in thionyl chloride cells. A similar effect appears to occur in sulfuryl chloride cells. At very low currents the measured apparent entropy voltage is 0.11V. However, at higher currents as shown in Figure 71 an apparent entropy voltage of 0.217V is found. This increase may well be due to an increase in lithium corrosion which is linearly dependent on current.

---

9. H.F. Gibbard, "Proceedings of the Symposium on Power Sources for Biomedical Implantable Applications and Ambient Temperature Lithium Batteries", B.B. Owens and N. Margalit, eds, The Electrochemical Society, 1980, p. 510.

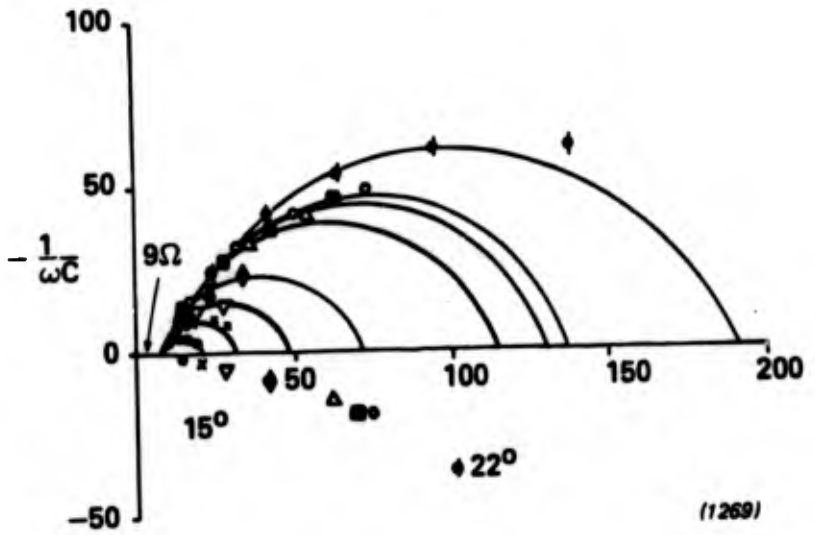

Figure 65 Complex Plane Impedance Spectrum of a Li/SO_2Cl_2 cell following termination of polarization

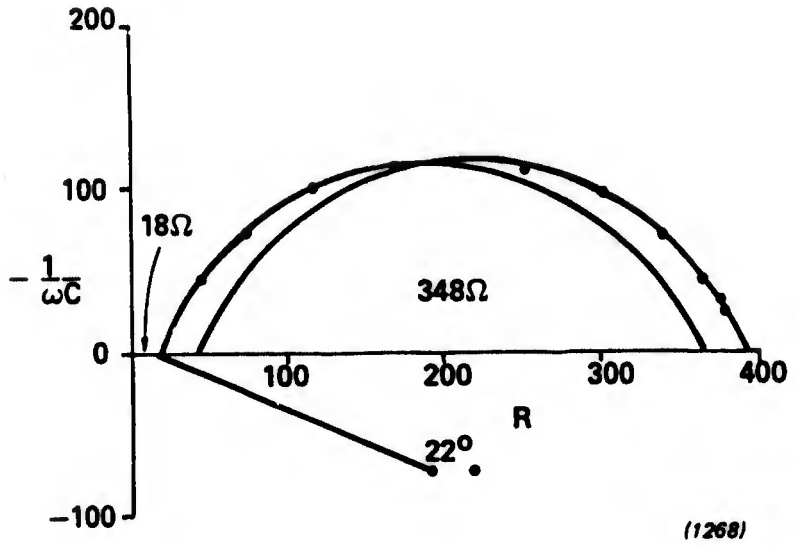

Figure 66 Impedance Spectrum of the Li/SO_2Cl_2 cell 11 days after polarization

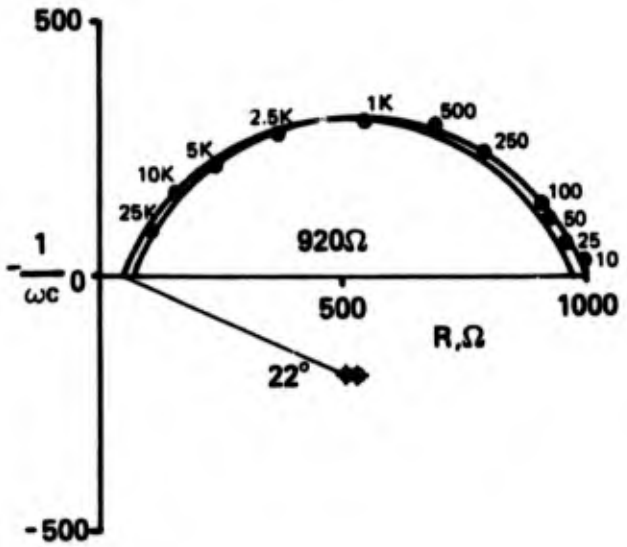

Figure 67 Impedance Spectrum of a Li/SO_2Cl_2 cell at rest 6 weeks after polarization

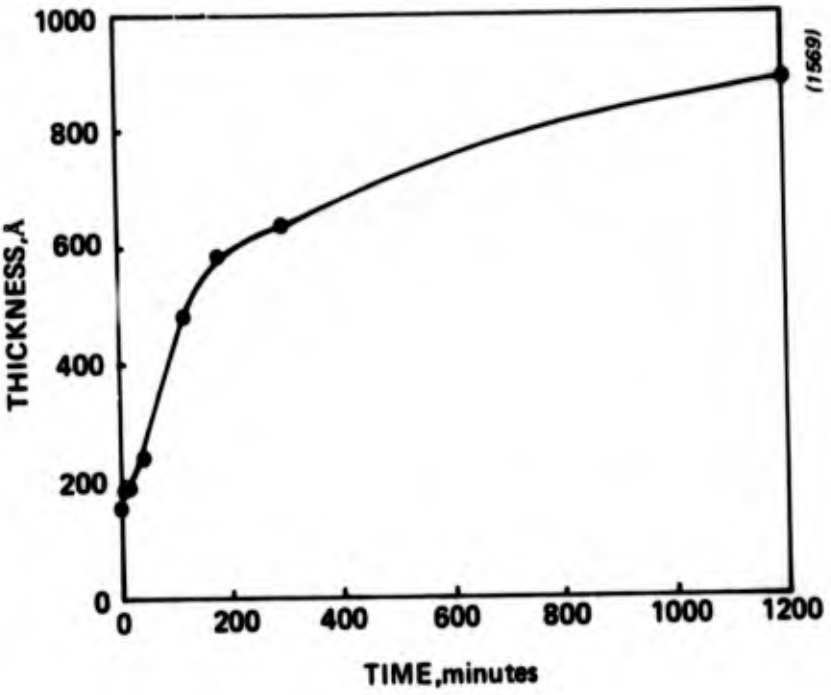

Figure 68 Film growth following Polarization in a Li/SO_2Cl_2 cell

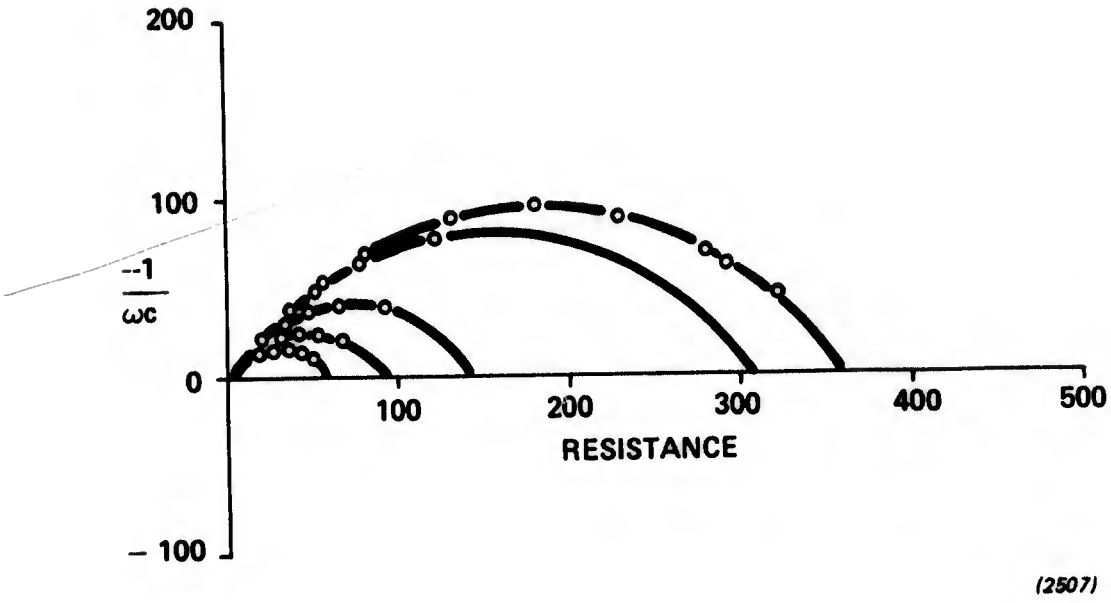

Figure 69 Complex Plane Impedance Spectra of a Lithium–Sulfuryl Chloride Cell Built with Added Liquid Chlorine 517hr after Fill at Open Circuit and in 100mV Steps from Open Circuit

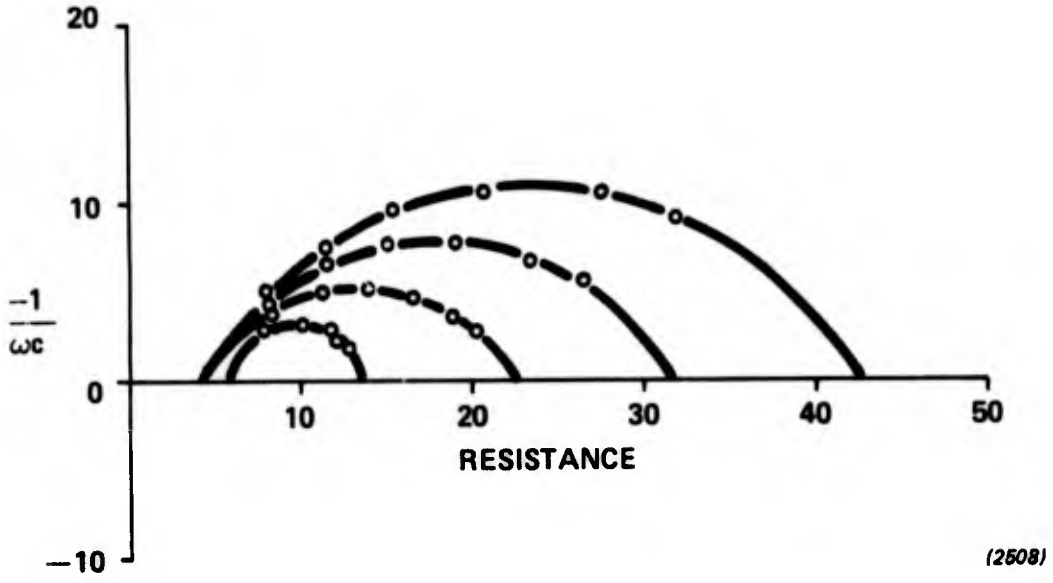

Figure 70 Complex Plane Impedance Spectra of a Lithium–Sulfuryl Chloride Cell Built with a Methylcyanoacrylate Coating on the Anode for Polarizations of 0, 50, 100, and 150mV from Open Circuit

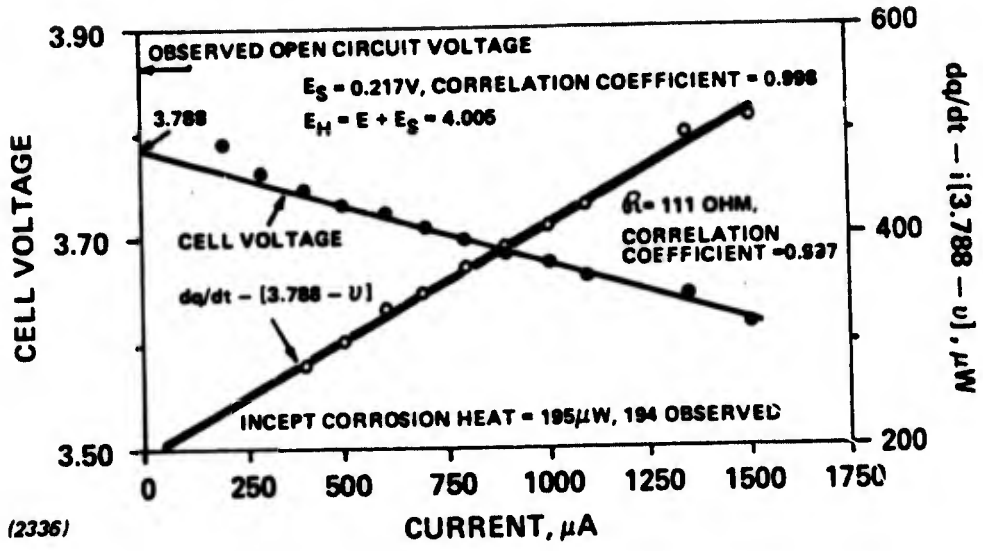

Figure 71 Steady State Second Law Data Treatment for a Li/SO_2Cl_2 Cell with Added Liquid Chlorine and a $SOCl_2$ Pretreated Anode Electrode Area = 5 cm^2

Table 4 Film Growth on Lithium in a Li/SO_2Cl_2 Cell Following Polarization

TIME MIN.	RESISTANCE Ω	CAPACITANCE $\mu F/cm^2$	THICKNESS Å	RESISTIVITY 10^{-7} Ω cm
0	12.0	0.618	158	2.5
5	23.0	0.524	186	4.1
15	38.0	0.509	192	6.5
40	64.4	0.403	242	8.8
120	104.5	0.201	487	7.1
180	121.0	0.166	588	6.8
300	127.5	0.151	646	6.5
1200	182.0	0.110	886	6.8
16000	348.0	0.069	1410	8.2
60000	920.0	0.052	1864	16.0

(1290)

III. MECHANISTIC STUDIES OF CELL OPERATION

III.1 Operation of the Bromine Additive

The generally accepted discharge reaction for a Li/SO_2Cl_2 cell is

$$2Li + SO_2Cl_2 = 2LiCl + SO_2 \qquad [2]$$

We favor addition of bromine to the electroltye. This addition can occur either as molecular bromine or as bromide;

$$2LiAlCl_3\,Br + SO_2Cl_2 = 2LiAlCl_4 + SO_2 + Br_2 \qquad [4]$$

We have found that reaction [4] proceeds to at least 80% completion using UV-visible spectroscopy.

Although bromide ion is chemically oxidized to bromine in SO_2Cl_2 we have obtained strong evidence summarized in Figure 72 that bromine is electrochemically reduced at a higher voltage vs. lithium than SO_2Cl_2 on carbon. The cyclic voltammograms in Figure 72 show two reduction peaks when bromine is present and only one lower voltage peak in its absence.

Based on these results it appears in a cell a cycle exists between electrochemically formed LiBr and chemically produced bromine and LiCl. This cycle may have two effects,

- A high capacity at high current densities (e.g., $>10mA/cm^2$) possibly because chemically produced LiCl is not as passivating as electrochemically produced LiCl.

- A greater high current density operating voltage as bromine is reduced at a lower over potential then SO_2Cl_2. As shown in Figure 73 cells with the additive are operable at current densities up to $50mA/cm^2$.

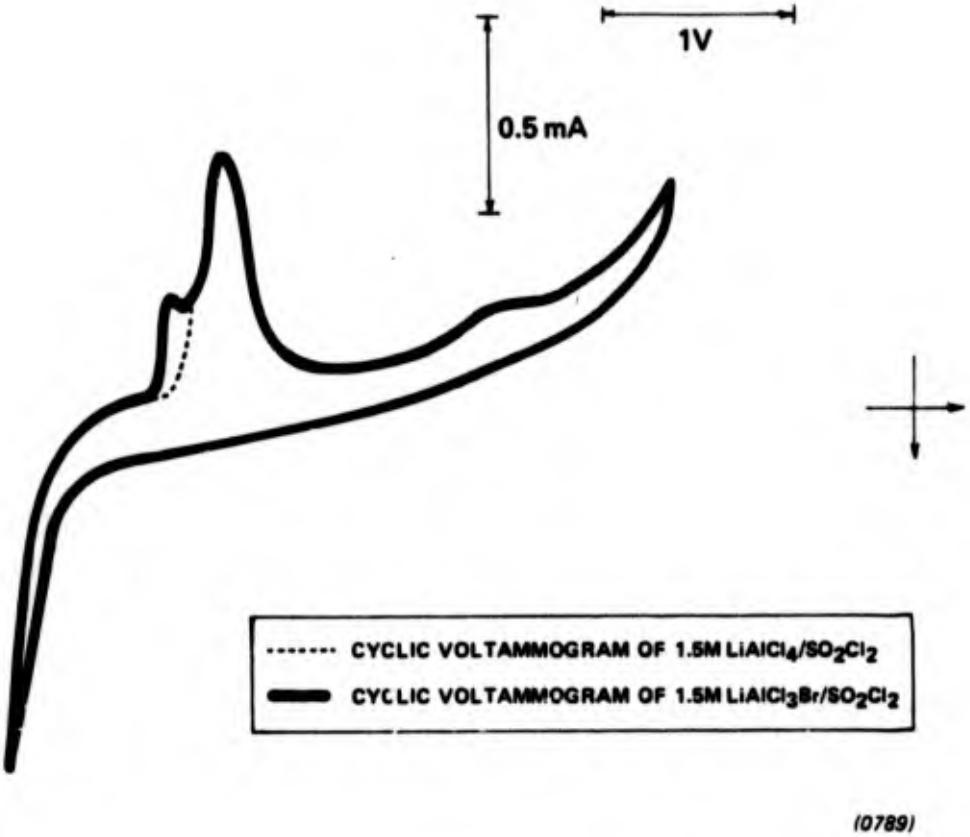

Figure 72 Cyclic Voltammogram on Glassy Carbon of 1.5M $LiAlCl_3Br/SO_2Cl_2$ and 1.5M $LiAlCl_4/SO_2Cl_2$

Scan Speed = 50 mV/sec

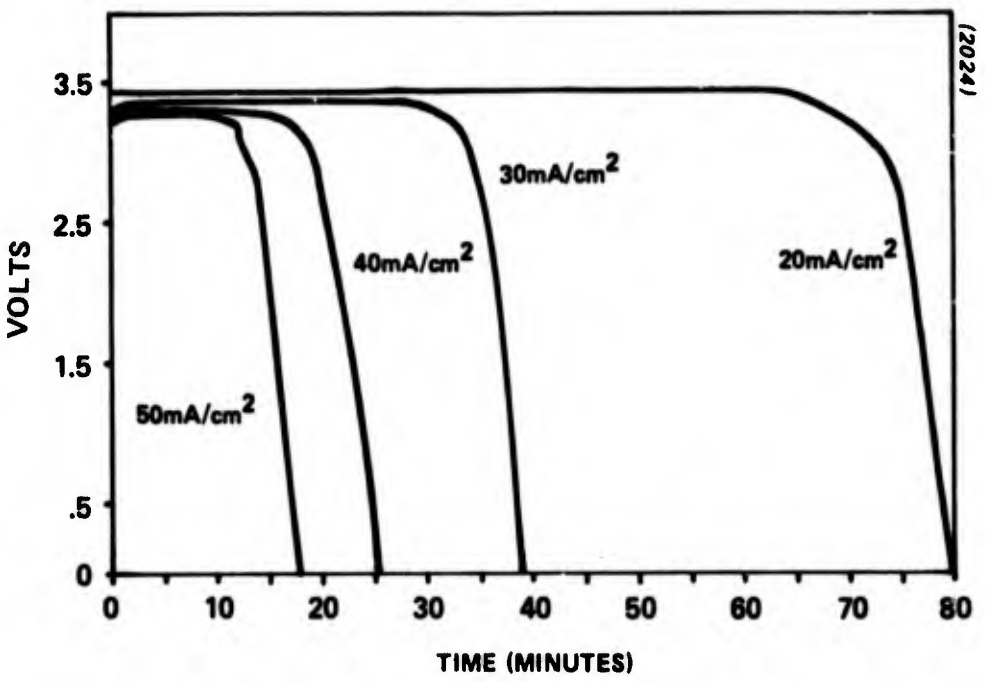

Figure 73 Discharge Behavior of Li/1.5M $LiAlCl_3Br$, SO_2Cl_2 Cells between 20 and 50 mA/cm^2

Bromine appears to act as a catalyst of the second kind. That is it is consumed in the discharge reaction but reformed by a subsequent chemical reaction. As shown in Figure 74 the concentration of bromine is almost constant during discharge (the slight decrease in Figure 74 may be due to evaporation).

III.2 Spectroscopic Studies of Cell Safety

One of the principal advantages of a Li/SO_2Cl_2 cell as opposed to a $Li/SOCl_2$ cell is the possibility of greater safety. One tool for assessing possible hazardous reactions in both cells is spectroelectrochemistry, where electrolyte is withdrawn from operating cells and spectroscopically analyzed. This approach has been of great value in the thionyl chloride system in following reactions during anode-limited cell reversal.

To assess the safety of Li/SO_2Cl_2 during anode limited reversal we have discharged a cell of the design shown in Figure 75 at $1mA/cm^2$ and periodically withdrew electrolyte samples for FTIR analysis. The spectra obtained during the discharge and anode limited reversal of this cell are given in Figures 76-81.

During normal discharge (Figures 76-78) the only observed change in the spectra is an increase in the SO_2 absorption (peak at $1330cm^{-1}$). Small peaks are evident at $1070cm^{-1}(SO^{+2})$ and an unidentified species which absorbs at $\sim 820cm^{-1}$. As reversal proceeds (Figure 79) the intensity of these peaks increases slightly and a small blip appears at $690cm^{-1}$.

The most surprising result obtained in this study is shown in Figure 80. At this point the cell had been in reversal for approximately 24 hours. Dramatic increases in both the 1070 and $820cm^{-1}$ absorbances are evident. This sudden increase is even more surprising if it is compared with the spectrum after approximately 100 hours of reversal given in Figure 81. As can be seen the intensity of both peaks returned to their previous levels.

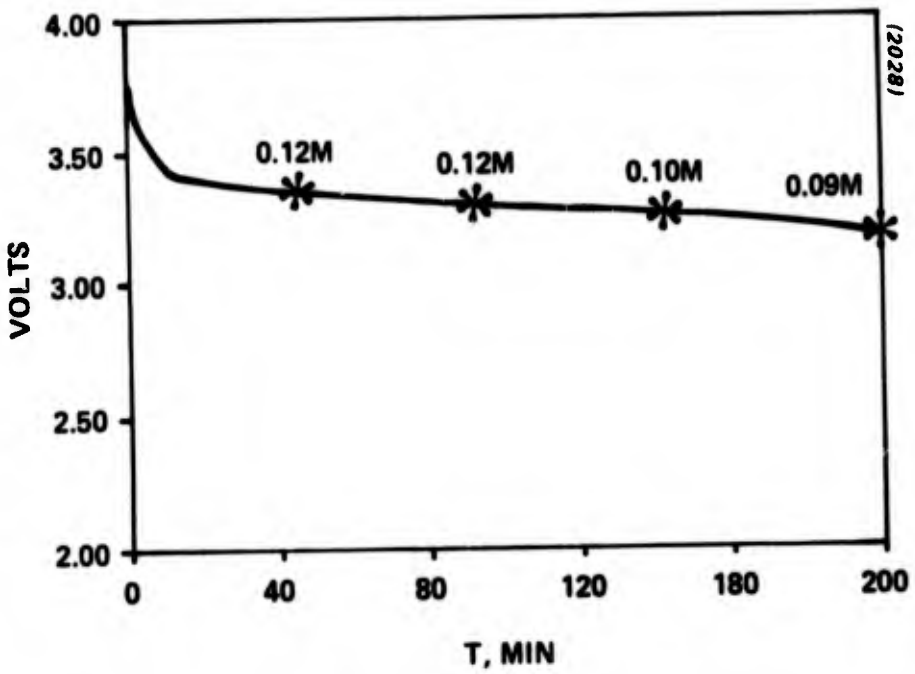

Figure 74 Lithium/Sulfuryl Chloride Bromine determination UV/VIS spectroscopy at 10mA/cm^2

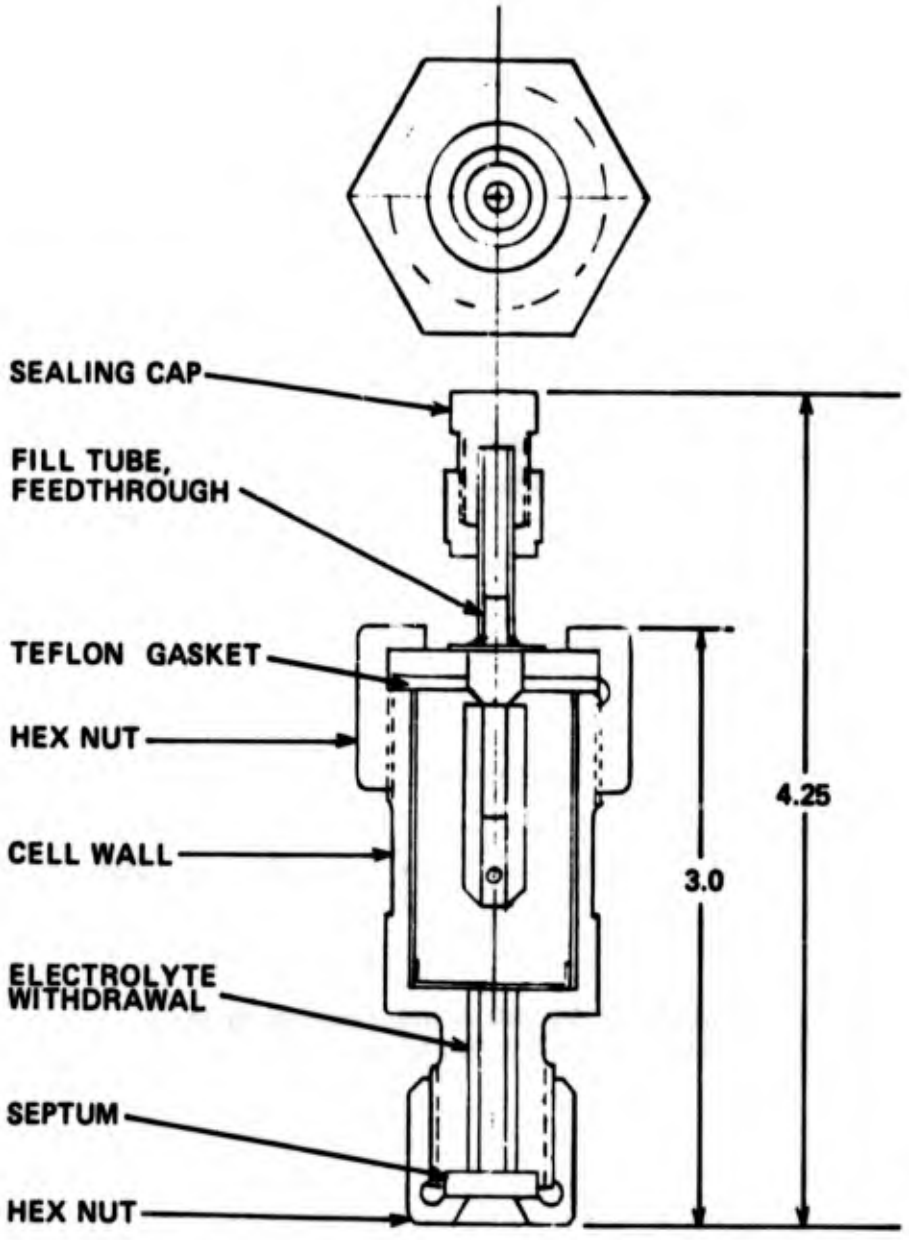

Figure 75 Electrochemical Cell Designed for Electrolyte Withdrawal

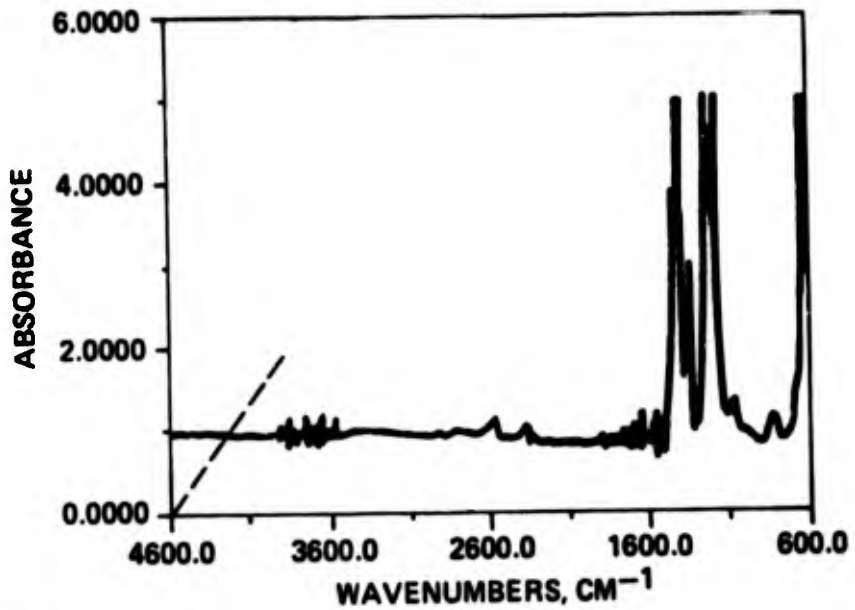

(2355)

Figure 76 Spectrum of Electrolyte at Open Circuit from a Li/SO_2Cl_2 Spectroelectrochemical Cell

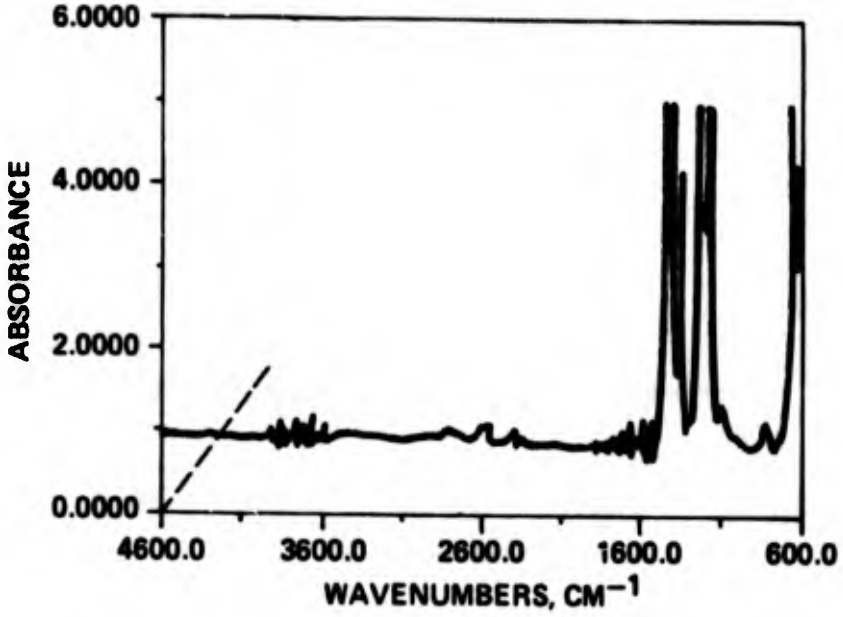

(2356)

Figure 77 Spectrum of Electroltye after 5.5 Hours of Discharge
$i = 1.0 mA/cm^2$, V = 3.680

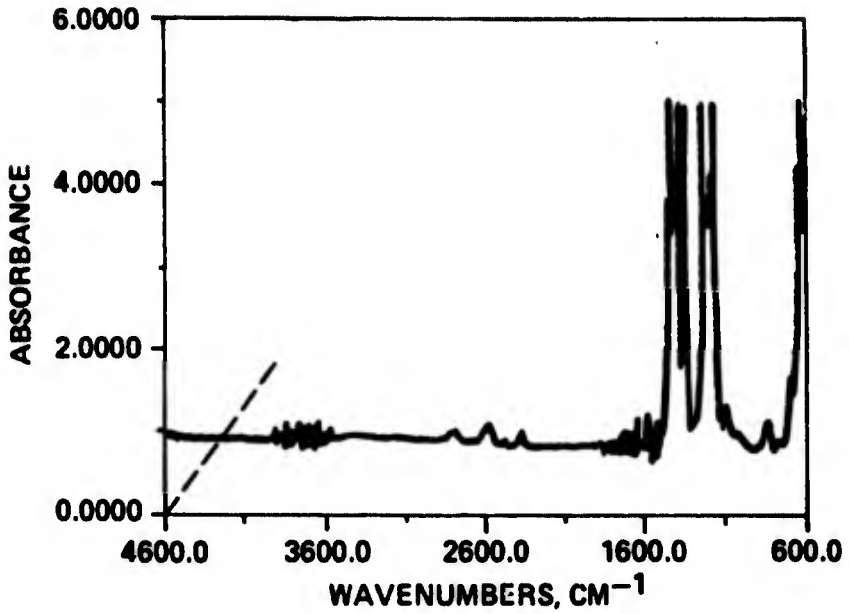

(2357)

Figure 78 Spectrum of Electrolyte after 20.5 Hours of Discharge
$i = 1.0 mA/cm^2$, V = 3.5 to –0.9V

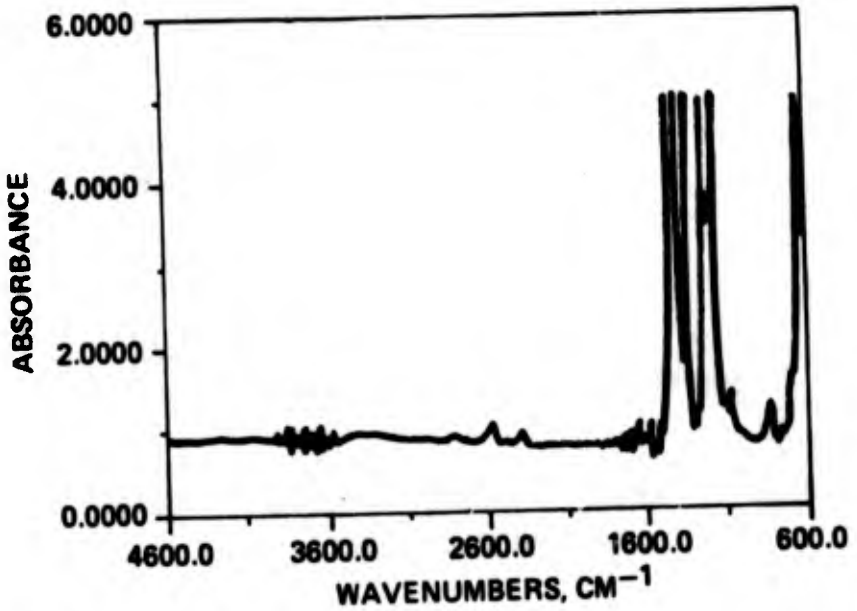

Figure 79 Spectrum of Electrolyte after 29 Hours of Discharge
$i = 1.0 mA/cm^2$, $V = -1.06V$

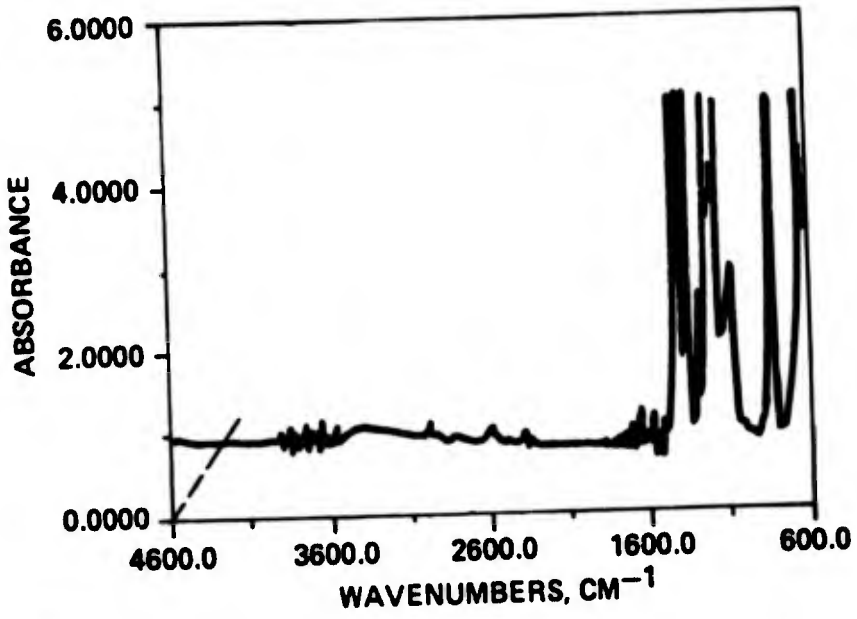

(2359)

Figure 80 Spectrum of Electrolyte after 45 Hours of Discharge
$i = 1.0 mA/cm^2$, $V = -1.03V$

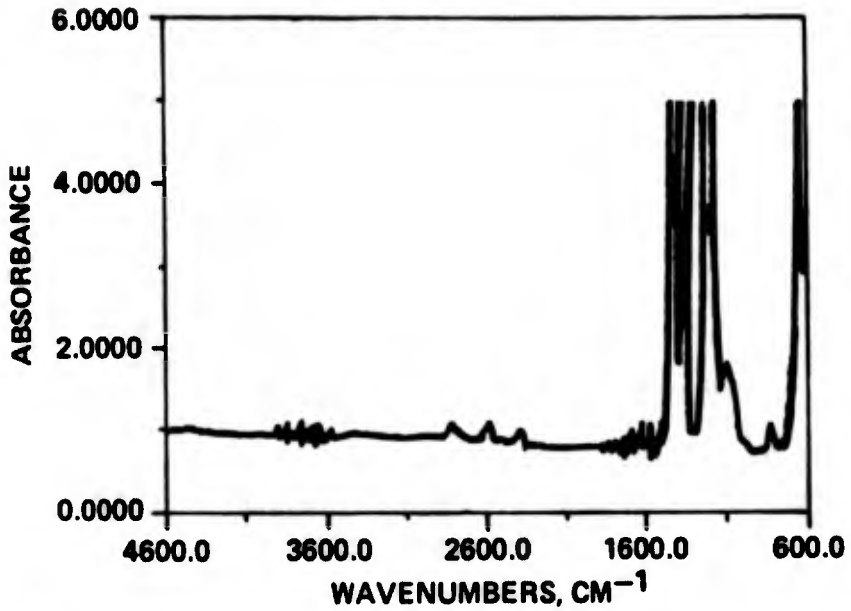

Figure 81 Spectrum of Electrolyte after 118 Hours of Discharge
$i = 1.0 mA/cm^2$, $V = -1.07V$

These preliminary results are somewhat disturbing with regard to cell safety. The sudden changes evidenced in Figure 80 appear to indicate an unpredictable transitory reaction. Such reactions could indicate a potential instability during anode limited reversal. In this regard it should be noted that we observed one near explosion (e.g., melting of internal nickel components, case swelling, venting) when a cell was accidentally driven into anode limited reversal.

A much more thorough parametic study will be required to identify possible hazardous reactions. In addition to reaction studies actual abuse testing will be required to determine if a hazard exists.

IV. ANODE PERFORMANCE CHARACTERIZATION

Lithium on exposure to sulfuryl chloride electrolyte develops a protective film which inhibits the spontaneous corrosion reaction at the interface. This film is essential to the storageability of Li/SO_2Cl_2 cells, but it also can affect adversely the performance of the cell. Upon storage of a Li/SO_2Cl_2 cell the film thickens causing voltage delay upon initiation of discharge. Voltage delay is, for our purposes, described as the time required from the onset of discharge for a cell to obtain a voltage of at least 2 volts. To control voltage delay, control of the film growth and the corrosion of the anode is needed.

Two approaches are suggested for minimizing voltage delay, choice of solute and coating of the anode. No work under this heading was performed with anode coatings though microcalorimetry of cells with methylcyanoacrylate coating is described in Section II. Most of the studies performed here involved the choice of solute.

In our electrolyte sulfuryl chloride is used with $LiAlCl_4$. Test cells, stored with this electrolyte for 2 and 7 days at 30°C and 60°C and discharged, performed poorly as seen in Figures 82 and 83. The voltage delay in the cells

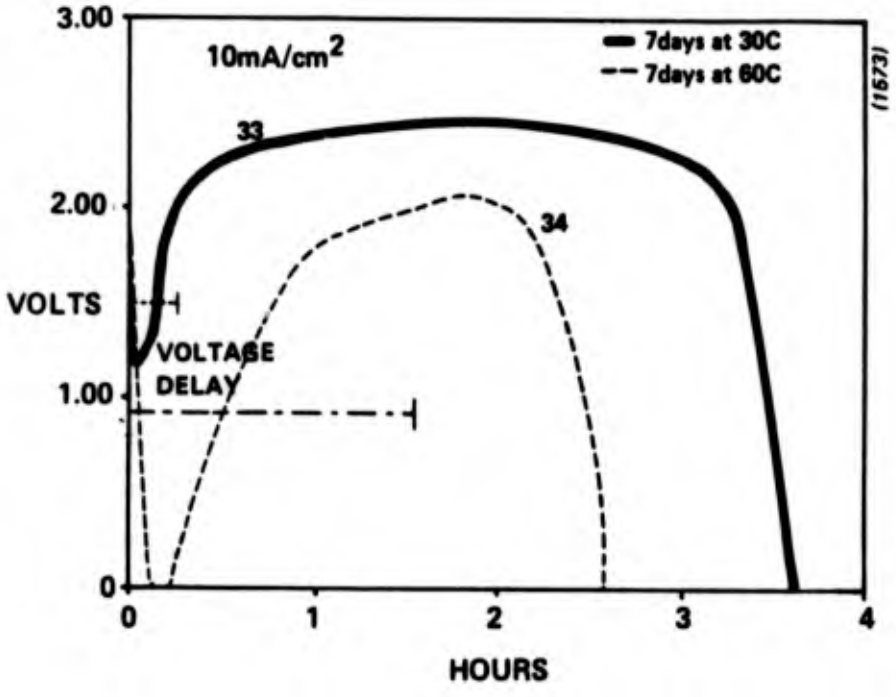

Figure 82 Discharge Curves Showing Voltage Delay after Seven Days Storage

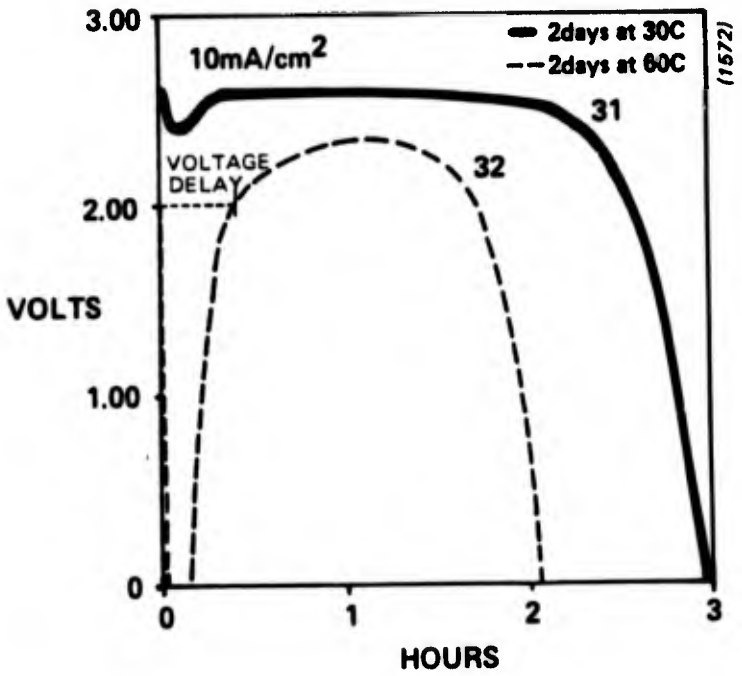

Figure 83 Discharge Curves Showing Voltage Delay After Two Days Storage

ranged from 15 to 90 minutes. Figures 84 and 85 illustrate the results achieveable by adding $LiAlCl_3Br$ to this electrolyte. Quite graphically the additive appears to prevent voltage delay.

Additional testing of the bromine additive indicates that some voltage delay does occur at high temperatures after seven days of storage, but the initial voltage and the severity of the drop in voltage is considerably less as seen in Figure 86 than in cells without the additive. The discharge curves indicate a 5-7 minute voltage delay after storage at 40°C and 60°C, but the voltage of neither of the cells drops below 1.5 volts, whereas in cells without the bromine additive, cell voltage falls below zero on the application of current.

These results prompted the following investigation. A 2^3 factorial experiment was performed to determine the effect the bromine addition has on cell performance. The effects of temperature and time of storage were also determined as well as interactions.

The experiment is as follows

Cell #		A	B	C
1A	1	-	-	-
2A	a	+	-	-
3A	b	-	+	-
4A	ab	+	+	-
5A	c	-	-	+
6A	ab	+	-	+
7A	bc	-	+	+
8A	abc	+	+	+

Factors:

A. Temperature - 25°C
+ 60°C

B. Additive - no additive
+ additive

C. Storage Time - 2 days
- 7 days

data accumulated were cell capacity

total watt-hours and the voltage delay

$i = 10mA/cm^2$

The test cell design used in this experiment is illustrated in Figure 87.

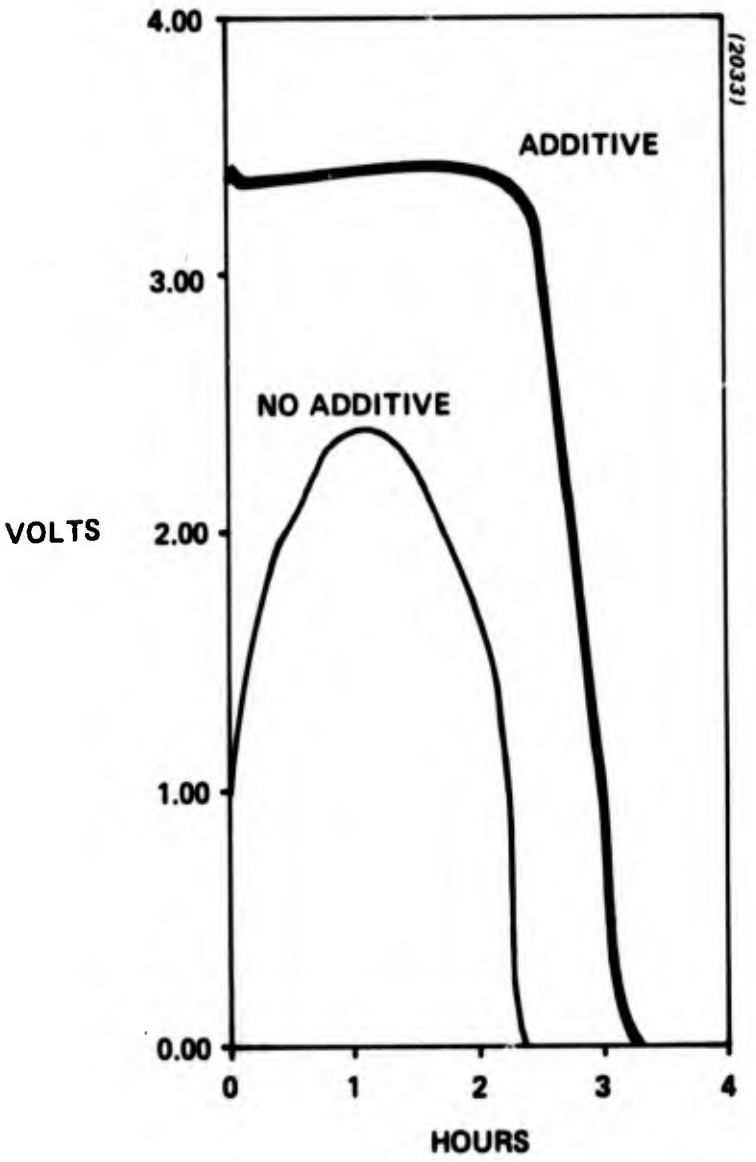

Figure 84 Discharge Curves of Li/SO_2Cl_2 2in diameter Test Cells stored at 25C for 2 days

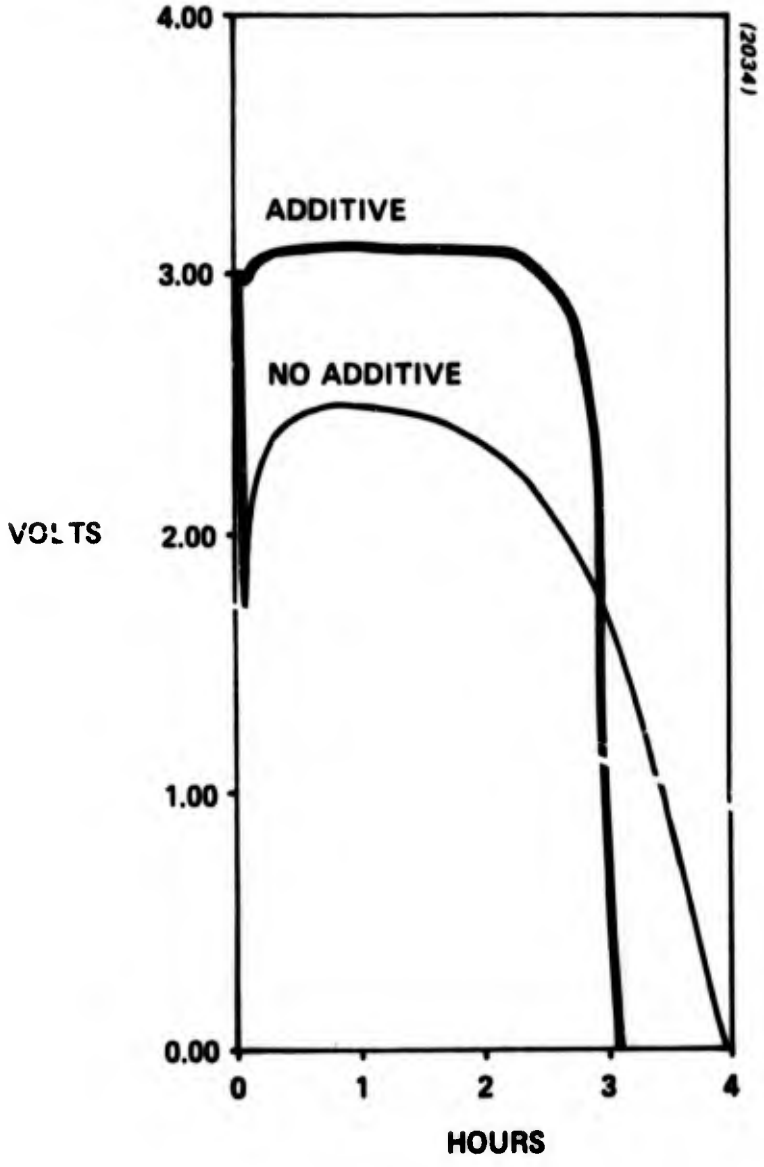

Figure 85 Discharge Curves of Li/SO_2Cl_2 2 in diameter Test Cells stored at 60C for 2 days

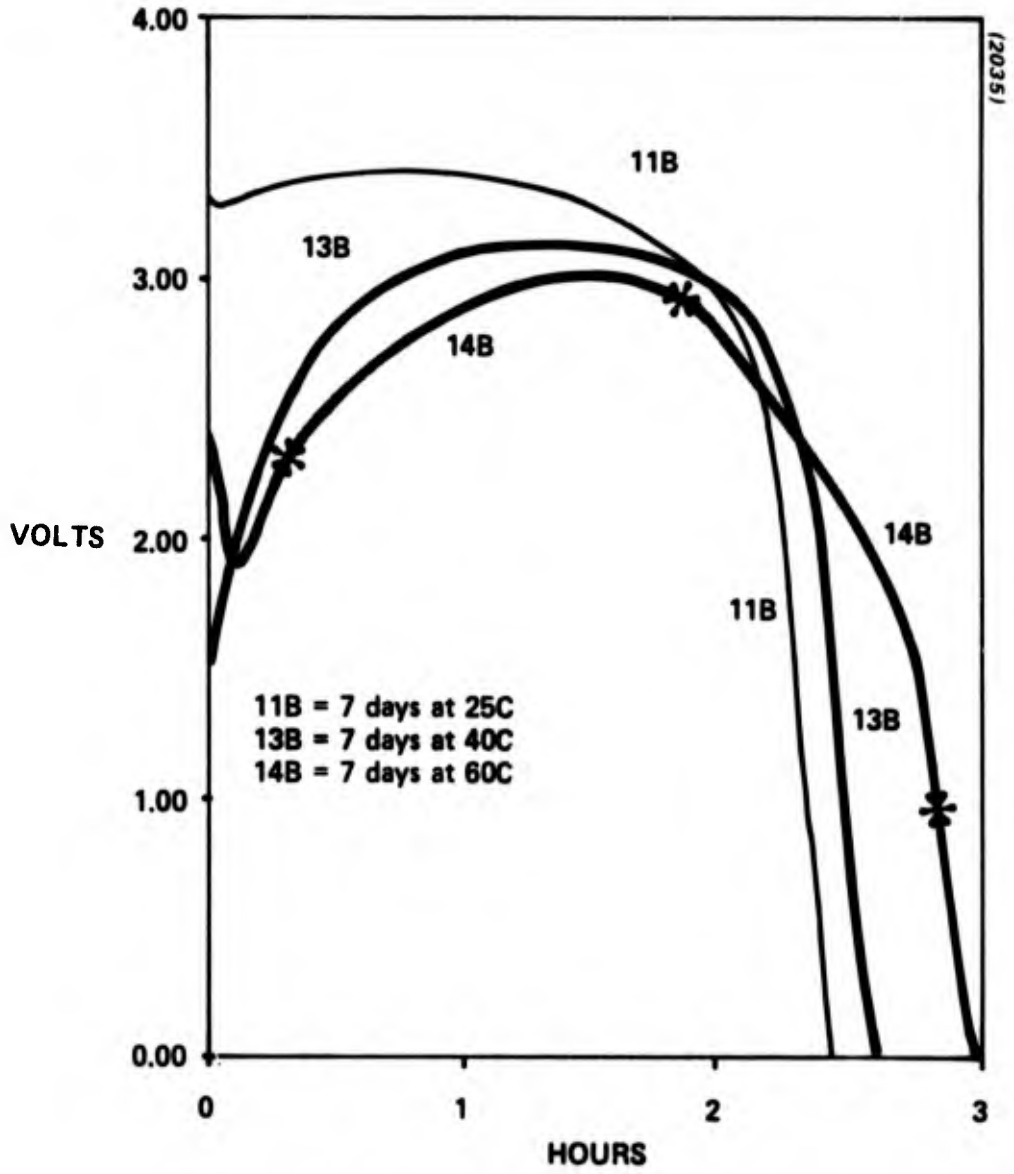

Figure 86 Discharge Curves of 11B, 13B, 14B (at 10mA/cm^2) with $LiAlBrCl_3$

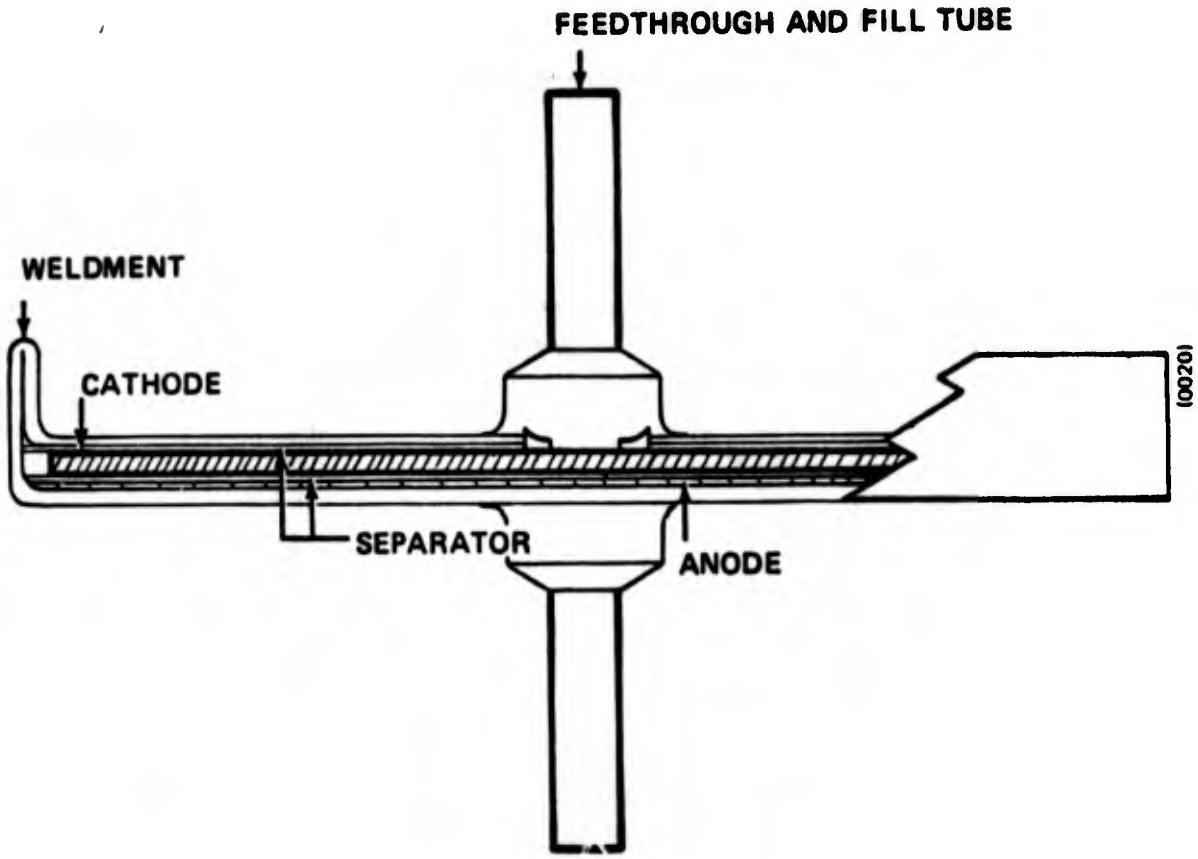

Figure 87 Schematic Cross Section and Description of 50mm diameter Cell used in Li/SO_2Cl_2 Studies

CATHODE: 90/10 Shawinigan Black/PTFE 0.35g pressed onto expanded Ni screen

ANODE: 20mil Lithium foil pressed onto expanded Ni screen

SEPARATOR: 5 mil Manniingles

INSULATOR: 10 mil Teflon sheet

The results of the experiment are seen in Table 5. Due to problems with storage life of the cells with the soldered feedthrough the seven day data are incomplete. Only one complete run of all eight treatments was acquired (run #3), and two additional runs of the top half of the experiment were obtained. Realizing that the top half of the experiment constitutes a 2^2 factorial experiment those eight observations were analyzed as such. The results of the analyses of variance are seen in Table 6; the watt-hour analysis and voltage delay analysis are both presented. Using the error estimate of the 2^2 factorial experiment the set of eight observations of the 2^3 experiment was statistically analyzed. The results of the analysis of variance for the watt-hour data and the voltage delay data are seen in Table 7 and 8 respectively.

From the analyses of variance on all the watt-hour data no significant effects are seen. This means that any increase or decrease in the data can be explained by experimental error.

By contrast the analysis of variance of the voltage delay data of the 2^3 factorial experiment shows three significant effects. From the analysis and the calculations of the treatments effects, we can determine that the bromide additive significantly reduces the voltage delay, the length of storage significantly increases the voltage delay and the combination of the bromide additive and the length of storage reduces voltage delay.

That the bromide additive reduced voltage delay and the length of storage increased it are certainly no surprise. The length of storage was shown by microcalorimetry and complex plane impedance measurements to increase film resistance which is thought to increase voltage delay, and the bromine additive was observed in our preliminary studies to inhibit voltage delay. The question of how the two interact is unclear. One explanation could be that as time passes a Br^- impurity becomes more incorporated in the films structure. This may cause the film to be more porous and conductive than a film from a cell stored for a shorter period of time with bromine.

TABLE 5

Voltage Delay and Total Watt-hours form 2^3 Factorial Experiment

	Voltage Delay (h)			Total Watt-hours		
	1	2	3	1	2	3
- - -	0.00	0.16	0.10	1.59	0.72	1.18
+ - -	0.10	0.75	0.07	0.92	1.17	1.04
- + -	0.00	0.00	0.00	1.42	1.05	1.05
+ + -	0.00	0.00	0.00	1.42	0.97	0.97
- - +			1.54			0.69
+ - +			0.90			0.78
- + +			0.00			0.89
+ + +			0.12			1.02

Table 6

Analysis of Variance of Voltage Delay Data of 2^2 Factorial Experiment

Source of Variation	Sum of Squares	Degree of Freedom	Mean Squares	F-Ratio
Replications	0.08	1		
Treatments	0.24	3		
Temperature (A)	0.059	1	0.059	1.18
Presence of (B)				
Additive	0.127	1	0.127	2.54
Interation: (AB)	0.059	1	0.059	1.18
Error	0.150	3	0.050	

Analysis of Variance of Total Watt-hours Data of 2^2 Factorial Experiment

Source of Variation	Sum of Squares	Degree of Freedom	Mean Square	F-Ratio
Replications	0.26	1		
Treatments	0.09	3		
Temperature (A)	0.011	1	0.011	0.10
Presence of (B)				
Additive	0.026	1	0.026	0.24
Interaction: (AB)	0.002	1	0.002	0.02
Error	0.32	3	0.107	

Table 7

Analysis of Variance of Watt-hour Data

Source of Variation	Sum of Squares	Degree of Freedom	Mean Square	F-Ratio
Temperature (A)	0.000	1	0.000	0.00
Presence of Additive (B)	0.007	1	0.007	0.07
Length of Storage (C)	0.092	1	0.092	0.86
Interaction:				
(AB)	0.001	1	0.001	0.01
(AC)	0.024	1	0.024	0.22
(BC)	0.051	1	0.051	0.48
(ABC)	0.000	1	0.000	0.00
Error*	0.320	3	0.107	

* Error estimate from replicated 2^2 factorial experiment

Table 8

Analysis of Variance of Voltage Delay Data

Source of Variation	Sum of Squares	Degree of Freedom	Mean Square	F-Ratio
Temperature (A)	0.038	1	0.038	0.76
Presence of Add. (B)	0.775	1	0.775	15.50**
Length of Storage (C)	0.714	1	0.714	14.28**
Interaction:				
(AB)	0.078	1	0.078	1.56
(AC)	0.030	1	0.030	0.60
(BC)	0.578	1	0.578	11.56**
(ABC)	0.067	1	0.067	0.63
Error *	0.15	3	0.050	

* Error estimate from replicated 2^2 factorial experiment

** Significant at 95% confidence level $F_{0.05}(1,3) = 10.13$

V. CATHODE PERFORMANCE CHARACTERIZATION

In this section four areas were investigated: i) baseline performance, ii) performance of cells with Cl_2 vs. cells w/Br_2, iii) low temperature performance, iv) cathode composition.

V.1. Experimental Method

The test vehicle for these studies consisted of 2 inch hermetically sealed cells with both electrodes electrically floating as shown in Figure 87. The anodes were composed of 20 mil Li pressed on 11 mil nickel mesh; the cathodes were composed of approximately 0.35 g of a Shawinigan Black (SB)/PTFE mixture pressed on 11 mil Ni mesh to a uniform thickness of 20 mil. Five mil Manninglas was used as the separator. Double distilled SO_2Cl_2 was used in the formulation of all electrolytes. The $LiAlCl_4$ and $LiAC_3Br$ were commercially prepared.

To insure reproducible results:

1) Electrolyte used was stored in stoppered flask and not stored for more than 3 days.
2) Upon filling of the cell, it was allowed to stand on open circuit for 10 minutes.
3) Cell discharged was carried out at constant current.
4) Capacity calculated was to a 2V cut-off.

V.2. Baseline Studies

In order to screen quickly cell treatments for those worthy of study, baseline data for Li/SO_2Cl_2 cells with a supporting electrolyte of 1.5M$LiAlCl_4$ were first accumulated. The cells used were constructed as shown in Figure 87 and were run over a range of current densities (1-20mA/cm^2). From the

baseline data in Table 9 the non-linearity of the capacity vs. current density is evident. This may be due to cathode swelling with wicking in of electrolyte and/or incomplete utilization of the cathode at higher current densities.

V.3. Cells with the Bromine Additive

Once the baseline data were accumulated testing of the bromide additive was initiated. The cells used for this study were identical to those used in the baseline study, but the electrolyte was $LiAlCl_4$/0.5M $LiAlCl_3Br/SO_2Cl_2$.

The discharge curves are seen in Figure 88, the capacity data is seen in Table 10, presented next to the baseline data. From the table it is quite evident that the bromine additive increases the capacity of the cell at all current densities. In addition, the additive results in a flatter, higher voltage discharge.

A further benefit of the Br_2 electrolyte is that it extends the usable range of current density of Li/SO_2Cl_2 cells. The original baseline data were taken up to current densities of $20mA/cm^2$. At $20mA/cm^2$ the capacity was only about 50% of theoretical, (0.450 Ah) at higher current densities the capacities are much less. In cells employing the bromine electrolyte the capacity is slightly above theoretical capacity (.450 Ah) and at 25 mA/cm^2 and 30 mA/cm^2 the capacity is 50% of the $20mA/cm^2$ capacity. This demonstrates that the bromine electrolyte allows a $20mA/cm^2$ discharge with no loss in capacity as compared to the theoretical capacity, and allows operation at current densities up to $30mA/cm^2$. In this range of current densities cells with the additive deliver at least twice the capacity of cells without the additive.

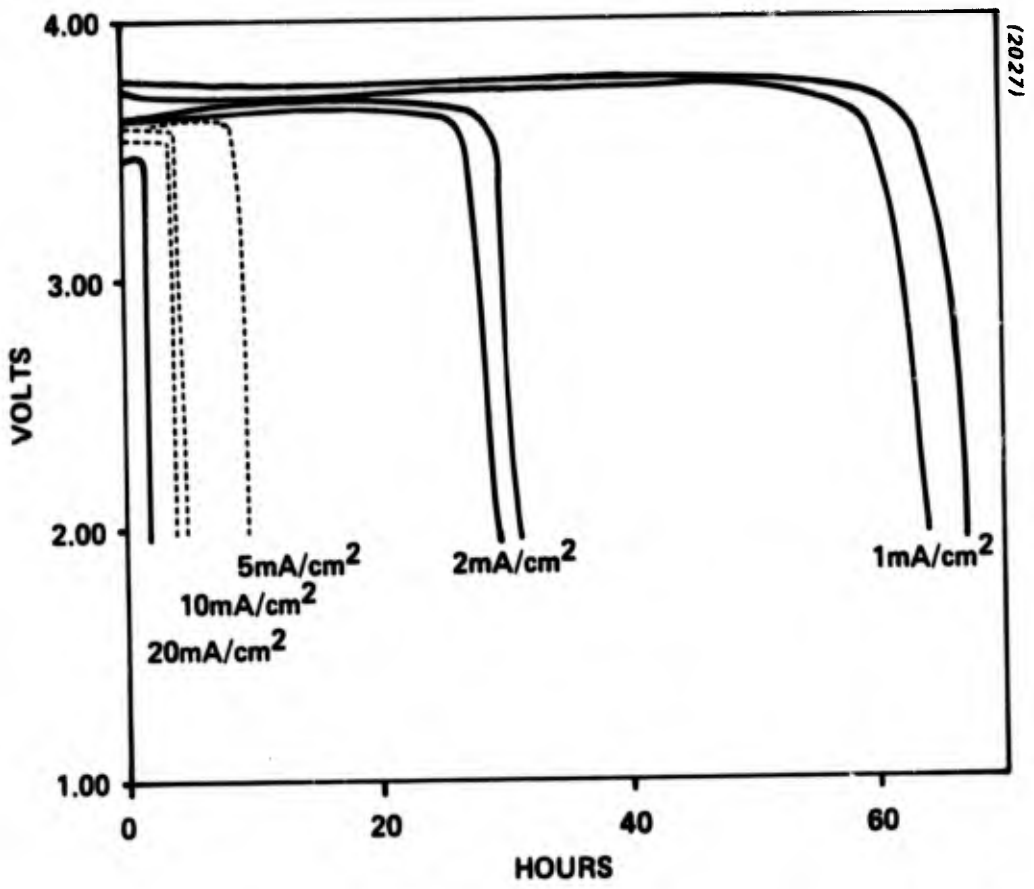

Figure 88 Dicharge Curves of Li/SO_2Cl_2 Cells with $LiAlBrCl_3$ at a Range of Current Densities

Table 9

Baseline Data for Li/SO_2Cl_2 Cells Using 1.5 M $LiAlCl_4/SO_2Cl_2$ Electrolyte

$I(mA/cm^2)$	Capacity (Ah)
1	N/A
2	0.888
	0.868
5	0.693
	0.660
10	0.459
	0.465
20	0.282
	0.270

Table 10
Baseline Data for Li/SO_2Cl_2 Cell With
$1.5MLiAlCl_4$ vs. Data for Li/SO_2Cl_2 Cells With
$1.0MLiAlCl_4$, 0.5M $LiAlCl_3Br$

$i(mA/cm^2)$	Baseline Capacity (Ah)	Bromine Electrolyte Capacity (Ah)
1	N/A	.992
	N/A	.951
2	888	.925
	868	.985
5	.693	.729
	.660	
10	.459	0.618
	.463	0.600
20	0.282	0.522
	0.270	
25	<0.1	0.212
		0.234
30	<0.1	0.225
		0.234

V.4. Cl_2 Addition vs. Br_2 Addition

Another additive considered for sulfuryl chloride is chlorine. Work by Liang (10) indicates that storage times of at least one year, using Cl_2 as an additive to SO_2Cl_2, are attainable with only an 8% loss in capacity (some voltage delay was evident). In addition an increase in the operating voltage and capacity of cells filled and immediately discharged are reported when the chlorine additive is employed.

The addition of Cl_2 was thus proposed for the Li/SO_2Cl_2 system. Using a double gas scrubbing apparatus seen in Figure 12 chlorine was added to a SO_2Cl_2/1.5M $LiAlCl_4$ solution. We also added Cl_2 as a liquid, trapped using a dry-ice/IPA trap, to SO_2Cl_2. The weight and volume change of the solution was used to calculate a final Cl_2 concentration of 0.5M. Simultaneous testing of two cells (Cl_2 added and $LiAlBrCl_3$) was performed. The discharge curves for the four cells run are given in Figure 89. Aside from the initial plateau, the curves for Cl_2 cells are comparable to cells run without an additive. Figure 90 shows curves one for each type of electrolyte, performed at $10mA/cm^2$. The bromine additive cell appears to have a higher capacity and average discharge voltage than either of the other two cells, but the difference in capacity is not significant within a 95% confidence interval.

This observation prompted further Br_2 vs. Cl_2 comparison. Comparison between Cl_2 and Br_2 was made at $20mA/cm^2$ and $30mA/cm^2$. Eight two inch cells as described above were fabricated using 90% SB/10% PTFE as the cathode mix. The electrolytes used were 1.0M $LiAlCl_4$, 0.5M $LiAlCl_3Br/SO_2Cl_2$ and 1.5M $LiAlCl_4$, 0.5M Cl_2/SO_2Cl_2. Four cells were discharged at 20 mA/cm^2 and 3 cells at 30 mA/cm^2 (one cell leaked upon filling). The results are seen in Table 11 and Figure 91.

---

10. C.C. Liang, M.E. Bolster and R.M. Murphy, J. Electrochem. Soc. 128 1631 (1981).

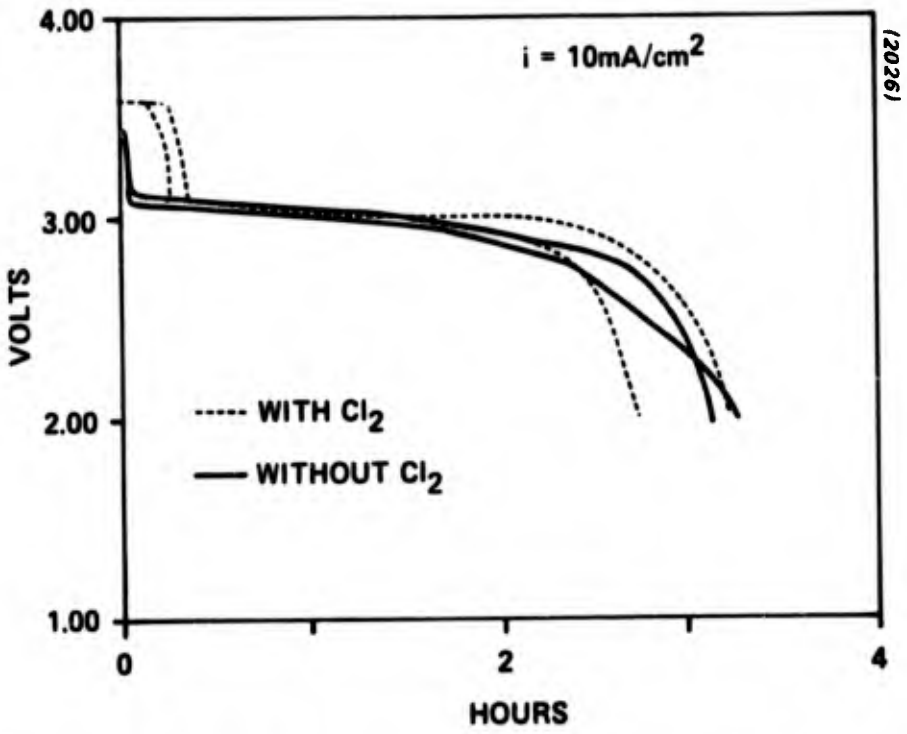

Figure 89 Discharge Curves of Li/SO_2Cl_2 Cells with and without Cl_2 Addition

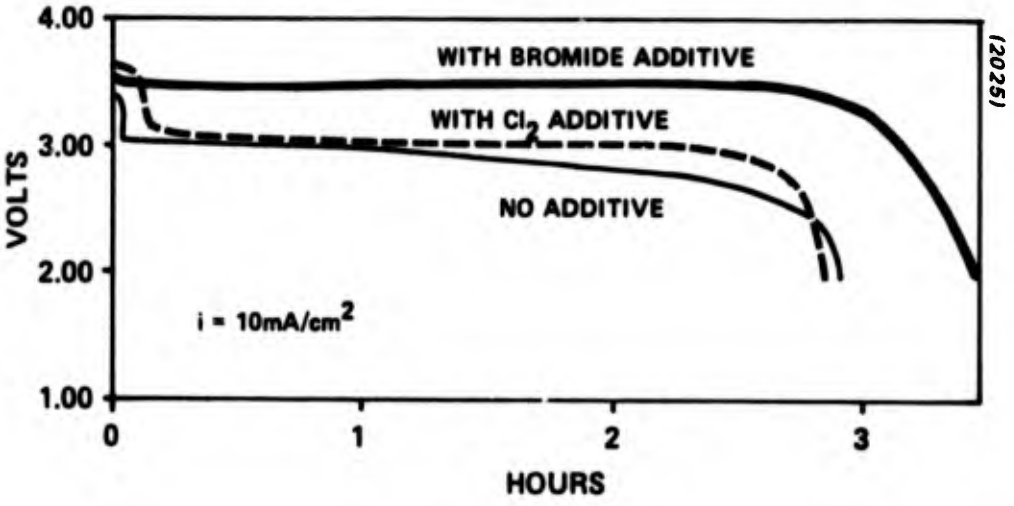

Figure 90 Discharge Curves of Li/SO_2Cl_2 Cells with Bromide Additive, Cl_2 Addition, and No Additives

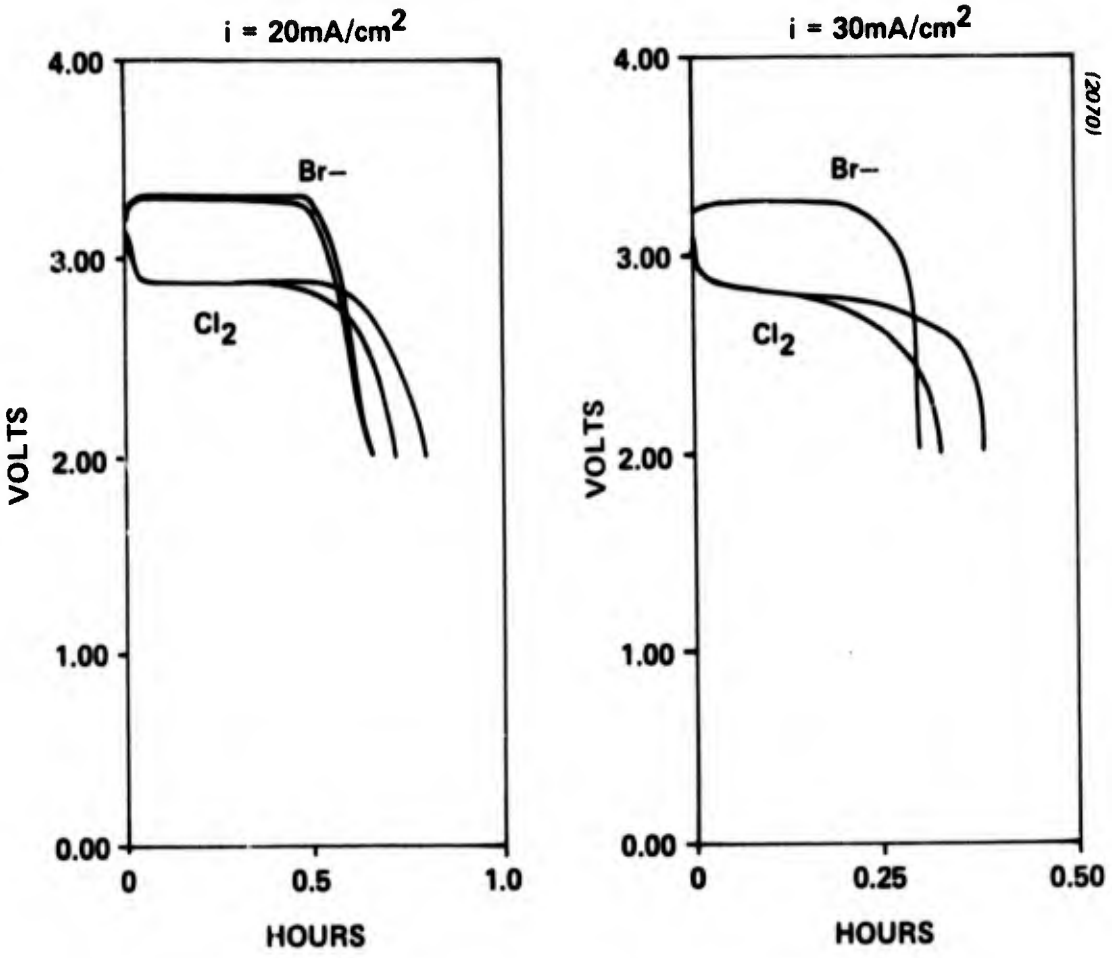

Figure 91 Discharge Curves of Li/SO_2Cl_2 Test Cells
Run at 20 and 30 mA/cm^2 with $LiAlCl_3Br$ Added and Cl_2 Added

Table 11

Average Capacities (in Ah) of Li/SO_2Cl_2 Cells
at $20mA/cm^2$ and $30mA/cm^2$ for Br^- and $C._2$ additives

	SO_2Cl_2/1.0M $LiAlCl_4$ 0.5M $LiAlCl_3Br$	SO_2Cl_2/1.5M $LiAlCl_4$ 0.5M Cl_2
$20mA/Cm^2$	0.198 ± 0.037	0.228 ± 0.037
$30mA/Cm^2$	0.139 ± 0.052	0.160 ± 0.037

From the table and the figure the Cl_2 cells appear to deliver at 20mA/cm^2 a higher capacity, but within a 95% confidence interval the difference between the two can be attributed to experimental error. The same is also true of the 30 mA/cm^2 data. Even though the bromide additive cells still operate at a higher voltage the differences in the capacities are not significant.

In view of the data the use of either $LiAlBrCl_3$ on Cl_2 as an additive is acceptable at current densities of 10mA/cm^2 or greater where cell capacity is the major concern.

V.5 Cell Performance at Low Temperature

A comparison between the capacity of cells with added Cl_2 versus cells added with the bromine additive was performed at -20°C. Some comparison were also done using standard electrolyte (SO_2Cl_2/1.5M $LiAlCl_4$). Cells were discharged at 10mA/cm^2 at -20°C and at 25°C for comparison.

The results of the runs are seen in Table 12. From the table we can see most of the differences can be attributed to experimental error. For example, when comparing standard electrolyte to Cl_2 containing electrolyte the differences between them are small when compared to the error. In at least one case though the differences cannot be explained entirely by error. In run 2 at -20°C the differences between the standard electrolyte data and the bromine additive data are significant indicating that at -20°C the standard electrolyte cells perform better than those with $LiAlCl_3Br$ added to them. With some reservations we can also conclude that since there is no significant difference between the Cl_2 data and standard electrolyte data that cells with Cl_2 added also perform better at -20°C than those with $LiAlCl_3Br$ added to them.

Table 12

Average Capacities of Cells Run
With Various Electrolytes at 25°C and -20°C

Run	Temp.	Standard Electrolyte	Cl_2 Added	Bromide Additive (0.5)	Bromide Additive (1.5)
1	25°C	0.360±0.076	0.419±0.056	-	-
2	25°C	0.303±0.078	-	0.395±0.056	0.285±0.078
3	-20°C	0.422±0.078	-	0.293±0.056	0.300±0.078
4	-20°C	0.323±0.056	0.329±0.056	-	-
1	-20°C	0.388±0.078	0.347±0.056	-	-
*2	-20°C	0.327±0.056	-	0.254±0.056	-

This preliminary study indicates that at lower temperatures the addition of bromine is deleterious to cell performance. Apparently the mechanism which utilizes bromine is temperature sensitive and less efficient at lower tempertures.

A final observation is that in those two runs in which 1.5M $LiAlCl_3Br$ was used no advantage could be seen over using only 0.5M $LiAlCl_3Br$.

V.6. Cathode Composition Studies

Most of the data obtained under this contract were taken from cells using 90% Shawinigan Black/10% PTFE binder as cathode material. This study was devised to compare the 90/10 cathode to the 95/5 cathode. A 2^3 factorial design experiment was developed for this study. The two additional factors are current density and the presence of the $LiAlCl_3Br$. The experimental design was as follows:

	A	B	C
1	−	−	−
a	+	−	−
b	−	+	−
ab	+	+	
c	−	−	+
ac	+		+
abc	−	+	+

Factors		
A.	Cathode composition	+ 95% SB/5% PTFE
		− 90% SB/10% PTFE
B.	Additive	+ w/B_2^-
		− $w/o\ B_2^-$
C.	Current density	+ 2 mA/cm^2
		− 10 mA/cm^2

Two runs of the above experiment were performed, and the results of those runs are seen in Table 13. The capacity and watt-hour data are both presented. The calculations of the treatment effects are seen in Table 14. The analysis of variance for the capacity and the watt-hour data are seen in Table 15 and Table 16 respectively.

In each of the analysis of variance the cathode composition and current density were both found to be significant. This means that for a given

Table 13

Effect of Cathode Composition on Cell Performance

	Run 1		Run 2	
	wh	Capacity (Ah)	wh	Capacity (Ah)
- - -	1.36	0.447	1.21	0.403
+ - -	2.45	0.804	1.69	0.567
- + -	1.86	0.540	1.48	0.426
+ + -	3.21	0.930	1.76	0.510
- - +	2.60	0.789	2.40	0.760
+ - +	3.33	1.010	3.24	0.997
- + +	2.56	0.710	2.58	0.718
+ + +	3.27	0.908	2.70	0.751

Table 14
Cathode Composition Study 2^3 Factorial Experiment

	Current Density 10mA/cm²				Current Density 1mA/cm²					
	No Additive		Br' Additive		No Additive		Br' Additive			
	90/10	95/5	90/10	95/5	90/10	95/5	90/10	95/5		
Run 1 Ah / Wh	0.447 / 1.36	0.804 / 2.45	0.540 / 1.86	0.930 / 3.21	0.789 / 2.60	1.010 / 3.33	0.710 / 2.56	0.908 / 3.27	6.138 / 20.64	
Run 2 Ah / Wh	0.403 / 1.21	0.567 / 1.69	0.426 / 1.48	0.510 / 1.76	0.760 / 2.40	0.997 / 3.24	0.718 / 2.58	0.751 / 2.70	5.132 / 17.06	
Total Ah / Total Wh	0.850 / 2.57	1.371 / 4.14	0.966 / 3.34	1.440 / 4.97	1.549 / 5.00	2.007 / 6.57	1.428 / 5.14	1.659 / 5.97	11.270 / 37.70	
									Factorial Gated Total	Sum of Squares
A	−	+	−	+	−	+	−	+	1.684 / 5.60	0.177 / 1.96
B	−	−	+	+	−	−	+	+	0.284 / 1.14	0.005 / 0.08
AB	+	−	−	+	+	−	−	+	0.274 / −0.68	0.005 / 0.03
C	−	−	−	−	+	+	+	+	2.016 / 7.66	0.254 / 3.67
AC	+	−	+	−	−	+	−	+	−0.306 / −0.80	0.005 / 0.04
BC	+	+	−	−	−	−	+	+	−0.654 / −2.06	0.027 / 0.26
ABC	−	+	+	−	+	−	−	+	−0.180 / −0.80	0.002 / 0.040

Table 15

Capacity Data Analysis of Variance

Source of Variation	Sum of Squares	Degree of Freedom	Mean Square	F-Ratio
Replications	0.063	1		
Treatments	0.475	7		
Cathode Composition (A)	0.177	1	0.177	16.74*
Presence of Additive (B)	0.005	1	0.005	0.47
Current Density (C)	0.254	1	0.254	24.03*
Interaction				
(AB)	0.005	1	0.005	0.47
(AC)	0.005	1	0.005	0.47
(BC)	0.027	1	0.027	2.55
(ABC)	0.002	1	0.002	0.19
Error	0.074	7	0.0105	

* Significant - $F_{(0.05)}\ (1,7) = 5.59$

Table 16

Watt-hour Data Analysis of Variance

Source of Variation	Sum of Squares	Degree of Freedom	Mean Squares	F-Ratio
Replications	0.80	1		
Treatments	6.08	7		
Cathode Composition (A)	1.96	1	1.96	16.94*
Presence of Additive (B)	0.08	1	0.08	0.69
Current Density (C)	3.67	1	3.67	31.71*
Interaction				
(AB)	0.03	1	0.03	0.26
(AC)	0.04	1	0.04	0.35
(BC)	0.26	1	0.26	2.25
(ABC)	0.04	1	0.04	0.35
Error	0.81	7	0.12	

$F_{0.05}\ (1,7) = 5.59$

thickness and weight of a cathode, a cathode made with 95/5 will perform significantly better than one made from 90/10 cathode mix.

The mechanism by which a 95/5 cathode is more efficient is not known, but it may lie in the fact that for a given weight of mix, 95/5 has more carbon than 90/10. This fact might translate into more active sites and therefore more capacity. The current density was also found to be significant. This is probably a result of inefficiencies of the electrode at higher current density.

It is interesting to note the lack of a significant coulombic capacity increase with the bromide additive. Trends observed in other studies have identified bromide addition as a way to improve cell capacity and discharge voltage. We certainly would have expected to see some effect in the watt-hour data (capacity x average discharge voltage) since the average discharge voltage is approximately 10% higher in cells using $LiAlCl_3Br$ but this is not seen indicating some loss in coulombic capacity.

These results further point to $LiAlCl_3Br$ as a questionable additive. At low temperatures cells using $LiAlCl_3Br$ perform with less capacity, at higher current densities ($20mA/cm^2$ and $30mA/cm^2$) cells with $LiAlCl_3Br$ perform only as well as those with Cl_2 added. We do observe little or no voltage delay in cells stored with the bromide additive, but the capacity is diminished over long periods of storage due to unimpeded corrosion. In most applications the positive effects of $LiAlCl_3Br$ addition are outweighed by the negative.

VI. CONDUCTIVITY AND DENSITY OF $SO_2Cl_2/LiAlCl_4$ SOLUTIONS

The conductivities and densities of SO_2Cl_2 solutions with 0.5M, 1.0M 1.5M and 2.0M $LiAlCl_4$ were determined from -20°C to 60°C at 20°C intervals. The results are presented in Table 17, and Figures 92 and 93.

VI.1. Conductivity

Procedure - 100ml of the desired solution was prepared from double distilled (second distillation over lithium) SO_2Cl_2 and commercially available $LiAlCl_4$. The solution was mixed for at least one and one half hours. Thirty-five ml of this solution were placed in a dry Jones-type conductivity cell (Beckman CEL 6J100). The cell was then placed in a refrigerated circulating bath at 20°C. After one hour a reading in ohms was taken using a Beckman conductivity bridge (RC-18A), and the temperature noted. Next the temperature of the bath was incresed to 40°C. After one hour at 40°C a second reading was taken and the temperature again noted. The above procedure was repeated at 60°C, 0°C and -20°C. All four solutions were run in a similar manner. The cell constant (in $meters^{-1}$) was determined, using 0.01 M KCl, before each series of measurements.

Results are presented in Table 17. The conductivity is reported in $(ohm\text{-}meter)^{-1}$, but the resistivity is in ohm-cm. Figure 92 is a plot of the inverse of the temperature in Kelvin versus the log of the conductivity.

VI.2. Density

Procedure - 50ml of one of the solutions prepared above was placed in a dry pre-weighed 50ml volumetric stoppered flask. The sealed flask was placed in a refrigerated circulating bath at 20°C for one hour. At the end of one hour the level in the flask was adjusted to 50ml. The flask was removed from the water bath, dried and weighed. The temperature of the bath was then in-

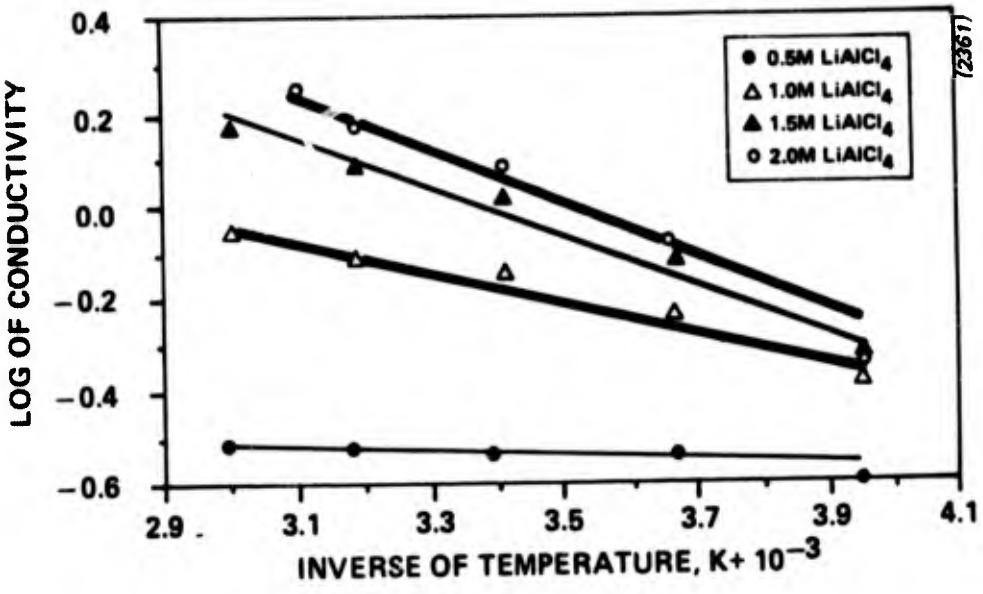

Figure 92 Inverse of Temperature (K) vs. Log of Conductivity of Sulfuryl Chloride with nM $LiAlCl_4$

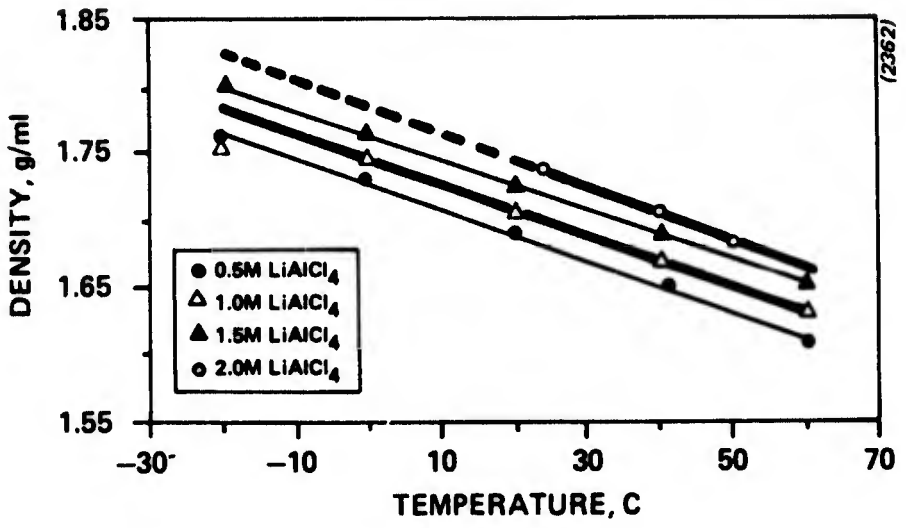

Figure 93 Temperature vs. Density of Sulfuryl Chloride with nM $LiAlCl_4$

Table 17

Density, Conductivity and Resistivity

of SO_2Cl_2/nM $LiAlCl_4$

(n=0.5M, 1.0M, 1.5M and 20M

from -20°C - 60°C

$LiAlCl_4$ Molarity	Temperature (°C)	Density (g/mL)	Conductivity (ΩM)-1	Resistivity (Ωcm)
0.5M	-20	1.762	0.252	397.45
	-0.5	1.731	0.289	345.30
	22	1.689	0.294	339.82
	41	1.651	0.301	332.67
1.0M	-20	1.759	0.423	139.88
	-0.5	1.747	0.587	171.61
	20	1.708	0.715	139.88
	40	1.672	0.780	128.23
	60	1.632	0.895	111.78
1.5M	-20	1.801	0.475	210.30
	-0.5	1.766	0.758	131.93
	20	1.726	1.030	97.03
	40	1.692	1.230	81.32
	60	1.656	1.476	67.77
2.0M	-20	N/A	0.456	219.34
	0	N/A	0.830	120.44
	20	1.737*	1.231	81.23
	40	1.705	1.505	66.43
	50	1.682	1.815**	55.09**

* @ 24°C

** @ 60°Ca

creased to 40°C. After one hour at 40°C, the level in the flask was adjusted to 50ml, the flask was again dried and weighed. The above procedure was repeated at 60°C, 0°C, and -20°C. The actual temperature was noted at each measurement.

The dry weight of the flask was determined before each series of measurements. In determining the density, the volume of the flask was adjusted for the different temperatures using the coefficient of expansion of glass.

Results are presented in Table 17 and Figure 93. At 60°C SO_2Cl_2 solutions containing 1.5 M and 2.0 M $LiAlCl_4$ boil. Using the method described above, obtaining an accurate level of a boiling solution is difficult and more prone to error, for this reason the accuracy of these measurements is less than the other ten measurements. This explains the density reading at 50°C for the 2.0 M solutions.

Also at temperatures 0°C and below SO_2Cl_2 with 2.0 M $LiAlCl_4$ is saturated using the method described above a mixed density is obtained as a result the plot drawn from -20°C to 20°C is the theoretical response assuming a linear dependency of density on temperature.

VII. CONCLUSIONS AND RECOMMENDATIONS

As a result of this work there does not appear to be any fundamental barrier to the development of a viable Li/SO_2Cl_2 cell capable of meeting Army storage and performance requirements. Although an acceptable in-cell corrosion rate was not demonstrated the ampule results demonstrate that this is a materials selection problem and not a fundamental characteristic of lithium in sulfuryl chloride solutions.

Though not a fundamental problem, selection of proper materials is far from trivial. For example, if a nickel case is required this may necessitate the use of ceramic-to-metal seals. This in turn will introduce problems with regard to the stability of the braze materials and the cost of such seals. A minimum close collaboration between the battery developer and seal fabricator will be required.

None of the chemistries tested was found to improve greatly the performance of fresh cells. Little benefit was seen with added chlorine. Although adding bromine results in a voltage advantage this did not lead to a statistically significant increase in total cell capacity. At current densities up to $20mA/cm^2$ the basic system delivers close to 100% of theoretical capacity. One may conclude from this that no improvement in room temperature performance is required.

Chlorine was found to improve decidedly anode storability. The improvement, however, was still not sufficient for long term storage of cells. Bromine, on the other hand, was found to effect adversely anode storage life. Our preliminary results suggest that the chlorine additive in combination with a methylcyanoacrylate anode coating is the preferred design for anode stability and minimum voltage delay for cells without optimum materials.

Finally, the principal reason for pursuing Li/SO_2Cl_2 technology for Army application is the possibility of greater safety. The preliminary spectroelectrochemical studies, however, indicate transitory reactions and the possible onset of cell instability. Any follow-on effort should as a major task element address safety issues in a parametric analytical fashion.

References

1. D.I. Chua, J.O. Crabb and S.L. Despande, "Proceedings of the 28th Power Sources Symposium", Atlantic City, N.J. 28 247 (1978).

2. A.N. Dey, "Proceedings of the 26th Power Sources Symposium", Atlantic City, N.J. 27 42 (1976).

3. W.K. Behl, "Proceedings of the 28th Power Sources Symposium", Atlantic City, N.J. 28 30 (1978).

4. W.K. Behl, J. Electrochem. Soc., 127 1444 (1980).

5. J.C. Hall, H.F. Gibbard and M.J. Montgomery, Fall Meeting of the Electrochemical Society, Extended Abstract No. 104, Los Angeles, California, October 14-19, 1979.

6. S. Gilman and W. Wade, J. Electrochem. Soc, 127, 1427 (1980).

7. N.A. Fleisher, "30th Power Sources Symposium", Atlantic City, N.J. (to be published).

8. C. Gabrielli, "Identification of Electrochemical Processes by Frequency Response Analysis", Solartron Instruments Group.

9. H.F. Gibbard, "Proceeding of the Symposium on Power Sources for Biomedical Implantable Applications and Ambient Temperature Lithium Batteries", B.B. Owens and N. Margalit, eds, The Electrochemical Society, 1980, p. 510.

10. C.C. Liang, M.E. Bolster and R.M. Murphy, J. Electrochem. Soc. 128 1631 (1981).

DISTRIBUTION LIST

Defense Technical Info Ctr
ATTN: DTIC-TCA
Cameron Station (Bldg 5)
Alexandria, VA 22314 (12)

HQDA (DAMA-ARZ-D/Dr. F.D. Verderame)
Washington, DC 20310 (1)

Cdr. Naval Surface Weapons Ctr
White Oak Laboratory
ATTN: Library, Code WX-21
Silver Spring, MD 20910 (1)

Cdr, Harry Diamond Laboratories
ATTN: Library
2800 Powder Mill Road
Adelphi, MD 20783 (1)

Commandant, Marine Corps
HQ, US Marine Corps
ATTN: Code LMC, INTS (In Turn)
Washington, DC 20380 (1)

Director
US Material Sys Anal Actv
ATTN: DRXSY-T
Aberdeen Prov Grnd, MD 21005 (1)

Rome Air Development Center
ATTN: Documents Library (TSLD)
Griffiss AFB, NY 13441 (1)

Cdr, USA Signals Warfare Lab
ATTN: DELSW-OS
Vint Hill Farms Station
Warrenton, VA 22186 (1)

AFGL/SULL
S-29
HAFB, MA 01731 (1)

Commander
USA Mobility Eqp Res & Dev Cmd
ATTN: DRDME-R
Fort Belvoir, VA 22060 (1)

Cdr, Harry Diamond Labs
ATTN: DELHD-CO,TD (In Turn)
2800 Powder Mill Road
Adelphi, MD 20783 (1)

Commander
US Army Electronics R&D Command
DELET-PR (S. Gilman)
Fort Monmouth, NJ 07703 (14)

Commander
US Army Electronics R&D Command
DELET-DT
Fort Monmouth, NJ 07703 (1)

NASA Scientific & Tech Info
Facility
Baltimore/Washington Intl Airpt
P.O. Box 8757, MD 21240 (1)

Commander
US Army Electronics R&D Command
DELET-DD
Fort Monmouth, NJ 07703 (1)

CMDR, MICOM
ATTN: DRCPM-HDE
Redstone Arsenal, AL 35809 (1)

Commander
US Army Electronics R&D Command
DELSD-L (Library)
Fort Monmouth, NJ 07703 (1)

Dr. H. Grady
Foote Mineral Company
Route 100
Exton, PA 19341 (1)

Commander
US Army Electronics R&D Command
DELSD-L-S (Stinfo)
Fort Monmouth, NJ 07703 (2)

Dr. D. Chua
Honeywell, Inc.
104 Rock Road
Horsham, PA 19044 (1)

Mr. Robert L. Higgins
Eagle-Picher Industries, Inc.
Electronics Division
P.O. Box 47
Joplin, Missouri 64801 (1)

Dr. Robert McDonald
GTE Sylvania/SSD
520 Winter Street
Waltham, MA 02154 (1)

Attn: Technical Library
Yardney Electric Company
82 Mechanic Street
Pawcatuck, CT 06379 (1)

Dr. J.L. Hartman
General Motors Corp.
Research Laboratories
General Motors Technical Center
12 Mile and Mounds Road
Warren, MI 48090 (1)

Dr. A.N. Dey
Duracell International, Inc.
Northwest Industrial Park
Burlington, MA 01803 (1)

Union Carbide Corporation
Parma Research Center
P.O. Box 6116
Cleveland, OH 44101 (1)

Dr. R. Hamlen
Exxon Research & Engineering Co.
Corporate Research Laboratory
Linden, NJ 07036 (1)

J. Dalfonso
Duracell International, Inc.
S. Broadway
Tarrytown, NY 10591 (1)

Dr. E.C. Gay
Argonne National Laboratories
9700 South Cass
Argonne, Il 60439 (1)

Dr. L. Heredy
North American Rockwell Corp
Atomics International Divison
Box 309
Canoga Park, CA 91304 (1)

Dr. Stefan Mitoff
General Electric R&D Center
P.O. Box 8
Schenectady, NY 12301 (1)

Dr. Keith Klinedinst
GTE Laboratories, Inc.
40 Sylvan Road
Waltham, MA 02254 (1)

Dr. J. Kennedy
University of California
Department of Science & Research
Santa Barbara, CA 93100 (1)

Dr. Eisenberg
Electrochimica
2485 Charleston Road
Mountain View, CA 94040 (1)

Mr. S. Charlip
Gulton Industries, Inc.
Metuchen, NJ 08840 (1)

J. Marshall
Sanders Associates, Inc.
24 Simon Street
Mail Stop NSI-2208
Nashua, NH 03060 (1)

Mr. B.J. Bragg
Propulsion and Power Division
Mail Code EP5
NASA-Johnson Space Center
Houston, Texas 77058 (1)

Stuart Chodosh
Power Conversion, Inc.
495 Boulevard
Elmwood Park, NJ 07407 (1)

Portfolio Manager
Hooker Chemicals & Plastics Corp
M.P.O. Box 8
Niagara Falls, NY 14302 (1)

Mr. J.R. Moden
Energy Conversion Branch Code 3642
Naval Underwater Systems Center
Newport Laboratory
Newport, RI 02840 (1)

Dr. Leonard Nanis
G207
S.R.I.
Menlo Park, CA 94025 (1)

Dr. Stuart Fordyce
NASA Lewis Research Center
Mail Stop 6-1
21000 Brookpark Road
Cleveland, OH 44135 (1)

Dr. J.J. Auborn, Rm 1A-317
Bell Laboratories
600 Mountain Avenue
Murrary Hill, NJ 07974 (1)

Mr. Myles Walsh
ECO Incorporated
P.O. Box 578
Buzzards Bay, MA 02532 (1)

Mr. Harvey Frank
Mail Stop 198-220
Jet Propulsion Laboratory
4800 Oak Grove Drive
Pasadena, CA 91103 (1)

S.B. Brummer
EIC, Inc.
Newton, MA 02158 (1)

Dr. D. Ernst
Naval Surface Weapons Center
White Oak Laboratory,
Code R-33 (M/S A026)
Silver Spring, MD 20910 (1)

A. Pignola
Altus Corp
1610 Crane Court
San Jose, CA 95112 (1)

J. Bene
MS 488
NASA Langley Research Center
Hampton, VA 23665 (1)

Dr. Frank Bis
Naval Surface Weapons Center
White Oak Laboratory, Code R-33
Silver Spring, MD 20910 (1)

Mr. Eddie T. Seo
Research and Development Division
The Gates Rubber Co.
999 S. Broadway
Denver, CO 80217 (1)

Dr. Jerry J. Smith
ONR Chemical Program
Arlington, VA 22217 (1)

Mr. Sidney Gross
Mail Stop 8C-62
Boeing Aerospace Company
P.O. Box 3999
Seattle, WA 98124 (1)

Mr. Lou Adams
Saft Corporation of America
711-A Industrial Blvd.
P.O. Box 1284
Valdosta, GA 31601 (1)

Dr. H.V. Venkatasetty
Honeywell Technology Center
10701 Lyndale Avenue, South
Bloomington, MN 55420 (1)

Dr. C. Liang
Electrochem Industries (E•I) Inc.
9990 Wehrle Drive
Clarence, NY 14031 (1)

Mr. Aiji Uchiyama
Jet Propulsion Laboratory-M.S. 198-220
4800 Oak Grove Drive
Pasadena, CA 91103 (1)

Dr. C. Schlaiker
Duracell International
Northwest Industrial Park
Burlington, MA 01803 (1)

Dr. Harvey N. Seiger
Harvey N. Seiger Associates
8 Beacon Hill Drive
Waterford, CT 06385 (1)

Dr. Fred Dampier
GTE Laboratories, Inc.
40 Sulvan Road
Waltham, MA 02254 (1)